Society for Science and Education
United Kingdom

ISSN: 2055 - 1266
Volume 1. Issue 5

Journal of Biomedical Engineering and Medical Imaging

TABLE OF CONTENTS

EDITORIAL ADVISORY BOARD

DISCLAIMER

All the contributions are published in good faith and intentions to promote and encourage research activities around the globe. The contributions are property of their respective authors/owners and the journal is not responsible for any content that hurts someone's views or feelings etc.

SOCIETY FOR SCIENCE AND EDUCATION UNITED KINGDOM

JBEMi JOURNAL OF BIOMEDICAL ENGINEERING AND MEDICAL IMAGING

ISSN: 2055-1266
VOLUME 1, ISSUE 5

An efficient neuro-fuzzy based segmentation of normal tissues in brain MRI (BMRI) using extensive feature set

M.Y.Bhanumurthy[1] and Koteswararao Anne[2]
[1]*Dept.of ECE, Vasireddy Venkatadri Institute of Technology, Guntur-522006, A.P, INDIA;*
[2]*Dean Academics, V.R.Siddhartha Engineering College, Vijayawada, A.P, INDIA;*
mybhanu@gmail.com; raoanne@gmail.com

ABSTRACT

Brain tissue Segmentation from the MRI images is having significance in the medical research field. The accurate Segmentation of the normal as well as the abnormal tissues is the complex assignment in this process. In this paper, a technique named Neuro-Fuzzy Based Segmentation (NFBS) is proposed for segmenting the normal features such as White Matter (WM), Gray Matter (GM) and Cerebro-Spinal Fluid (CSF) in the MRI Brain images. (1) Feature extraction (2) Classification (3) Segmentation are the three stages offered in this work. At first, the features such as energy, entropy, homogeneity, contrast and correlation from MRI Brain Images are extracted. Next, by utilizing Neuro-Fuzzy classifier, the Classification process is carried out and for this process, the feature set is specified as the input. From the outcome of Classification, the images are categorized into normal as well as abnormal. The further procedure Segmentation is performed according to this outcome only. The normal MRI images are segmented into normal tissues like White Matter (WM), Gray Matter (GM) and Cerebro-Spinal Fluid (CSF). All the tissues are individually segmented by special methods such as Gradient method, Orthogonal Polynomial Transform method. Utilizing MATLAB platform, the implementation of the proposed technique is made. The experimentation is carried out on the MRI Brain Images by BrainWeb data sets. The performance of the proposed technique is assessed with the help of the metrics namely FPR, FNR, Specificity, Sensitivity and Accuracy. Therefore, using our proposed techniques with enhanced classification, the normal tissues of MRI Brain images are segmented accurately.

Keywords:- Segmentation, Classification, Neuro-Fuzzy Logic, Normal and abnormal tissues, Gradient Method, Orthogonal Polynomial Transform.

1 Introduction

The brain is the frontal most part of the central nervous system. It forms the Central Nervous System (CNS) along with the spinal cord. The Cranium, a bony box in the skull guards it. Because of our brain in practical we do lots of things like, to think, act, reason, walk, talk, the list is never-ending. Brain Tumors are one of the syndrome caused in the brain. In an uncontrolled behavior cells reproduces themselves that causes abnormal growth which is called tumor. A benign brain tumor contains benign (harmless) cells and has different manner. This tumor can be cured only by surgery. A malignant brain tumor is very critical. Because of its location and it contains of cancer cells it may be termed as malignant. A malignant

DOI: 10.14738/jbemi.15.429
Publication Date: 09th September 2014
URL: http://dx.doi.org/10.14738/jbemi.15.429

brain tumor invented of cancerous cells which possibly will spread or begin in other locations in the brain or spinal cord. Hence it cannot function correctly as it can attack and destroy healthy tissues.

By means of Magnetic Resonance Imaging (MRI) doctors and researchers can examine noninvasively the structure and function of the brain. In fact, the MRI image is a thin horizontal slice of the brain. The white area at lower left is the tumor. It looks white as MRI scans develops the tissue variation. In reality, the tumor is on the right side of the brain. In recent times, various people utilize the MRI data to explore the relation among white matter development and neural diseases particularly the anatomy image is combined with those images from diffusion tensor imaging. And the accuracy of segmenting white matter is a key problem when it is utilized to lead the fibre tack [1-2]. Attention deficit hyperactivity disorder (ADHD) [3] is as well required to segment white matter.

Various algorithms have been proposed for brain MRI segmentation recently. Different algorithms for segmenting MRI of data [4-8] are watershed algorithm, eSneke algorithm and genetic algorithm. Those algorithms are based on the homogeneity of image. Actually, we have to solve the problem with new technique as the intensity in homogeneity is impact on every image. The majority well-liked techniques are consisted thresholding [8], region-growing [9] and clustering. The complete mechanical intensity-based algorithms include high sensitivity to different noise artifacts that is intra-tissue noise and inter-tissue intensity contrast reduction. Thresholding is very ease and competence. The intensity histogram of the image is bimodal if the target is plainly noticeable from background, and by simply selecting the valley bottom as the threshold point, it can be easier to obtain the optimal threshold. On the other hand, in the majority of real images, there are not plainly noticeable marks among the target and the background. Clustering is the majority well-liked approach for segmentation of brain MR images and naturally executes better than the other techniques [10]. Wells [9] buildups a latest statistical approach based on the expectation-maximization (EM) algorithm, however the results are too reliant on the initial values, very time consuming and just looking for local maximum point.

Segmentation is an significant implement in medical image processing and it has been helpful in several applications, namely: detection of tumors, detection of the coronary border in angiograms, surgical planning, measuring tumor volume and its response to therapy, automated classification of blood cells, detection of micro calcifications on mammograms, heart image extraction from cardiac cine angiograms, etc [11]-[14]. It may be helpful to categorize image pixels into anatomical regions in some applications such as bones, muscles, and blood vessels, while in others into pathological regions, such as cancer, tissue deformities, and multiple sclerosis lesions. To detach an image into regions that are homogeneous with respect to one or more characteristics is the primary objective in segmentation process [10]. The aim is to separate the whole image exactly into sub regions included gray matter (GM), white matter (WM) and cerebrospinal fluid (CSF) spaces of the brain [15] in magnetic resonance (MR) images processing. As, in a number of neurological disorders like multiple sclerosis (MS) and Alzheimer's disease, the volume changes in total brain, WM, and GM can give major notification about neuronal and axonal loss [16].

The remaining of the paper is prepared as follows: After this Introduction part the next section surveys several works that have already segmenting the tissues in the MRI Brain images. Section 3 explains our proposed technique of segmenting the tissues of BMRI images utilizing Neuro-Fuzzy Classifier. The

outcomes regarding the performance of our proposed work are specified in the Section 4 and as a final point; our paper is summed up with the conclusion part in Section 5.

2 Literature Survey

Researchers proposed for many researches for the brain image segmentation. A short access of several researches is offered here. Arnaldo Mayer and Hayit Greenspan [20] have offered an automated segmentation framework for brain MRI volumes based on adaptive mean-shift grouping in the joint spatial and intensity feature space. The technique was authorized both on simulated and real brain datasets, and the outcomes were compared with state-of-the-art algorithms. The benefits over intensity based GMM EM schemes as well as additional state-of-the-art techniques were established. Moreover they proved that by means of the AMS framework, segmentation of the normal tissues is not degraded by the presence of abnormal tissues. The algorithm gave good outcomes on noisy and biased data while only a rudimental bias field improvement part executed and no spatial prior was extracted from an atlas. And thanks to the adaptive mean-shift ability to work with non-convex clusters in the joint spatial intensity feature space and also the mean-shift noise smoothing behavior.

Mert R. Sabuncu et al. [21] have examined a generative model that guides to label fusion style image segmentation techniques. They originated several algorithms that merge transmitted training labels into a single segmentation estimate in the proposed framework. An expert gave a dataset of 39 brain MRI scans and equivalent label maps and we analytically compared these segmentation algorithms with Free Surfer's broadly-used atlas-based segmentation tool. Their outcomes established that the proposed framework yields an accurate and robust segmentation tools that are employed on large multi-subject datasets. They utilized one of the enhanced segmentation algorithms to calculate hippocampal volumes in MRI scans of 282 subjects, in a second experiment. A assessment of these measurements across clinical and age groups signifies that the proposed algorithms were adequately sensitive to detect hippocampal volume variations related with earlier Alzheimer's disease and aging.

By utilizing a subject-specific tissue probabilistic atlas produced from longitudinal data, Feng Shi et al. [22] have offered a framework for presenting neonatal brain tissue segmentation. Proposed method has received the benefit of longitudinal imaging study in their system, i.e., by means of the segmentation outcomes of the images obtained at a late time to direct the segmentation of the images obtained at neonatal stage. Compared to the two population-based atlases the testing outcomes revealed that the subject-specific atlas has better performance. And moreover the proposed algorithm attained comparable performance as manual raters in neonate brain image segmentation. By attaining optimal segmentation results in a broad range of 0.3–0.6, the atlas sharpness parameter has been shown robust appearance. For the selection of late time-point image, the segmentation accuracy remains alike when the atlas was developed by either one-year-old or two-year-old image.

Juin-Der Lee et al. [23] have offered the most statistical segmentation methods in the literature and have presumed that either the intensity allocation of every tissue variety was Gaussian, or the logarithmic transformation of the raw intensity was Gaussian. As an alternative of setting up further classes to model "mixels," they proposed a power transformation approach to carry out automatic segmentation of brain MR images into CSF, GM, and WM. By instinct it was understandable that the familiar Box-Cox power transformation model was capable to give a statistically significant and helpful solution to proposed difficulty. To include both Gaussian intensity distributions as well as non-Gaussian

distributions, the shape parameter utilized to widen the traditional Gaussian mixture models. And the parameters can be expected by means of the EM algorithm. They authorized the approach against four real and simulated datasets of normal brains from the IBSR and BrainWeb. Testing's on real data from the IBSR have shown that compared with other techniques utilized presently, the proposed approach attains higher Jaccard indexes. The power transformation approach maintains the simplicity of the Gaussian mixtures, and in addition it has the prospective to simplify the multivariate versions personalized for segmentation by means of multi-modality images.

Dalila Cherifi et al. [24] have illustrated normal tissue's recognition than tumor extraction (applied for GBM and MS diseases). To detach the abnormal tissues they have offered brain recognition techniques. Based on thresholding utilized for tumor extraction (GBM and MS diseases) they have proposed and applied the technique. They have originated that the local thresholding provides a good outcomes comparing with the others. They have accomplished that when they merge median filter, local thresholding and post processing in such a way that the resultant algorithm is tougher. For tissue recognition and tumor extraction they have executed categorization based on EM segmentation technique. Comparing with thresholding particularly for detecting the small regions of necrotizing tissue which was inside Anaplastic cells (pseudo-Palisading necrosis) for GBM tissue, proposed technique provided us better outcomes; and it mainly for the reason that of parameters that utilized in this algorithm.

Nagesh Vadaparthi et al. [25] have offered a paper in which particular cases like Acoustic neuroma, it was presumed that there was an option of hearing loss, dizziness and other symptoms associated to brain. Surgery can cure various acoustic neuromas. Hence, it was required to segment the image more correctly, which assisted to recognize the damaged tissues to be repaired and can be corrected by surgery. And so a new novel segmentation algorithm based on Skew Gaussian distribution was proposed in proposed paper, which assisted to recognize the tissues more correctly. Because of the basic structure of Skew Gaussian distribution it was suitable for symmetric and asymmetric distribution. The performance evaluation was succeeded by utilizing quality metrics. The outcomes proved that, proposed developed algorithm outperforms the existing algorithm. Various models were exploited to recognize the diseases, although due to the utility of non-ionizing radiation, MRI brain segmentation has achieved popularity over the other models.

Usually noise is generated by equipments, environment and also the performance of operator in MRI Brain images which creates serious incorrectness in the outcome of Segmentation procedure. Several of the unverified techniques did not deal with the intensity and in-homogeneity artifacts. And also the managed techniques undergo with the shortcomings of manual intervention for providing a priori notification. Pathological tissues demonstrate inconsistency in their structures. The shape of these tissues is deformable, the location of them across the patients may differ extensively, and also their characteristics of texture and intensity might vary. These difficulties of the existing schemes are generally un-solvable. A few techniques do not consider the large deformation of brain structures. The practice of brain atlas might show the way to false learning, though such deformations occurs.

3 Proposed Methodology

Initially, the input BMRI images are given to our proposed work NFBS. The feature sets are extracted from these input images. From these feature sets, the images are classified into two kinds of tissues normal and abnormal using the Neuro-Fuzzy classifier. Then the normal tissues are segmented using various techniques. The normal tissues that are segmented are White Matter (WM), Gray Matter (GM) and Cerebro-Spinal Fluid (CSF). The proposed work is illustrated in Fig. 1.

1.1 Phases of NFBS

For our proposed method, to segment the BMRI images effectively, the three phases are presented which are as follows:

I. Feature set Extraction
II. Neuro-Fuzzy classifier based Classification
III. Classified tissue's Segmentation

3.1.1 Phase I: Extraction of extensive feature sets

In order to classify the given Brain MRI images, the features from these MRI images are initially extracted. In our work, the statistical features such as Energy, Entropy, Homogeneity, Contrast and Correlation are extracted from these input BMRI images.

Energy

Energy is also called as uniformity. Within [0,1] the range of energy is presented. The value of energy for a constant image is 1. The equation for finding energy is,

$$E_g = \sum_{i,j} p(i,j)^2 \tag{1}$$

where, $p(i,j)$ is the pixel value at the point i,j of the BMRI image of size $M \times N$.

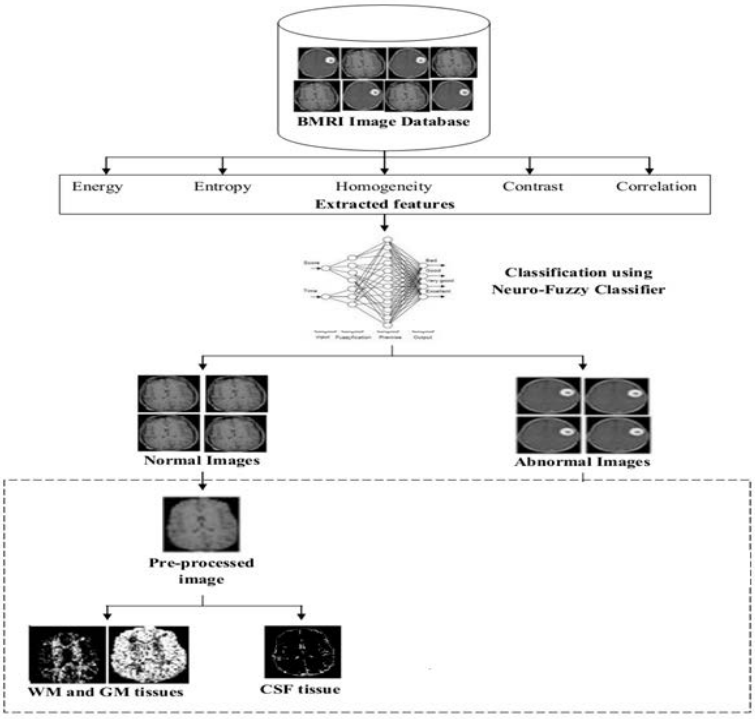

Figure 1: Proposed NFBS block diagram

Entropy

Entropy helps to characterize the texture of the BMRI image and to find out the distribution variation in a region of the image. Entropy is calculated as follows,

$$E_p = \sum_{k=0}^{G-1} Pb_k \left(\log_2 Pb_k\right) \tag{2}$$

where, Pb_k is the probability of kth gray level and the kth gray level is calculated using $\frac{Z_k}{M \times N}$. In this, Z_k represents the total number of pixels in the image with kth gray levels. G indicates the total number of gray levels.

Homogeneity

Homogeneity provides the closeness of the elements. It has the range of [0,1]. It is computed as,

$$H_m = \sum_{i,j} \frac{p(i,j)}{1+|i-j|} \tag{3}$$

Contrast

The intensity contrast between a pixel of an image and the neighbor of that pixel throughout the whole image is defined by this Contrast measure. For a constant image, the contrast is set as 0. It is specified as,

$$C_n = \sum_{i,j} |i-j|^2 \, p(i,j) \tag{4}$$

Correlation

It tells about the correlation between a pixel and its neighbor over the whole BMRI image. Its range is [-1,1]. If an image has the value of correlation as 1 means, then it indicates the perfectly positively correlated image and if it is -1 means, then it shows the image is perfectly negatively correlated. The correlation of a constant image is not a number.

$$C_r = \sum_{i,j} \frac{(i-\mu_i)\,(j-\mu_j)\,p(i,j)}{\sigma_i\,\sigma_j} \tag{5}$$

where, μ_i, μ_j, σ_i, σ_j are the means and standard deviations of the partial probability density functions P_i, P_j.

Mean, $$\mu = \frac{1}{MN}\sum_{i=1}^{M}\sum_{j=1}^{N} p(i,j)^2$$

Standard Deviation, $$\sigma = \sqrt{\frac{1}{MN}\sum_{i=1}^{M}\sum_{j=1}^{N}(p(i,j)-\mu)^2}$$

Variance, $$Var = \sqrt{\sigma}$$

Thus the feature correlation of the images is calculated using the mean and variance equations. Hence, all the feature sets $E_g, E_p, H_m, C_n,$ *and* C_r are extracted from the input BMRI images directly.

3.1.2 Phase II: Classification using Neuro-fuzzy classifier

The BMRI images are classified using the Neuro-Fuzzy classifier. The extracted features $E_g, E_p, H_m, C_n,$ *and* C_r are given as the input to the Neuro-Fuzzy Classifier for classifying all the given BMRI images into 2 classes such as Normal BMRI images and Abnormal BMRI images. The Neuro-fuzzy system has a three-layered architectural design; the following diagram fig. 2 shows the basic structure of the neuro-fuzzy classifier system. Neuro-Fuzzy classifier is a fuzzy based system that is trained by a learning algorithm derived from Neural Networks. The learning algorithm only performs on the local information and provides the local modifications in the fuzzy system. In general, a neuro-fuzzy system generates very powerful solutions instead of using the system components individually.

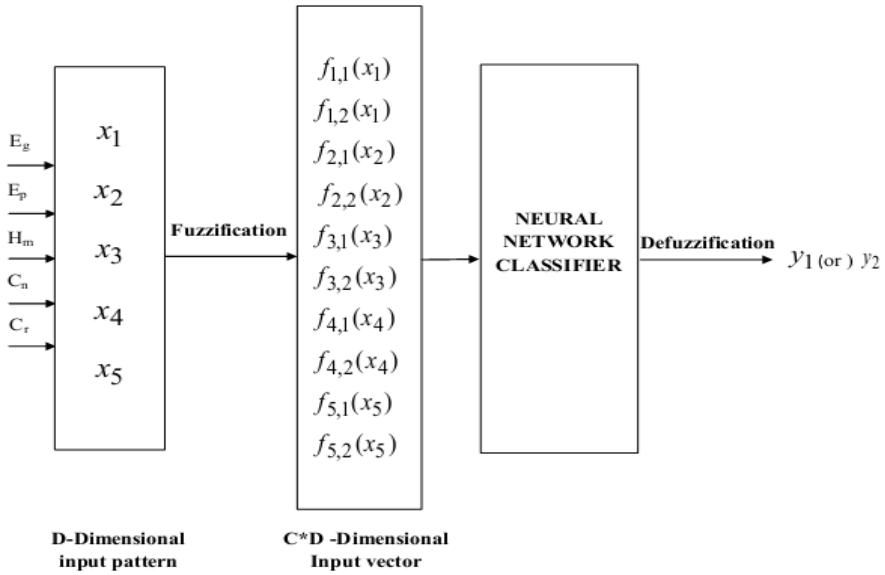

Figure 2: Architecture of Neuro-Fuzzy classifier

Fuzzification

The input values are the extracted features $E_g, E_p, H_m, C_n,$ *and* C_r, which are received by the system as the input and then these input feature values are fuzzified using membership functions (MF) that facilitates the membership of each features to different classes. The hidden and inter-related information are extracted from the features to the classes through the MF, which leads to get more accuracy of the classification phase using Neuro-fuzzy classifier. The membership matrix comprises with 5 rows and 2 columns, in which the number of rows is equal to the number of features and the number of columns is equal to the number of classes.

The membership matrix $f_{d,c}(x_d)$ produced, describes the degree of belonging of different features (D) to different classes (C).

where, x_d - d^{th} feature value of pattern X .

d - 1, 2, …, D, here number of features is 5.

c - 1, 2, …, C, here number of classes is 2.

The representation of pattern is as follows,

$$X = [x_1, x_2, x_3, x_4, x_5]^T \tag{6}$$

In this a π–type MF is used as the membership function to classify the images. It is a bounded function having a shape similar to that of the Gaussian/exponential function. The π–type MF has fuzzifier (m) as the parameter that can be tuned corresponding to the need of the problem. This controls the generalization capability by choosing a proper value of the fuzzifier m and gives more flexibility for

classifying the images. The steepness of the Gaussian function is controlled by varying the fuzzifier value, which is defined as follows,

$$\pi(X;a,r,b) = \begin{cases} 0, & if\ X \le a \\ 2^{m-1}\left[\dfrac{(X-a)}{(r-a)}\right]^m, & if\ a < X \le p \\ 1-2^{m-1}\left[\dfrac{(r-X)}{(r-a)}\right]^m, & if\ p < X \le r \\ 2^{m-1}\left[\dfrac{(X-r)}{(b-r)}\right]^m, & if\ r < X \le q \\ 1-2^{m-1}\left[\dfrac{(b-X)}{(b-r)}\right]^m, & if\ q < X < b \\ 0, & if\ X \ge b \end{cases} \quad (7)$$

The value r is the center of MF, and $r = \dfrac{(p+q)}{2}$, in which p and q are the two crossover points. The membership function after the fuzzification process is expressed for a pattern X as follows,

$$F(X) = \begin{bmatrix} f_{1,1}(x_1) & f_{1,2}(x_1) \\ f_{2,1}(x_2) & f_{2,2}(x_2) \\ f_{3,1}(x_3) & f_{3,2}(x_3) \\ f_{4,1}(x_4) & f_{4,2}(x_4) \\ f_{5,1}(x_5) & f_{5,2}(x_5) \end{bmatrix} \quad (8)$$

All rows and columns in the membership matrix are cascaded and converted into a vector by this cascading. This generated vector V_i is given as the input to the Neural Network (NN).

Neural Network

In this, Feed Forward Multi-layer Perceptron classifier is used which has three layers such as input layer, hidden layer and output layer.

The total number of input nodes of the NN is equal to the product of the number of features and classes. In this paper the product of 5 features and 2 classes is 10, which is the number of input nodes of the NN. The total number of output nodes from the NN is same as that of the number of classes, and here 2 output nodes are generated from the NN. The total number of hidden nodes is equal to the square root of the product, of the number of input nodes and output nodes. The structure for the Neural Network is given in fig.3.

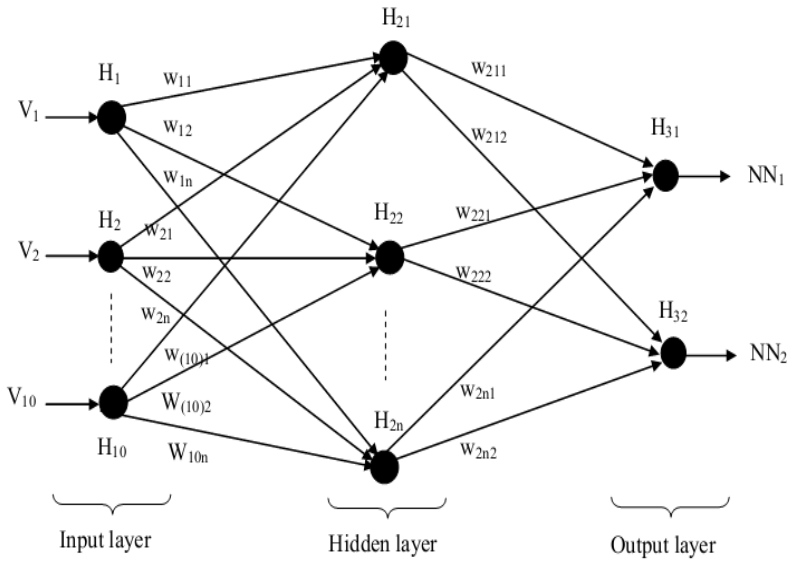

Figure 3: Neural Network classifier

Defuzzification

Then the defuzzification process is carried out on the output nodes of NN, by performing a MAX (maximum) operation. The output is a single value, y_1 or y_2 for a given BMRI image. From this value, we can able to classify whether the given input BMRI image is normal or abnormal.

3.1.3 Phase-III: Segmentation of classified tissues

Utilizing Neuro-fuzzy classifier the BMRI images are classified and after that the images are comprised only in any of the two different images normal and abnormal or pathological images. From the normal images, the normal tissues like White Matter (WM), Gray Matter (GM), and Cerebro-Spinal Fluid (CSF) are segmented. Prior to the segmenting of these normal images, one of the procedure named as pre-processing is carried out only on the normal images, not on the abnormal images. Almost it is very simple to place the CSF tissue of the normal BMRI images in the area that surrounds the cortex by use of the pre-processing technique. For segmenting the tissues, the segmentation stage is sustained after that on both the classified images efficiently.

Pre-processing of normal BMRI images

In order to apply the Morphological operations [26] on the images, firstly, the classified BMRI normal images are transformed into gray scale images. Next, the brain cortex is stripped in the gray scale image by means of Region Based Binary Mask Extraction procedure. In general, the brain cortex can be observed as the ring around the brain tissues in BMRI images. The Skull Stripping technique is used for these images to eradicate the ring that surrounds the brain tissues. Utilizing Skull Stripping technique, normal BMRI image is attained after the pre-processing is denoted as I_{SS} .

BMRI image tissue's Segmentation

The segmentation of the tissues of both the normal and abnormal images takes place after the normal BMRI images gets pre-processed. In the normal BMRI images, the normal tissues namely WM, GM and CSF are used for segmentation. Herein, WM and GM are segmented by means of Gradient technique and CSF is segmented by use of Orthogonal Polynomial Transform (OPT) technique.

Segmentation of WM and GM

For segmenting the White Matters and Gray Matters, the pre-processed skull stripped image I_{SS} is subjected into gradient technique. The Gaussian Convolution filter that utilized in this technique makes the image I_{SS} into smoothed image I_S. After that, the smoothed image I_S is subjected with Gradient operation. The gradient of two variables x and y are specified as follow:

$$\nabla I_S(x,y) = \frac{\partial I_S}{\partial x}\hat{e} + \frac{\partial I_S}{\partial y}\hat{f} \tag{9}$$

The gradient values are useful to mark the current edges in the image that are specified in the following equations (10) and (11).

$$S = x_{(e)}{}^2 + y_{(f)}{}^2 \tag{10}$$

$$EM = \frac{1}{(1+S)} \tag{11}$$

The process of Binarization is then carried out on the edge marked image EM. In this Binarization procedure, the value of gray level of every pixel in EM image is estimated by means of a global threshold value T_g. The resultant binarized image after the Binarization process is I_B.

By use of Morphological Opening and Closing operation, the small holes and small objects from the image I_B is eliminated. Currently, in our work, the WM and GM normal tissues of normal BMRI images are segmented by means of the intensity values.

$$I_{WG} = \begin{cases} WM, & if\ I_{B_i} = 1 \\ GM, & if\ I_{B_i} = 0 \end{cases} \tag{12}$$

The exacting part is segmented into White Matter, if the intensity value of the image part is one and then it is considered as Gray Matter part, if the intensity value is zero, and subsequently the images are segmented according to the equation (12).

Segmentation of CSF

CSF tissue from the image I_{SS} is segmented by Orthogonal Polynomial Transform (OPT) using the formula given below:

$$I_{CSF} = Sin\left(\frac{I_{SS_{(i)}}{}^{3}}{100}\right)^{2} + \left(0.05 * rand(|I_{SS}|)\right) \quad (13)$$

At present, the CSF tissue I_{CSF} from the normal image is segmented efficiently. Therefore, the normal tissues WM, GM and CSF are segmented from the pre-processed image I_{SS} .

4 Results and Discussions

Our proposed NFBS for the effective segmentation of normal tissues is implemented using the MATLAB platform on the Brain MRI images from the dataset. The data set description is given below in detail.

4.2 Dataset Description:

BrainWeb dataset is utilized with different BMRI images for our proposed work. Based on standard tissue segmentation mask, BrainWeb datasets give MRI brain images with unreliable image quality. The datasets are too based on an anatomical structure of a normal brain, which results from the tasks of registering and preprocessing of 27 scans from the same individual with segmentation. Different kinds of tissues are well identified in this dataset, both the types of tissue memberships “fuzzy” and “crisp” are assigned to each voxel. The sample Brain MRI images from the BrainWeb data set are specified in the fig. 4 given below.

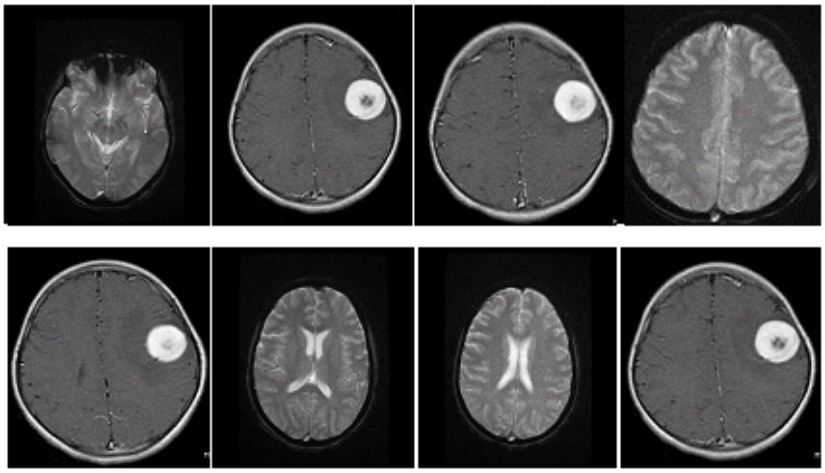

Figure 4: Sample BMRI images from dataset.

Our proposed work is estimated by means of 23 BrainWeb MRI images. 9 images are normal and the remaining 14 images are abnormal among 23 MRI images. At first, the BMRI images from this dataset is taken and offered to the procedure of our proposed NFBIS. Five of the statistical characteristics from these BMRI images are extracted. Then for the categorization of images these extracted features are utilized. In order to categorize the particular images into normal and abnormal images, Neuro-Fuzzy classifier is utilized as the classifier in this proposed NFBIS work.

The classified normal and abnormal images are specified in the fig. 5 given below.

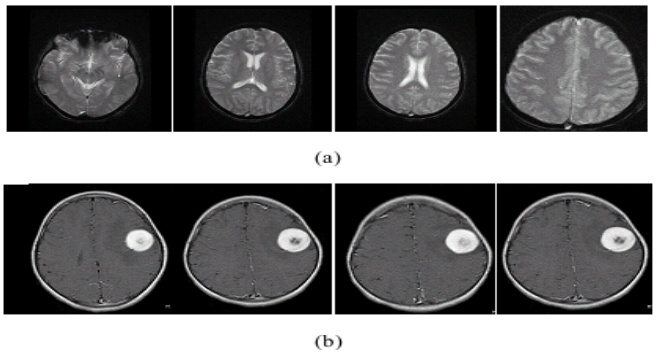

Figure 5: Normal and Abnormal Images

Subsequently, the Segmentation is performed on the classified BMRI images. The first step in the segmentation of normal images is the Skull Stripping Method which is carried out on the classified images by means of pre-processing. The normal image after pre-processing is specified in fig. 6 given below:

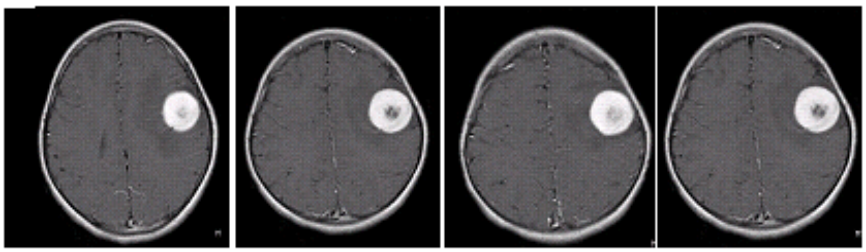

Fig. 6: Normal BMRI images after pre-processing

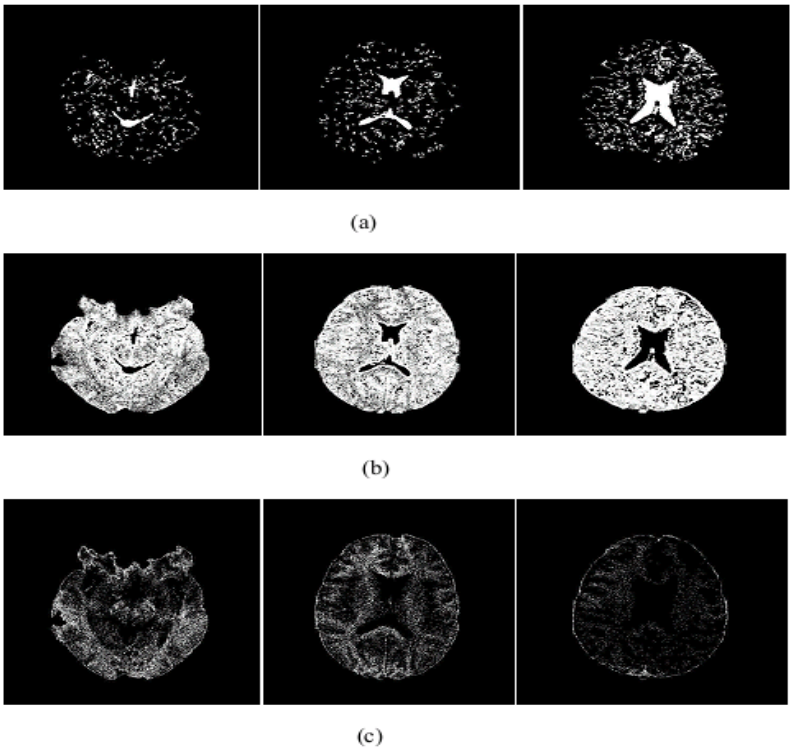

Figure 7: Segmentation of normal images. (a) WM (b) GM (c) CSF

The segmentation is performed on these pre-processed images, following the pre-processing of normal images. The normal tissues of these images are White Matter, Gray Matter and Cerebro-Spinal Fluid. WM and GM segmentation is carried out by utilizing Gradient technique and the segmentation of CSF tissue is made by utilizing OPT technique, respectively. The images of normal tissues subsequent to the segmentation procedure are specified in the fig. 7 given below.

4.3 Performance Evaluation

By utilizing the performance measures namely False Positive Rate, False Negative Rate, Sensitivity, Specificity and Accuracy, the performance of the system is estimated. The basic count values such as True Positive (TP), True Negative (TN), False Positive (FP) and False Negative (FN) are used by these measures. Both the categorization of normal and abnormal images and the segmentation efficiency of every normal tissue is examined by our proposed work, which are clarified in detail in the next sections.

4.3.1 Results of Classification Evaluation

The BrainWeb images include both the normal and abnormal images in our work. These images are categorized into normal and abnormal individually by the procedure of Neuro-Fuzzy classifier. The efficiency of the classifier is examined by the metrics False Positive Rate, False Negative Rate, Sensitivity, Specificity and Accuracy. The explanation of TP, TN, FP, FN values for the categorization of normal and abnormal images is specified in the table I given below.

Table I: Description of TP, TN, FP, FN values for the classification of normal and abnormal images

Description	Classified as normal image	Classified as abnormal image
Actually normal image	TP	FN
Actually abnormal image	FP	TN

False Positive Rate (FPR)

The percentage of cases where an image was classified to normal images, but in fact it did not.

$$FPR = \frac{FP}{FP + TN} \tag{16}$$

False Negative Rate (FNR)

The percentage of cases where an image was classified to abnormal images, but in fact it did.

$$FNR = \frac{FN}{FN + TP} \tag{17}$$

Sensitivity

The proportion of actual positives which are correctly identified is the measure of the sensitivity. It relates to the ability of test to identify positive results.

$$Sensitivity = \frac{Number\ of\ true\ positives}{Number\ of\ true\ positives + Number\ of\ false\ negatives} \times 100 \quad (18)$$

Specificity

The proportion of negatives which are correctly identified is the measure of the specificity. It relates to the ability of test to identify negative results.

$$Specificity = \frac{Number\ of\ true\ negatives}{Number\ of\ true\ negatives + Number\ of\ false\ positives} \times 100 \quad (19)$$

Accuracy

We can compute the measure of accuracy from the measures of sensitivity and specificity as specified below.

$$Accuracy = \frac{TP + TN}{TP + TN + FP + FN} \times 100 \quad (20)$$

Above eqns. (16-20) are as well appropriate for finding the efficiency of segmentation of the tissues WM, GM and CSF.

The subsequent table II explains the categorization efficiency outcomes for the normal and abnormal images with various metric values.

Table II: Effectiveness of classification results using Neuro-Fuzzy classifier for the normal and abnormal images

Metrics	Values
TP	8
TN	14
FP	0
FN	1
FPR	0
FNR	6.667
Sensitivity	88.9%
Specificity	100%
Accuracy	95.65%

In our proposed work, we can establish the efficiency of categorization for the normal and abnormal images by means of Neuro-Fuzzy classifier from the above table II. False Positive Rate and False Negative Rate values are 0 and 6.667, respectively, which explains that our proposed work has low error rate in categorizing images. Properly categorized percentages of normal images are specified by Sensitivity. Neuro-fuzzy classifier offers very high (88.9%) values for the metric sensitivity, in which only one of the normal image is categorized as abnormal. In addition, Specificity is another metric that specifies the percentage of abnormal images properly categorized. The classifier provides 100% specificity rate by categorizing the entire actual abnormal images into abnormal images in our work. The highest value in sensitivity and specificity and also the lowest value in the error rates False Positive Rate and False Negative Rate open a mode to raise the categorization correctness outcome with the value 95.65%. Therefore we can show that in proposed work categorization of BMRI BrainWeb images offers high classification accuracy.

4.3.2 Results of Segmentation Evaluation

Every normal image is segmented for the WM, GM and CSF tissues after the categorization. The efficiency of this segmentation of all the tissues are examined by the metrics False Positive Rate, False Negative Rate, Sensitivity, Specificity and Accuracy as specified in the eqns. (16-20). The explanation of TP, TN, FP, FN values for the segmentation of normal image tissues is specified in the following table III.

Table III: Description of TP, TN, FP and FN values for the segmentation of normal images

Description	Segmented as WM tissue	Segmented as not a WM tissue
Actually WM tissue	TP	FN
Actually not a WM tissue	FP	TN

Each image is taking the test either has or does not have the tissue (WM, GM, CSF). The test outcome can be positive (predicting that the image has the particular tissue) or negative (predicting that the image does not have the particular tissue).

Three types of tissues are offered such as WM, GM and CSF in normal images. At first, these three tissues are segmented from the normal images and the segmentation efficiency values are tabularized in the following table IV with different estimation metrics of different images.

Table IV: WM segmentation results for various images

Images	TP	TN	FP	FN	FPR	FNR	Specificity (in %)	Sensitivity (in %)	Accuracy (in %)
Img 1	693	253393	8058	5166	0.0308870	0.883860	96.9179	11.8279	95.0529348
Img 2	1457	239434	21253	3519	0.0810368	0.704334	91.8473	29.2805	90.6754046
Img 3	693	256043	5408	7871	0.0209167	0.919750	97.9315	8.09201	95.0821251
Img 4	1215	252815	8114	6701	0.0314603	0.850268	96.8903	15.3486	94.4893898
Img 5	6512	227682	27950	10063	0.1104886	0.622534	89.0663	39.2880	86.0352599

Segmentation of White matter gives very good accuracy outcomes. The subsequent fig. 8 explains the corresponding graph for the values in table IV.

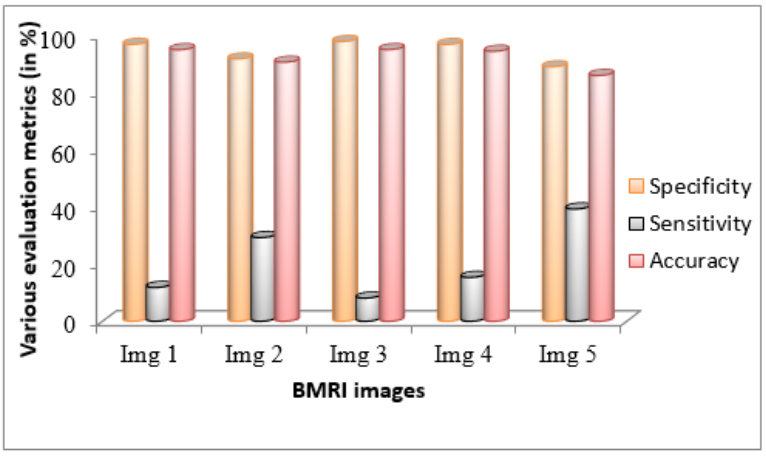

Figure 8: Sensitivity, Specificity and Accuracy results of WM segmentation

We can attain the WM segmentation efficiency from the above table IV and its corresponding graph in fig. 8. The FPR and FNR values are very low for our proposed work. These low values offer a way to raise the segmentation accuracy. The specificity for the image 3 is very high (97.93%) as compared with the other four images. Image 1, 2, 4 and 5 contain 96.91%, 91.84%, 96.89% and 89.06% of specificity metrics, respectively. These values are also high for our proposed NFBIS, which guides to make high accuracy of segmentation of WM tissue. But the sensitivity values for these five images are low values of 11.82%, 29.28%, 8.09%, 15.34% and 39.28% for images 1, 2, 3, 4 and 5, respectively. Though these values are low, it does not change the segmentation accuracy of WM tissue. Therefore, we can obtain very good accuracy values of 95.05%, 90.675%, 95.08%, 94.48% and 86.035% for the images 1, 2, 3, 4 and 5, respectively. Generally, our proposed work gives 92.264% of accuracy for the WM tissue segmentation.

The table V shows the GM segmentation outcomes with different images.

Table V: GM segmentation results for various images

Images	TP	TN	FP	FN	FPR	FNR	Specificity (in %)	Sensitivity (in %)	Accuracy (in %)
Img 1	29279	211105	21760	24172	0.0903	0.451690	90.655	54.777	83.9575
Img 2	13731	234678	13735	34343	0.0514	0.714504	94.470	28.562	83.7841
Img 3	55115	188526	18503	9537	0.0844	0.147501	91.062	85.248	89.6790
Img 4	29685	221767	10692	36912	0.0470	0.555322	95.400	44.574	84.0819
Img 5	32333	217357	12454	30587	0.0565	0.489560	94.580	51.387	85.2967

Corresponding graph of table V is designed in Fig. 9 with different BMRI images for the GM segmentation. The evaluation outcome illustrates whether our proposed work is good or not.

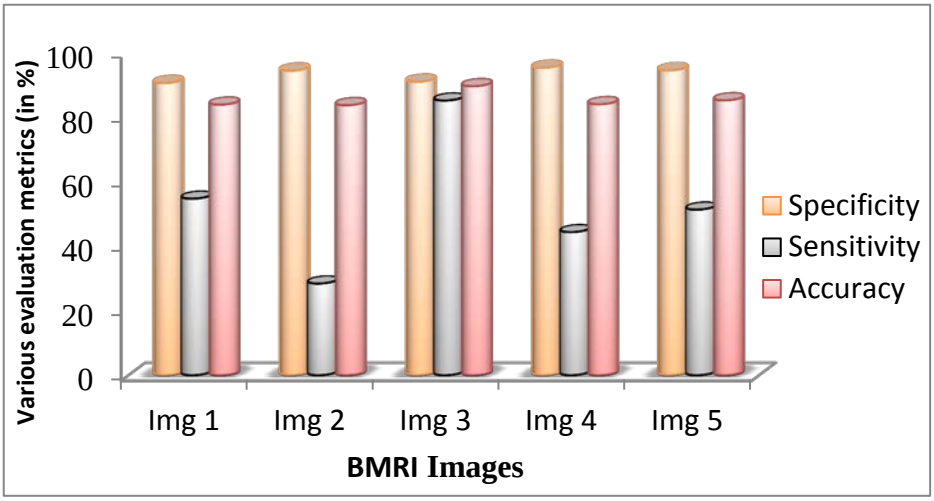

Figure 9: Sensitivity, Specificity and Accuracy results of GM segmentation

We can attain the GM segmentation efficiency from the table V and Fig. 9. The FPR and FNR values are very low for the GM segmentation of our proposed work. The segmentation accuracy can be improved with the help of these low values of FPR and FNR. The specificity for the Images 1, 2, 3, 4 and 5 have 90.65%, 94.47%, 91.06%, 95.4% and 94.58% of specificity metric, respectively. These values are high for our proposed NFBIS, which guides to create high accuracy of segmentation of GM tissue. However the

sensitivity values for these five images are medium values (not very low) of 54.77%, 28.56%, 85.24%, 44.57% and 51.38% for images 1, 2, 3, 4 and 5, respectively. Although these values are not high, it also does not change the segmentation accuracy of GM tissue. Hence, we can achieve good accuracy values of 83.95%, 83.78%, 89.67%, 84.08% and 85.29% for the images 1, 2, 3, 4 and 5, respectively. Overall, our proposed work grants 85.359% of accuracy for the GM tissue segmentation. Anyway, it is good outcome for our proposed work.

The table VI illustrates the CSF segmentation outcomes with different images.

Table VI: CSF segmentation results for various images

Images	TP	TN	FP	FN	FPR	FNR	Specificity (in %)	Sensitivity (in %)	Accuracy (in %)
Img 1	787	256986	4371	16587	0.0167280	0.951058	98.3275	4.5297571	92.48092
Img 2	2512	254993	4639	31817	0.0191407	0.928281	98.2132	7.3174284	87.59835
Img 3	192	260102	1850	10867	0.0070851	0.982321	99.2937	1.7361425	95.34194
Img 4	541	257445	4158	10166	0.0155631	0.944853	98.4105	5.0527692	94.73981
Img 5	29	260976	1139	1786	0.0043074	0.985582	99.5654	1.5977961	98.89175

Corresponding graph of table VI is designed in Fig. 1 with different BMRI images for the CSF segmentation. The evaluation outcomes illustrates whether our proposed work is good or not.

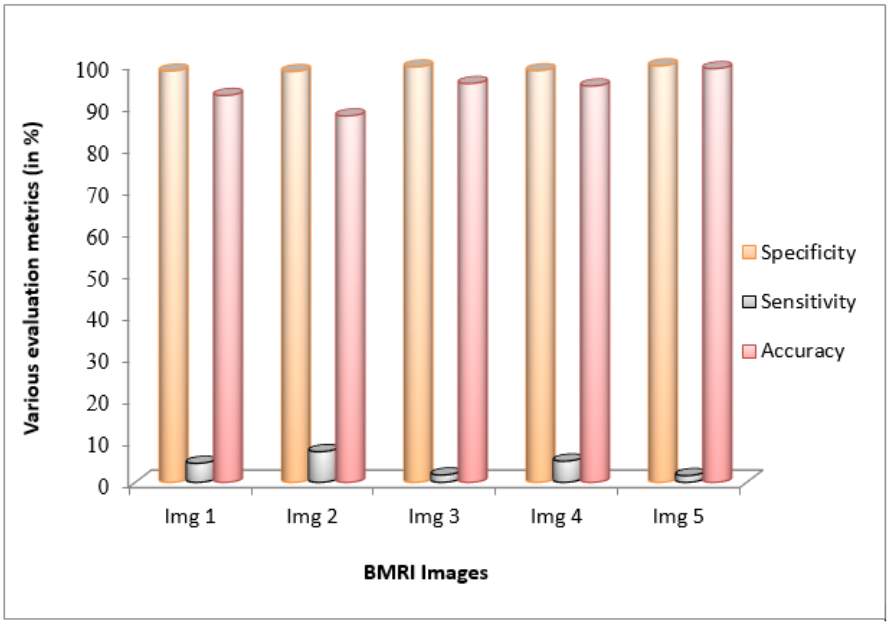

Figure 10: Sensitivity, Specificity and Accuracy results of CSF segmentation

The segmentation of CSF outcomes is attained with diverse evaluation metric values. From the outcomes, it is clearly recognized that our proposed work efficiently segments the CSF tissues by presenting 93.81% of accuracy on average. This development in the accuracy of CSF segmentation is achieved by the lower error rate values of FPR and FNR. Also, the specificity values of each image are very high by assisting 98.32%, 98.21%, 99.29%, 98.41% and 99.56% for image 1, 2, 3, 4, and 5, respectively. However, the sensitivity values are very low for our work. Even these values are low, by no

means it lessen the outcomes of segmentation accuracy values. Our proposed work offers low value for the FPR and FNR additionally with this. Moreover it makes the segmentation accuracy of CSF tissue in our proposed work to be improved.

4.3.3 Comparative Analysis for our proposed work with the existing works

For the categorization of normal and abnormal brain images our proposed work makes use of Neuro-Fuzzy classifier. We can establish that our proposed work helps to attain very good accuracy for the categorization of images utilizing Neuro-Fuzzy classifier from the above sections 4.2.1 and 4.2.2. And also we can establish this categorization accuracy outcome by comparing other classifiers. We have utilized Artificial Neural Network and Fuzzy C-Means for our comparison in our work. The comparison outcomes are presented in the following table VII.

Table VII: Comparison results for the image classification with other classifiers

Metrics	Fuzzy C-Means	Artificial Neural Network	Neuro-Fuzzy in our proposed work
TP	0	1	8
TN	14	9	14
FP	0	5	0
FN	9	8	1
FPR	0	0.3571	0
FNR	0.3913	0.4706	6.667
Sensitivity (in %)	0	11.11	88.9
Specificity (in %)	100	64.29	100
Accuracy (in %)	60.87	43.48	95.65

Below specified fig. 11 explains the comparison outcomes of the classifiers for the BMRI image categorization with different metrics. The improved accuracy outcomes of categorization of BMRI images into normal and abnormal images are presented by our proposed work. In comparison with the classifier Neuro-Fuzzy, both the Fuzzy C-Means and Artificial Neural Networks gives very less accuracy values for the categorization of images. The sensitivity for the Fuzzy C-Means and Artificial Neural Networks are 0% and 11.11%, which is low in compared with our classifier, Neuro-Fuzzy 88.9%. The specificity is 100% for our classifier and for the Fuzzy C-means classifier. However the accuracy is 95.65% for our Neuro-fuzzy classifier and the fuzzy C-means and ANN contain only low categorization accuracy results of 60.87% and 43.48%, respectively. From these outcomes, it is known that by means of Neuro-Fuzzy classifier in our work provides very good for the categorization purpose as it gives improved accuracy outcomes. Therefore, our work shows that it is worth for the categorization and segmentation of BMRI images.

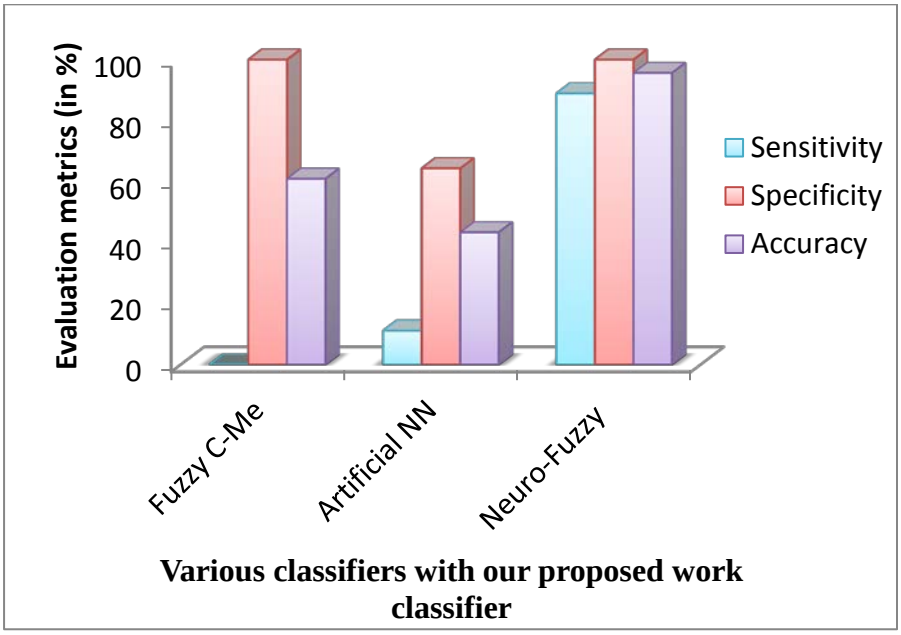

Figure 11: Comparison graph for the image classification with other classifiers

5 CONCLUSION

A Neuro Fuzzy based BMRI image segmentation technique with three phases – Feature Extraction, Classification and Segmentation was proposed in this paper. The features from the BMRI images were extracted and then specified to the Neuro-Fuzzy classifier. The classification of normal and abnormal images was made by this Neuro-Fuzzy classifier and these classified images were segmented efficiently by our proposed method. The testing was performed with the BrainWeb images dataset. The performance measures False Positive Rate, False Negative Rate, sensitivity, specificity and accuracy were evaluated for our proposed method. The testing was prepared for establishing the accuracy of both the classification of images into normal and abnormal and segmentation of every normal tissue. The efficiency of the classification of images is very high by presenting very good accuracy outcomes and also the segmentation of each tissue offers very accurate outcomes. From the outcomes, we have showed that the Neuro-Fuzzy classifier utilized in our proposed work outperforms the other classifiers Fuzzy C-Means and ANN by facilitated very good accuracy of 95.65% in categorizing the images into normal and abnormal.

REFERENCES

[1]. P. Hagmann, J.P. Thiran, L. Jonasson, "DTI mapping of human brain connectivity: statistical fibre tracking and virtual dissection", NeuroImage, 2003.

[2]. M.C. Davidson, K. M. Thomas. and B. J. Casey, "Imaging the developing brain with fMRI", Mental Retardation and developmental disabilities research reviews, 2003.

[3]. V. A. Grau, U. J. Mewes, M. Alcaniz, "Improved watershed transform for medical image segmentation using prior information", IEEE Trans. on Medical Imaging, 2004, 23(4): 447-458

[4]. H Lv., K. H. Yuan, S. L. Bao, "An eSnake model for medical imaging segmentation", Progress in Natural Science, 2005.

[5]. D. L. Pham and J. L. Prince, "Adaptive fuzzy segmentation of magnetic resonance images," IEEE Trans. Med. Imag., 1999.

[6]. A. F. Goldszal, C. Davatzikos, D. L. Pham, M. X. H. Yan, et al, "An image processing system for qualitative and quantitative volumetric analysis of brain images," J. Comput. Assist. Tomogra., 1998.

[7]. Arnold J.B., Liow, J.-S., Schaper, K.A., et al., "Qualitative and quantitative evaluation of six algorithms for correcting intensity nonuniformity effects". NeuroImage, 2001.

[8]. R. Moller., R. Zeipelt. "Automatic segmentation of 3D-MRI data using a genetic algorithm, Medical Imaging and Augmented Reality", 2001. Proceedings. International Workshop on, 10-12 June 2001:278 – 281.

[9]. W. M.Wells, III,W. E. L. Grimson, R. Kikinis. "Adaptive segmentation of MRI data", IEEE Trans. Medical Imaging , 1996.

[10]. J. C. Bezdek, L.O. Hall, L. P. Clarke, "Review of MR image segmentation techniques using pattern recognition," Med. Phys., vol. 20, No. 4, pp. 1033-1048, 1993.

[11]. Suetens, E. Bellon, D. Vandermeulen, M. Smet, G. Marchal, J. Nuyts, L. Mortelman, "Image segmentation: methods and applications in diagnostic radiology and nuclear medicine," European Journal of Radiology, vol. 17, pp. 14-21, 1993.

[12]. A. Goshtasby, D. A. Turner, "Segmentation of Cardiac Cine MR Images for extraction of right and left ventricular chambers," IEEE sTrans. Med. Imag., vol. 14, No. 1, pp. 56-64, 1995.

[13]. D. Brzakovic, X. M. Luo, P. Brzakovic, "An approach to automated detection of tumors in mammograms," IEEE Trans. Med. Imag., vol. 9, No. 3, pp. 233-241, 1990.

[14]. J. F. Brenner, J. M. Lester, W.D. Selles, "Scene segmentation in automated histopathology: techniques evolved from cytology automation," Pattern Recognition, vol. 13, pp. 65-77, 1981.

[15]. K. Lim, A. Pfefferbaum, "Segmentation of MR brain images into cerebrospinal fl¬uid spaces, white and gray matter," J. Comput. Assist. Tomogr., vol. 13, pp. 588-593, 1989.

[16]. Zhang Y, Brady M, Smith S. "Segmentation of brain MR images through a hidden Markov random field model and expectation-maximization algorithm,". IEEE Trans Med. Imag., pp. 45–57, 2001.

[17]. L. Lemieux, G. Hagemann, K. Krakow, and F. G. Woermann, "Fast, accurate, and reproducible automatic segmentation of the brain in T1-weighted volume MRI data, "Magn. Reson. Med., vol. 42, pp. 127–135, 1999.

[18]. R. Pohle and K. D. Toennies, "Segmentation of medical images using adaptive region growing," Proc. SPIE— Med. Imag., vol. 4322, pp. 1337–1346, 2001.

[19]. S. Shen, W Sandham, M. Grant and A. Ster, "MRI Fuzzy Segmentation of Brain Tissue Using Neighborhood Attraction with Neural Network Optimization", IEEE Trans. On Information Technologyis Biomedicine, vol. 9, No. 3, 2005.

[20]. Arnaldo Mayer and Hayit Greenspan, "An Adaptive Mean-Shift Framework for MRI Brain Segmentation", IEEE Transactions On Medical Imaging, Vol. 28, No. 8, August 2009.

[21]. Mert R. Sabuncu, B.T. Thomas Yeo, Koen Van Leemput, Bruce Fischl and Polina Golland, "A Generative Model for Image Segmentation Based on Label Fusion", Ieee Transactions On Medical Imaging, 2009.

[22]. Feng Shi, Yong Fan, Songyuan Tang, John H. Gilmore, Weili Lin, Dinggang Shen, "Neonatal brain image segmentation in longitudinal MRI studies", Elsevier Inc., 2009.

[23]. Juin-Der Lee, Hong-Ren Su, Philip E. Cheng*, Michelle Liou, John A. D. Aston, Arthur C. Tsai, and Cheng-Yu Chen, "MR Image Segmentation Using a Power Transformation Approach", IEEE Transactions On Medical Imaging, Vol. 28, No. 6, June 2009.

[24]. Dalila Cherifi, M.Zinelabidine Doghmane, Amine Nait-Ali , Zakia Aici,Salim Bouzelha, "Abnormal tissus extraction in MRI Brain medical images", IEEE, 2011.

[25]. Nagesh Vadaparthi, Srinivas Yarramalle, Suresh Varma Penumatsa, "Unsupervised Medical Image Segmentation On Brain MRI Images Using Skew Gaussian Distribution", IEEE-International Conference on Recent Trends in Information Technology, ICRTIT 2011.

[26]. Soumya Maitra, "Morphological Edge Detection Using Bit-Plane Decomposition in Gray Scale Images", In Proceedings of INDIACom, 2011.

SOCIETY FOR SCIENCE AND EDUCATION UNITED KINGDOM

JBEMi JOURNAL OF BIOMEDICAL ENGINEERING AND MEDICAL IMAGING

ISSN: 2055-1266
VOLUME 1, ISSUE 5

Soft-computing: An Objective Approach in Varied Diabetes Recognition

Obi J.C[1] and Imianvan A.A[2].
[1&2] *Department of Computer Science, University of Benin, Benin City. Nigeria.*
tripplejo2k2@yahoo.com ; tonyvanni@yahoo.com

ABSTRACT

Diabetes is a chronic disorder caused by elevated glucose within the blood stream. The predominant indicator of diabetes include a glucose level of more 125mg/dl in addition to frequent thirst, unusual thirst, extreme fatigue blurred vision and frequent infection. Existing approach for the recognition of diabetes are to two classes (Type I and Type II) in addition to their subjective approach. This research paper proposed an objective approach utilizing soft-computing techniques for the recognition of five class of diabetes.

Keywords: Fuzzy Logic, Fuzzy Set, Fuzzy Linguistic variables Genetic Algorithm, Neural Network,

1 Introduction

Diabetes; once considered a rare disease in sub-Saharan Africa is one of the most predominate health issue across Africa. In 2010, over 12 million people in sub-Saharan Africa are estimated to have diabetes, and 330,000 people die annually from diabetes-related conditions (DLF, 2011). Over the next 20 years, it is predicted that sub-Saharan Africa will have the highest growth in the number of people with diabetes of any region in the world, which is expected to double in 20 years, reaching 23.9 million by 2030 (DLF, 2011).

In Nigeria about 2million persons are living with diabetes, many people are living with the condition unaware of the seriousness of the disease and its consequences as those diagnosed are often poorly managed due to lack of resources or because the health care professionals vested with such care have limited knowledge about diabetes and how to provide good care. Diabetes might overtake those suffering from Tuberculosis, Malaria, HIV/AIDS, and other terminal diseases by the year 2030 if adequate attention was not paid toward the provision of health education; monitoring, treatment and management are not provided to the masses quickly (Kemi, 2012).

Diabetes is a chronic, debilitating disease requiring life-long management which invariably reduces the risk of serious, long-term complications such as kidney infection, liver disease and glaucoma etc. Offering the long-term monitoring and treatment needed is not easy for the healthcare systems of sub-Saharan Africa in general and Nigeria in particular, which are more focused on treatment and management of acute infection. Awareness of the early symptoms of diabetes is low, even among healthcare professionals. 85% of diabetes cases are undiagnosed, remaining without treatment and increasing the chances of untimely death (DLF, 2011). The professional knowledge in these regions if

DOI: 10.14738/jbemi.15.402
Publication Date: 29th September 2014
URL: http://dx.doi.org/10.14738/jbemi.15.402

available is tied mainly to type I and type II diabetes and rest in the hand of senior consultants and physicians. Other forms of diabetes such as gestational, Maturity onset Diabetes of the Young (MODY) and Latent Autoimmune Diabetes in Adulthood (LADA) are really difficult to comprehend from the physician standpoint due to their obsolete knowledge, lack of experience and exposure.

This research paper proposed an objective soft-computing approach utilizing the three fundamental concepts; neural network, genetic algorithm and fuzzy logic as a means for recognition five class of diabetes.

2 Review of Related Literature

The Multiple Knot Spline Smooth Support Vector Machine (MKS-SSVM) proposed by Shanti et al., (2009) is an algorithm for data mining techniques extending the original smoothing techniques introduced by Lee and Mangasarian (2001) to generate a smooth function which approximate the plus function for enhancing the performance, accuracy and result of Smooth Support Vector Machine (SSVM). The plus function which is the modification of the original three order spline function was the focal point of their research which was applied to the diagnosis of Type I diabetes utilizing the Pima Indian Dataset. SSVM and MKS-SSVM were chosen as material and method. The result of their research presented MKS-SSVM as significantly improving performance, accuracy and obtaining promising result to help diagnosis compared to SSVM although their computational time were Identical.

Madhavi and Bamnote (2012) proposed a predictive modeling of clinical data using a hybrid of neuro-fuzzy (soft-computing techniques) and data mining techniques for type I and type II diabetes recognition. The first phase of the system is preprocessing of diabetes data which is achieved utilizing soft-computing techniques. The second phase applies the different classification algorithm to the preprocessed data. The classification algorithm aims at identifying the characteristics that indicate the group to which each case belong. Decision-tree, neural network, multivariate adaptive regression spline (MARS), rule induction and K-Nearest are some of the mining techniques utilized. The performance of the proposed predictive model is measured utilizing Accuracy and Receiver Operator Characteristic Curve (AROC). In conclusion effective predictive model is achievable using preprocessing and data mining techniques for diabetes recognition.

Artificial Neural Networks (ANNs) constitute a class of flexible nonlinear models designed to mimic biological neural systems. An ANN is a mathematical model or computational model based on biological neural networks (Gutiérrez, 2011), as an interconnected group of artificial neurons, which carries out computation using a connectionist approach. Typically, a biological neural system consists of several layers, each with a large number of neural units (neurons) that can process the information in a parallel manner. The models with these features are known as ANN models (Robert, 2000). ANNs have been widely applied to solve many difficult problems in different areas, including pattern recognition (matching), signal processing, language learning, electronic medical record processing, tele-diagnosis and computer networking (Robert, 2000). Neural network utilize dataset. The data set is divided into three distinct sets: training, testing and validation sets. The training set is the largest set and is used by neural network to learn patterns present in the data. The testing set is used to evaluate the generalization ability of a supposedly trained network. A final check on the performance of the trained

network is made using validation set. Learning methods in neural networks can be broadly classified into three basic types Supervised, unsupervised and reinforced learning (Diogo et al. 2008):

The theory of fuzzy logic provides a mathematical strength to capture the uncertainties associated with human cognitive processes, such as thinking and reasoning. In standard set theory, an object does or does not belong to a set. There is no middle ground. In such bivalent systems, an object cannot belong to both its set and its compliment set or to neither of them. This principle preserves the structure of the logic and avoids the contradiction of object that both is and is not a thing at the same time (Zadeh, 1965). However, fuzzy logic is highly abstract and employs heuristic (experiment) requiring human experts to discover rules about data relationship (Angel and Rocio, 2011).

Fuzzy classification assumes the boundary between two neighboring classes as a continuous, overlapping area within which an object has partial membership in each class (Kuang et al., 2011). Fuzzy logic highlights the significant of most applications in which categories have fuzzy boundaries, but also provides a simple representation of the potentially complex partition of the feature space. (Sun and Jang**,** 1993 and Ahmad, 2011) Conventional approaches of pattern classification involve clustering training samples and associating clusters to given categories. The complexity and limitations of previous mechanisms are largely due to the lack of an effective way of defining the boundaries among clusters. This problem becomes more intractable when the number of features used for classification increases (Christos and Dimitros, 2008).

The Genetic Algorithm (GA) is a search and optimization technique based on the principles of genetics and natural selection. They represent processes in nature that are remarkably successful at optimizing natural phenomena. They are capable of solving other types of problems, using genetic operators abstracted from nature; they form a mechanism suitable for a variety of search problems. These algorithms encode a potential solution to a specific problem on a simple chromosome-like data structure and apply recombination operators to these structures so as to preserve critical information. Genetic algorithms are often viewed as function optimizer. The main idea is survival of the fittest (natural selection). Genetic algorithm is composed of three main genetic operators namely; **Selection:** is a way for the genetic algorithm to move toward promising regions in the search space. **Mutation:** is a genetic operator that changes one or more gene values in a chromosome. The mutation process helps to overcome trapping at local maxima. **Crossover:** Exchanging Chromosomes portions of genetic materials.

3 Methodology, Design and Result

Carefully observing these reviewed literatures propagated these drawbacks:

a) *Existing diabetes models are tied to two classes; type I and type II, with none of these existing models capable to diagnose the three current classes of diabetes namely; Gestational diabetes, Maturity Onset Diabetes of the Young (MODY) and Latent Autoimmune Diabetes in Adulthood (LADA).*
b) *The fuzzy scaled membership function boundary was in most cases subjective (assumed) and not based on objective (scientific) approach which is achievable utilizing a search and optimization techniques which has invariably lead to flaw medical diagnosis in most cases.*

3.1 The Proposed Soft-computing Model

The proposed model is a Hybrid architectural framework which harnessing the three fundamental soft-computing techniques with the aim of provide class distinction for the differential recognition of varied diabetes identification utilizing the predominant fuzzy set, in addition with the occurrence factors thereby establishing a conclusive boundary. Unlike the current approaches, in which success or failure are based on the wills and experiences of relevant personnel designing and administrating the approach in other to elicit relevant recognition points. This model is artificial intelligence based; therefore success and failure are not dependent on human intuitions, but success, is closely linked within tuned-up approaches within the system components.

The Dataset present in Table 3.1 was obtained through a research survey, utilizing questionnaires as the research tool. The quantitative and qualitative questionnaires comprises of two phase. The first phase contains demographic information's while the second phase tele-medical information. A total of fifty questionnaires were constructed and distributed to various expert diabetes medical professional spread across eight teaching hospitals within five Geo-political regions in Nigeria. All questionnaires administrated were retrieved without mutilation. In other to generate a Fuzzy Linguistic variable dataset, all questionnaires responds were tuned utilizing the proposed Adapted Fuzzy Cluster Mean Equation:

$$AFCME = \sum (A, B, C, D, E)*X \quad (3.1)$$

Where *A, B, C, D and E = Picked Questionnaires Questions Options (PQQO)*

X (0.02) = Assigned Question Option Fuzzy Range Value (AQOFRV)

Unpicked options = 0.00

Utilizing the Genetic Algorithm Procedures proposed by (obi and Imainavan, 2013), the generated membership function derived from our tuned questionnaires were optimized to obtain the fuzzy membership function boundary of 0.53 specified in Table 1, which is invariably attached to the linguistic variable represented as **Serious,** while **Moderate** is 0.4 and 0.3 and below **Minor**

Table 1: Optimized Dataset for the Varied Form of Diabetes (Scale 0.00 - 1.00)

Symp. Codes	Symptoms/ Fuzzy Set (Parameters)	Degree of Membership Function for the Varied Forms of Diabetes *(Scale ranging from 0.00 -1.00)*				
		Cluster 1 (Type I)	Cluster 2 (Type II)	Cluster 3 (Gestational)	Cluster 4 (MODY)	Cluster 5 (LADA)
P01	Frequent urination	*0.50*	0.00	0.00	0.00	*0.50*
P02	Unusual thirst	*0.50*	0.00	0.00	0.00	*0.50*
P03	Extreme hunger	*0.50*	0.00	0.00	0.00	*0.50*
P04	Unusual weight loss	*0.50*	0.00	0.00	0.00	*0.50*
P05	Extreme fatigue	*0.50*	0.00	0.00	0.00	*0.50*
P06	Irritability	0.00	0.00	*0.50*	*0.50*	0.00
P07	Frequent infections	0.00	0.00	*0.50*	*0.50*	0.00
P08	Blurred vision	0.00	*0.50*	0.00	*0.50*	0.00
P09	Slow to heal cuts/bruises	0.00	*0.50*	*0.50*	0.00	0.00
P10	Tingling/numbness in hands/feet	0.00	*0.50*	0.00	*0.50*	0.00
P11	Regular skin/gum/ bladder infections	0.00	*0.50*	*0.50*	0.00	0.00
P12	Nausea and vomiting	0.00	*0.50*	*0.50*	0.00	0.00
P13	*Hemoglobin A1c test (HbA1c)* >10	0.20	0.20	*0.20*	*0.20*	0.20
P14	*Rapid Weight loss*	0.00	0.00	0.00	*0.50*	*0.50*
P15	Leg Cramp	0.20	0.20	*0.20*	*0.20*	0.20

3.2 Fuzzy Integration

The fuzzy partition for each input feature consists of clinical symptoms of for the varied forms of diabetes (frequent urination, unusual thirst, extreme hunger, unusual weight loss, extreme fatigue, irritability, frequent infection, blurred vision, slow to heal cuts/bruises, tingling/numbness in hands/feet, regular skin/bladder/gum infection, nausea/vomiting, hemoglobin A1c test (HbA1c) >10, rapid weight loss and leg cramp). However, it can occur that if the fuzzy partition for the varied forms of diabetes is not set up correctly, or if the number of linguistic terms for the input features is not large enough, then some patterns will be misclassified. The linguistic label serious is the base point for classification.

a) *Not diagnose with a class diabetes (C_1)*
b) *Might be diagnose with a class of diabetes (C_2)*
c) *Diagnose with a class of diabetes (C_3)*

If the patient is exhibiting at least three or less of the symptoms of a class of diabetes THEN (C_1), if the patient is exhibiting exactly four of the symptoms of a class of diabetes THEN (C_2) and if the patients is exhibiting five or more of the symptoms of a class of diabetes THEN (C_3).

The Fuzzy IF-THEN Rules that can be generated from the initial fuzzy partitions of the classification of varied for diabetes is thus:

R1: IF the patient exhibit *frequent urination* and its *serious* THEN class C_1.

R2: IF the patient exhibit *frequent urination* and *unusual thirst* and both symptoms are *serious* THEN class C_1.

R3: IF the patient exhibit *frequent urination, unusual thirst and extreme hunger* and these symptoms are *serious* THEN class C_1.

R4: IF the patient exhibit *frequent urination, unusual thirst, extreme hunger* and *unusual weight loss* and these symptoms are *serious* THEN C_2.

R5: IF the patient exhibit *frequent urination, unusual thirst, extreme hunger, unusual weight loss* and *extreme fatigue* and these symptoms are *serious* THEN class C_3.

R6: IF the patient exhibit *frequent urination, unusual thirst, extreme hunger, unusual weight loss, extreme fatigue* and *irritability* and these symptoms are *serious* THEN class C_3.

R7: IF the patient is exhibits *frequent urination, unusual thirst, extreme hunger, unusual weight loss, extreme fatigue, irritability* and *frequent infection* and these symptoms are *serious* THEN class C_3.

R8: IF the patient exhibits *frequent urination, unusual thirst, extreme hunger, unusual weight loss, extreme fatigue, irritability, frequent infection* and *blurred vision* and these symptoms are *serious* THEN class C_3.

R9: IF the patient exhibit frequent urination, unusual thirst, extreme hunger, unusual weight loss, extreme fatigue, irritability, frequent infection, blurred vision and slow to heal cuts/bruises and these symptoms is serious THEN class C_3.

R10: IF the patient exhibit frequent urination, unusual thirst, extreme hunger, unusual weight loss, extreme fatigue, irritability, frequent infection, blurred vision, slow to heal cuts/bruises and tingling/numbness in hands/feet and these symptoms are serious THEN class C_3.

R11: IF the patient exhibit frequent urination, unusual thirst, extreme hunger, unusual weight loss, extreme fatigue, irritability, frequent infection, blurred vision, slow to heal cuts/bruises, tingling/numbness in hands/feet and regular skin/bladder/gum infection and these symptoms are serious THEN class C_3.

R12: IF the patient exhibit frequent urination, unusual thirst, extreme hunger, unusual weight loss, extreme fatigue, irritability, frequent infection, blurred vision, slow to heal cuts/bruises, tingling/numbness in hands/feet, regular skin/bladder/gum infection and nausea/vomiting, *and these symptoms are serious* THEN class C_3.

R13: IF the patient exhibit frequent urination, unusual thirst, extreme hunger, unusual weight loss, extreme fatigue, irritability, frequent infection, blurred vision, slow to heal cuts/bruises, tingling/numbness in hands/feet, regular skin/bladder/gum infection, nausea/vomiting, and *hemoglobin A1c* test (*HbA1c*) >10 and these symptoms are serious THEN class C_3.

R14: IF the patient exhibits frequent urination, unusual thirst, extreme hunger, unusual weight loss, extreme fatigue, irritability, frequent infection, blurred vision, slow to heal cuts/bruises, tingling/numbness in hands/feet, regular skin/bladder/gum infection, nausea/vomiting, *hemoglobin A1c test (HbA1c)* >*10* and *rapid weight loss and these symptoms are serious* THEN class C_3.

R15: IF the patient exhibits frequent urination, unusual thirst, extreme hunger, unusual weight loss, extreme fatigue, irritability, frequent infection, blurred vision, slow to heal cuts/bruises, tingling/numbness in hands/feet, regular skin/bladder/gum infection, nausea/vomiting, *hemoglobin A1c* test (*HbA1c*) >10*, rapid weight loss and* Leg Cramp and these symptoms are serious THEN class C_3.

3.3 Diabetes Diagnosis

If a patient is exhibiting five or more symptoms of diabetes with linguistic label serious in collaboration with a Glucose level ≥ *125mg/dl*, Age range = *Teenager*, Origin = *Caucasians* and pancreas obliteration = *swift* Then **Type I**

If a patient is exhibiting five or more symptoms of diabetes with linguistic label serious in collaboration with a Glucose level ≥ *125mg/dl*, Age range = *Post Adult*, Origin = *Blacks* and Pancreas Obliteration = *swift* Then **Type II**

If a patient is exhibiting five or more symptoms of diabetes with linguistic label serious in collaboration with a Glucose level ≥ *125mg/dl*, Age range = *Pre-manopause*, Origin = *Plus* Then **Gestational**

If a patient is exhibiting five or more symptoms of diabetes with linguistic label serious in collaboration with a Glucose level ≥ *125mg/dl*, Age range = *Teenager*, and mutated dominant gene = *present* and Origin = Caucasians Then **MOYD**

If a patient is exhibiting five or more symptoms of diabetes with linguistic label serious in collaboration with a Glucose level ≥ 125mg/dl, Age range = Pre- Adult, Origin = Caucasian and pancreas obliteration = *Progressive* Then **LADA**

The proposed model is depicted on Figure 1,

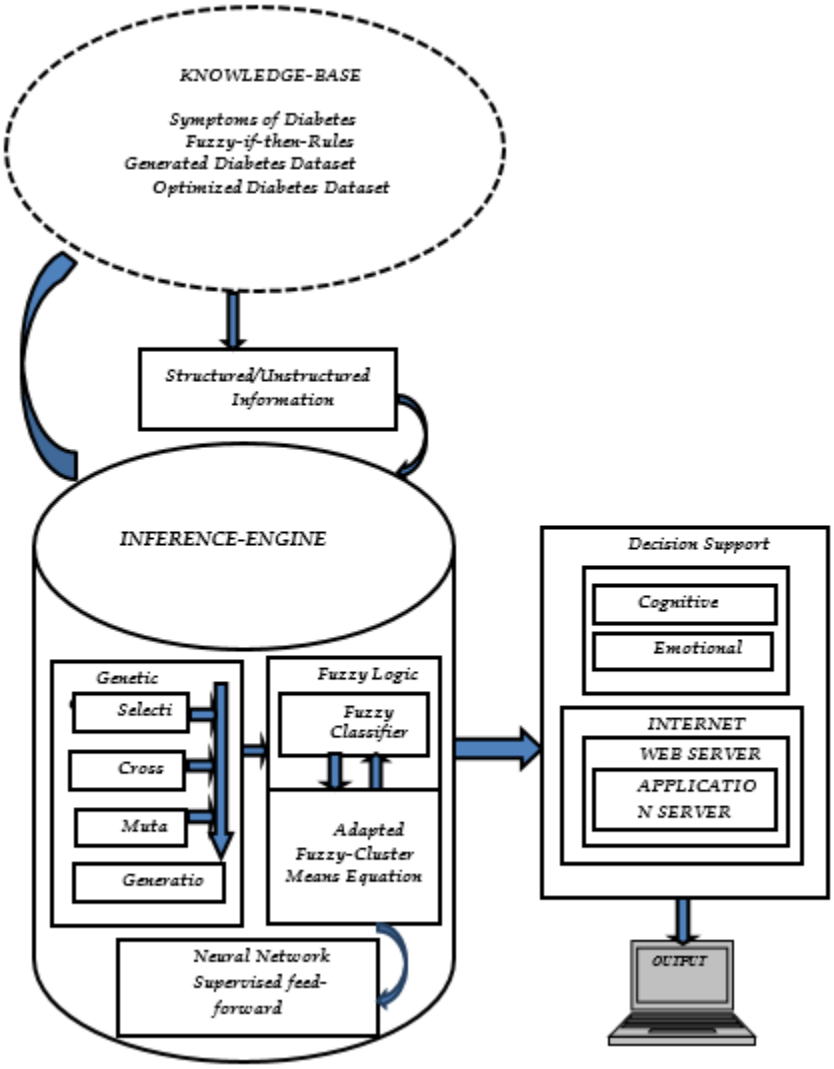

Figure 1: Soft computing Architecture for the Diagnosis of varied forms of Diabetes

3.4 Unified Modeling Language (UML)

Unified Modeling Language (UML) is a standard modeling language used for modeling software systems. The focus of UML is on creating simple, well documented and easy to understand software models. Use case and Sequence Diagram where utilized for depicting the two main view of the proposed system.

Figure 2 and 3 shows the user case model for varied forms of diabetes of our proposed system.

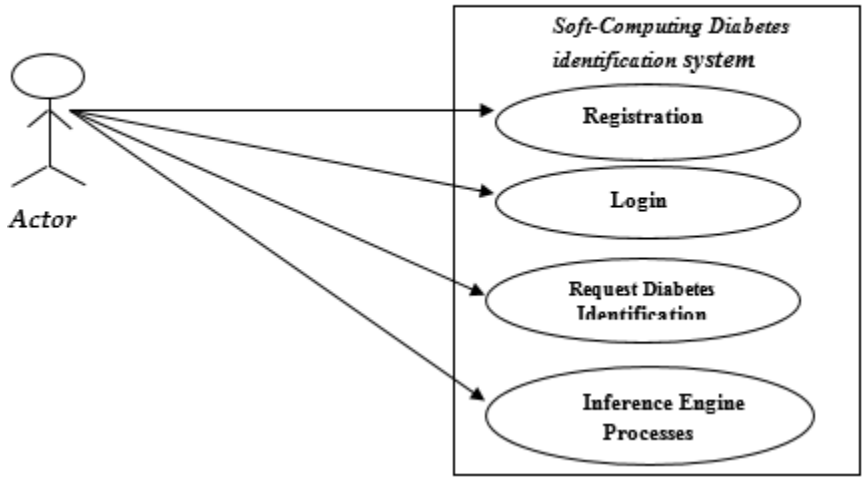

Figure 2: Use Case Diagram modeling Diabetes software System

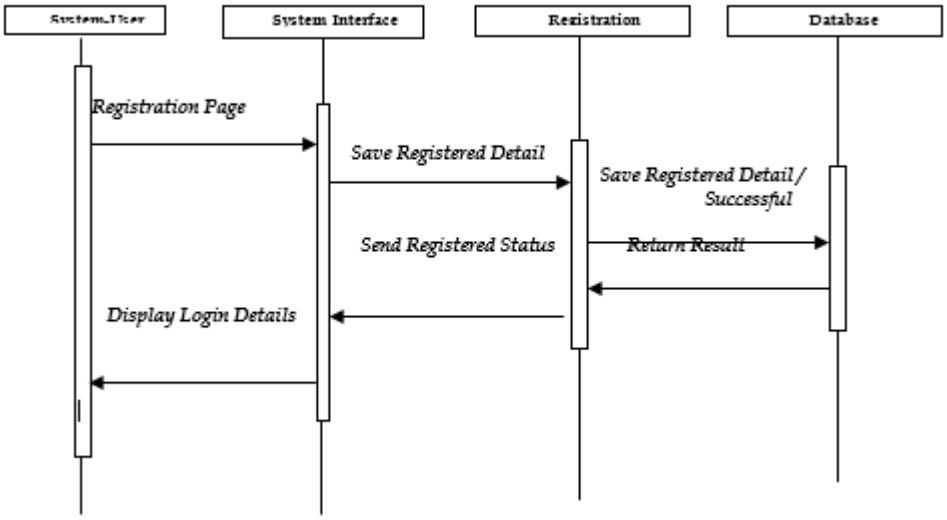

Figure 3: 18 Sequence Diagram modeling Registration Process

4 Implementation and Results

Matrix Laboratory (MATLAB) serves as our simulation tool in achieving the our results because of its interactive environment for algorithm development, data visualization, data analysis, and numerical approach which was relevant to our numerical dataset which was more appropriate than with spreadsheets or traditional programming languages, such as C/C++ or Java.

4.1 Results

The system was successfully installed and tested on the following operating systems: Microsoft Windows (XP, Vista & 7), Ubuntu 9 and Solaris 10. The system was validated with online records of Diabetes cases with slight deviation from results, corrections were effected. University of Benin

Teaching Hospital (UBTH) provided a communicative framework for testing the system on a one-on-one basis. Our simulation results are presented on Table 2 and 3 respectively.

Table 2: Subjective Diagnosis Approach

	Diabetic Patient	Type I	Type II	Gestational	MODY	LADA	Diabetes (Nil)
1.	Patient A	-		-	-	-	-
2.	Patient B	-		-	-	-	-
3.	Patient C	-		-	-	-	-
4.	Patient D	-		-	-	-	-
5.	Patient E	-		-	-	-	-
6.	Patient F	-		-	-	-	-
7.	Patient G	-		-	-	-	-
8.	Patient H	-		-	-	-	-
9.	Patient I	-		-	-	-	-
10.	Patient J	-		-	-	-	-

Table 3: Soft-Computing Expert System

		Varied Classes of Diabetes					
	Diabetic Patient	Type I	Type II	Gestational	MODY	LADA	Diabetes (Nil)
1.	Patient A	-	-	-	-	-	
2.	Patient B	-	-	-	-	-	
3.	Patient C	-		-	-	-	-
4.	Patient D	-		-	-	-	-
5.	Patient E	-		-	-	-	-
6.	Patient F	-		-	-	-	-
7.	Patient G	-		-	-	-	-
8.	Patient H	-	-			-	-
9.	Patient I	-	-			-	-
10.	Patient J	-	-			-	-

5 Conclusion

A soft-computing system has been design, developed, implemented and simulated for the recognition of five class of diabetes diagnosis utilizing the fundamental concepts of soft-computing. Unlike previous approaches in which successfully and failure are tied fully to human intuition, this is an objective system.

REFERENCES

[27]. Ahmad H. (2011), "Fuzzy approach to Likert Spectrum in Classified levels in surveying researches" retrieved http://www.tjmcs.com.

[28]. Angel C. and Rocio R. (2011), "Documentation management with Ant colony Optimization Meta-heuristic: A Fuzzy Text Clustering Approach Using Pheromone trails" retrieved from soft computing in Industrial applications, Advances in intelligent and soft Computing, vol. 96, 2011, 261-70, DOI: 10.1007/978-3-642-20505-1_23

[29]. DLF: Diabetes Leadership Forum (2011), "Diabetes: the hidden pandemic and its impact on Sub-Saharan Africa"retrieved online from www.novonordisk.com/...diabetes/.../Sub-Saharan%20Africa%20BB.

[30]. Diogo F. P., Flávio R.S. O. and Fernando B. L. N (2008), "Multi-objective abilities in the Hybrid Intelligent Suite for decision support" retrieved from http://ieeexplore. ieee.org/xpl/freeabs_all.

[31]. Gutiérrez P.A. (2011), "Hybrid Artificial Neural Networks: Models", retrieved online from *http:// dl.acm.org/citation.cfm?id=20233*

[32]. Kemi O. (2012), "Three Nigerians Suffering from Diabetes" retrieved online from http://nationalmirroronline.net/index.php/health/health-news/42251.html

[33]. Kuang Y. H.; Ting-H. C. and Ting-Cheng Chang (2011), "Determination of the threshold value β of variable precision rough set by fuzzy algorithms" retrieved from http://www.sciencedirect.com/science/article/pii/S0888613X11000831

[34]. Madhavi G. and Bamnote K. (2012), Predictive Diagnosis Model" Clinical Microbiology Reviews, Vol.13, No.1, Pp. 76-82.

[35]. Robert F. (2000) "Introduction to Neuro-Fuzzy Systems: Advances in Soft Computing Series", Springer-Verlag, Berlin/Heidelberg, Germany.

[36]. Shanti W. P., Abdullah E., Jasni M. Z, and Rahayu S.P. (2009), "A New Smoth Vector Machine and Its Applications in Diabetes Disease Diagnosis", Journal of Computer Science Vol. 5(12): 1003-1008

[37]. Sun C.T. and Jang J.S. (1993) "A neuro-fuzzy classifier and its applications", in: Proc. IEEE Int. Conference on Neural Networks, San Francisco, pp.94–98.

[38]. Zadeh L.A. (1965), "Fuzzy sets. Information and Control", Vol.8, pp.338-353.

SOCIETY FOR SCIENCE AND EDUCATION UNITED KINGDOM

JBEMi JOURNAL OF BIOMEDICAL ENGINEERING AND MEDICAL IMAGING

ISSN: 2055-1266
VOLUME 1, ISSUE 5

Fuzzy Supervised Neural Training Algorithm for varied Diabetes recognition

[1]Imianvan A.A. & [2]Obi J.C.

[1,2]Department of Computer Science, University of Benin, P.M.B. 1154. Benin City, Nigeria.

tonyvanni@yahoo.com; tripplejo2k2@yahoo.com

ABSTRACT

Diabetes is a metabolic disorder associated with Blood Glucose Level. Most of the approaches applied in diagnosis are subjective in nature at best and tied toward Type I and Type II diabetes recognition, with none geared toward form of diabetes recognition. Fuzzy Supervised Neural Network Training Algorithm has been designed and implemented with Matrix Laboratory (MATLAB) and Hypertext Preprocessor as the simulation language. This paper demonstrates the practical application of algorithm techniques in medical diagnosis in determining patient's status.

Keywords: Supervised-Neural-Network, Fuzzy set, Fuzzy Logic, Algorithm

1 Introduction

In Nigeria about 2million persons are living with diabetes, many people are living with the condition unaware of the seriousness of the disease and its consequences as those diagnosed are often poorly managed due to lack of resources or because the health care professionals who care for them have poor knowledge about diabetes and how to provide good care. Diabetes might overtake those suffering from Tuberculosis, Malaria, HIV/AIDS, and other terminal diseases by the year 2030 if adequate attention was not paid toward the provision of health education; monitoring, treatment and management are not provided to the masses quickly (Kemi, 2012).

Diabetes is a chronic, debilitating disease requiring life-long management which invariably reduces the risk of serious, long-term complications such as kidney infection, liver disease and glaucoma etc. Offering the long-term monitoring and treatment needed is not easy for the healthcare systems of sub-Saharan Africa in general and Nigeria in particular, which are more focused on treatment and management of acute infection. Awareness of the early symptoms of diabetes is low, even among healthcare professionals. 85% of diabetes cases are undiagnosed, remaining without treatment and increasing the chances of untimely death (DLF, 2011). The professional knowledge in these regions if available is tied mainly to type I and type II diabetes and rest in the hand of senior consultants and physicians. Other forms of diabetes such as gestational, Maturity onset Diabetes of the Young (MODY) and Latent Autoimmune Diabetes in Adulthood (LADA) are really difficult to comprehend from the physician standpoint due to their obsolete knowledge, lack of experience and exposure.

DOI: 10.14738/jbemi.15.403
Publication Date: 29th September 2014
URL: http://dx.doi.org/10.14738/jbemi.15.403

Diabetes is a very difficult disease to monitor and manage in Africa and Nigeria. However, early identification (diagnosis) and treatment of the disease reduces the life-threatening effect and prevents deaths ultimately. The diagnosis of diabetes, therefore, is an important key in the fight against diabetes in terms of treatment and long-term management, where possible. It therefore calls for the attention of health workers in this regard.

This research paper is geared toward proposing an implementing a supervised forward neural network algorithm for the identification of five class of diabetes.

2 Review of Related Literature

The theory of fuzzy logic provides a mathematical strength to capture the uncertainties associated with human cognitive processes, such as thinking and reasoning. In standard set theory, an object does or does not belong to a set. There is no middle ground. In such bivalent systems, an object cannot belong to both its set and its compliment set or to neither of them. This principle preserves the structure of the logic and avoids the contradiction of object that both is and is not a thing at the same time (Zadeh, 1965). However, fuzzy logic is highly abstract and employs heuristic (experiment) requiring human experts to discover rules about data relationship (Angel and Rocio, 2011).

Fuzzy classification assumes the boundary between two neighboring classes as a continuous, overlapping area within which an object has partial membership in each class (Kuang et al., 2011). Fuzzy logic highlights the significant of most applications in which categories have fuzzy boundaries, but also provides a simple representation of the potentially complex partition of the feature space. (Sun and Jang**,** 1993 and Ahmad, 2011) Conventional approaches of pattern classification involve clustering training samples and associating clusters to given categories. The complexity and limitations of previous mechanisms are largely due to the lack of an effective way of defining the boundaries among clusters. This problem becomes more intractable when the number of features used for classification increases (Christos and Dimitros, 2008).

Artificial Neural Networks (ANNs) constitute a class of flexible nonlinear models designed to mimic biological neural systems. An ANN is a mathematical model or computational model based on biological neural networks (Gutiérrez, 2011), as an interconnected group of artificial neurons, which carries out computation using a connectionist approach. Typically, a biological neural system consists of several layers, each with a large number of neural units (neurons) that can process the information in a parallel manner. The models with these features are known as ANN models (Robert, 2000). ANNs have been widely applied to solve many difficult problems in different areas, including pattern recognition (matching), signal processing, language learning, electronic medical record processing, tele-diagnosis and computer networking (Robert, 2000). Neural network utilize dataset. The data set is divided into three distinct sets: training, testing and validation sets. The training set is the largest set and is used by neural network to learn patterns present in the data. The testing set is used to evaluate the generalization ability of a supposedly trained network. A final check on the performance of the trained network is made using validation set. Learning methods in neural networks can be broadly classified into three basic types Supervised, unsupervised and reinforced learning (Diogo et al. 2008).

Supervised learning is the machine learning task of inferring a function from supervised training data. The training data consist of a set of training examples. In supervised learning, each example is a pair

consisting of an input object (typically a vector) and a desired output value (also called the supervisory signal). A supervised learning algorithm analyzes the training data and produces an inferred function, which is called a classifier (if the output is discrete) or a regression function (if the output is continuous).

Unsupervised learning studies how systems can learn to represent particular input patterns in a way that reflects the statistical structure of the overall collection of input patterns. By contrast with Supervised Learning or Reinforcement Learning, there are no explicit target outputs or environmental evaluations associated with each input; rather the unsupervised learner brings to bear prior biases as to what aspects of the structure of the input should be captured in the output. Unsupervised learning is important since it is likely to be much more common in the brain than supervised learning (Benedetti et al., 2005).

Reinforcement learning, one of the most active research areas in artificial intelligence, is a computational approach to learning whereby an agent tries to maximize the total amount of reward it receives when interacting with a complex, uncertain environment. In Reinforcement Learning, provide a clear and simple account of the key ideas and algorithms of reinforcement learning. Their discussion ranges from the history of the field's intellectual foundations to the most recent developments and applications. The only necessary mathematical background is familiarity with elementary concepts of probability (Richard and Andrew, 2011).

The two most widely used neural networks are the feed-forward networks and recurrent or interactive (feedback) networks, kohonen's self-organizing network, Adaptive resonance Theory (ART) and Counter propagation network are others (Chakraborty, 2010).

Feed-forward ANNs allow signals to travel one way only; from input to output. There is no feedback (loops) i.e. the output of any layer does not affect that same layer. They are extensively used in pattern recognition (Chakraborty, 2010).

This multi-layered structure of a feed-forward network is designed to function as a biological neural system. The input units are the neurons that receive the information (stimuli) from the outside environment and pass them to the neurons in a middle layer (i.e., hidden units). These neurons then transform the input signals to generate neural signals and forward them to the neurons in the output layer. The output neurons in turn generate signals that determine the action to be taken. It is important to note that all information from the units in one layer is processed simultaneously, rather than sequentially, by the units in an "upper" layer (kuan and white, 1994).

Feedback Network or Recurrent Neural Networks: Feedback networks can have signals travelling in both directions by introducing loops in the network. Feedback networks are dynamic; their 'state' is changing continuously until they reach an equilibrium point. They remain at the equilibrium point until the input changes and a new equilibrium needs to be found (Chakraborty, 2010).

Kohonen's Self-Organizing Network is a two-layer, feed-forward network (Beale and Jackson, 1990 and Dayhoff, 1990).The first is an input layer and the second is a grid or map arranged in a one or two-dimensional array. The second layer is known as a competitive layer. Incoming patterns are classified by the nodes that they activate in the competitive layer. Similarities among patterns are mapped into

closeness relationships on the competitive layer. After training, the pattern relationships and groupings are observed from this layer.

Adaptive Resonance Theory (ART) is an unsupervised, competitive learning algorithm (Beale and Jackson, 1990). It is a two-layer network arranged in feedback and feed-forward connection. The layers have different functions, unlike the Multilayer or Kohonen networks. The first layer can be either an input or a comparison layer and the second layer can be either an output or a recognition layer. Both are interchangeable during training.

3 Methodology and Design

Existing diabetes models are tied to two classes; type I and type II, with none of these existing models capable to diagnose the three current classes of diabetes namely; Gestational diabetes, Maturity Onset Diabetes of the Young (MODY) and Latent Autoimmune Diabetes in Adulthood (LADA).

Numerous algorithm has be proposed for solving real work problems such tele-diagnosis through tele-surgery, but still date few Fuzzy-neural network algorithm has be proposed for training, validating and recognition or diagnosis for diabetes which span five class.

3.1 The Proposed Fuzzy Supervised Neural Network Training Algorithm

The proposed Algorithm imbibe artificial intelligence techniques in tying the symptoms of diabetes to the differential diagnosis of five class in addition with the occurrence factors thereby establishing a conclusive boundary. Unlike the current approaches, in which success or failure are based on the wills and experiences of relevant personnel designing and administrating the approach in other to elicit relevant recognition points. This algorithm is artificial intelligence based; therefore success and failure are not dependent on human intuitions, but success, is closely linked within tuned-up approaches within the carefully and systematic implemented. The Algorithm is depicted on Figure 1

INPUT:

Types of Diabetes (TYPE1, TYPE2, GESTATIONAL, MODY, LADA)

No. of Symptoms (P1, P2,…, Pn) = 15

P; Fuzzy parameters (Symptoms Codes)

Degree of membership function

≥ 0.50 = High degree membership function (serious)

≤ 0.50 = Low degree Membership Function (minor)

Fuzzy predefined Rules

More than five symptoms = Not diagnose with a class diabetes

Exactly four symptoms = Might be diagnose with a class of diabetes

Three symptoms and below = Diagnose with a class of diabetes

Glucose Level (125md/dl) = High

Age Range (R)

1 – 21yrs of age = teenager

30 – 40yrs of age = pre-Adult

> 41yrs of age = post-Adult

12 – 50 = pre-menopause

Origin (descent)

Caucasians; Americans, Europe's, Asians, North- Africa, Half-caste

Blacks; African, Black-Americans, Blacks Indians, Half-caste

Plus; either Caucasians or blacks

// INITIALIZATION

1. Randomly pick a patient *K;*
2. Save identification (diagnosis) Result in *Knot;*

// Loop till terminal point

3. For P = 1 to n do;

// Type 1 diabetes

4. Diagnose for Type 1 Diabetes;
5. If TYPE I symptoms is *serious*, patient age range is *teenager*, glucose level is *high,* patient origin is *Plus* and pancreas destruction is *swift* THEN Type 1;
6. Else if
7. Might be Type 1; (*exhibiting fours symptoms of Type I Diabetes*)
8. Else
9. Not Type 1;

// Type 2 diabetes

10. Diagnose for Type 2 Diabetes;
11. If TYPE 2 symptoms is *serious*, patient age is *post-Adult,* glucose level is *high* and patient origin is *black* THEN Type 2;
12. Else if
13. Might be Type 2; (*exhibiting fours symptoms of Type II Diabetes*)
14. Else
15. Not Type 2;

//Gestational diabetes

16. Diagnose for Gestational Diabetes;
17. If Gestational symptoms is *serious,* patient age is *pre-menopause,* glucose level is *high,* patient origin is *plus* and patient is *pregnant* THEN Gestational diabetes;
18. Else if (*exhibiting fours symptoms of Gestational Diabetes*)
19. Might be Gestational Diabetes;
20. Else
21. Not Gestational Diabetes;

// MODY diabetes

22. Diagnose for MODY Diabetes;

23. If MODY symptoms is *serious,* patient age is *teenager,* glucose level is *high,* patient origin is *caucasians* and mutated autosomal dominant gene is *present* THEN MODY diabetes;
24. Else if (*exhibiting fours symptoms of MODY Diabetes*)
25. Might be MODY diabetes;
26. Else
27. Not MODY diabetes;

// LADA diabetes

28. Diagnose for LADA Diabetes;
29. If LADA symptoms is *serious;* patient age is *pre-Adult,* glucose level is *high,* patient origin is *Caucasians* and pancreas destruction is *progressive* THEN LADA diabetes;
30. Else if (*exhibiting fours symptoms of LADA Diabetes*)
31. Might be LADA diabetes;
32. Else
33. Not LADA diabetes;

//Save results in *Knot;*

34. Return diabetes result for patient K

Figure 1: The Proposed Fuzzy Supervised Neural Network Training Algorithm

4 Implementation and Discussion

The implementation of our result was dual fold; the neural training dataset was handled conveniently utilizing Matrix Laboratory (MATLAB) which serves as our simulation tool in achieving the our results because of its interactive environment for algorithm development, data visualization, data analysis, and numerical approach which was relevant to our numerical dataset which was more appropriate than with spreadsheets or traditional programming languages, such as C/C++ or Java. After pruning the dataset utilizing MATLAB, the algorithm was fully implemented utilizing Hypertext Preprocessor (PHP), which served as the language of implementation.

4.1 Discussion

The implemented algorithm provides an interactive base in determining varied diabetes diagnosis objectively as opposed to the subjective approach which is achievable utilizing the algorithm. The result was satisfactory having been able to distinct diagnosis several diabetic patient and subsequently classified into varied classes.

5 Conclusions

This paper has demonstrates the practical application of fuzzy supervised diabetes training algorithm in the medical sector in determining and diagnosing varied diabetes identification.

REFERENCES

[1]. Ahmad H. (2011), "Fuzzy approach to Likert Spectrum in Classified levels in surveying researches" retrieved http://www.tjmcs.com.

[2]. Angel C. and Rocio R. (2011), "Documentation management with Ant colony Optimization Meta-heuristic: A Fuzzy Text Clustering Approach Using Pheromone trails" retrieved from soft computing in Industrial applications, Advances in intelligent and soft Computing, vol. 96, 2011, 261-70, DOI: 10.1007/978-3-642-20505-1_23

[3]. Benedetti S., Saverio M., Anna G. S. and Gian L.M. (2005), "Electronic nose and neural network use for the classification of honeypot" retrieved from *citeseerx.ist.psu. Edu/viewdoc /download?doi=10.1.1.128.pdf*

[4]. Beale R. and Jackson I. (1990), "Neural Computing: An Introduction" *dl.acm.org/citation.cfm?id=121342.*

[5]. Chakraborty R.C. (2010), "Soft computing- Introduction: Soft-computing Lecture 1-6, notes"retrieved from http://myreaders.inro

[6]. Christos S. and Dimitros S. (2008) "Neural Network", retrieved from http://www.docstoc.com/docs/15050/neural-networks

[7]. Dayhoff, J.E. (1990), "Neural Network Architecture: An Introduction" retrieved from https://catalyst.library.jhu.edu/?q=%22Dayhoff%2C+Judith

[8]. Diogo F. P., Flávio R.S. O. and Fernando B. L. N (2008), "Multi-objective abilities in the Hybrid Intelligent Suite for decision support" retrieved from http://ieeexplore. ieee.org/xpl/freeabs_all.

[9]. DLF: Diabetes Leadership Forum (2011), "Diabetes: the hidden pandemic and its impact on Sub-Saharan Africa" retrieved online from www.novonordisk.com/…diabetes/…/Sub-Saharan%20Africa%20BB.

[10]. Gutiérrez P.A. (2011), "Hybrid Artificial Neural Networks: Models", retrieved online from http:// *dl.acm.org/citation.cfm?id=20233*

[11]. Kuan C. M. and White H. (1994), "Artificial neural networks: An econometric perspective", Econometric Reviews, Vol.13, Pp.1-91 and Pp.139-143.

[12]. Kuang Y. H.; Ting-H. C. and Ting-Cheng Chang (2011), "Determination of the threshold value β of variable precision rough set by fuzzy algorithms" retrieved from http://www.sciencedirect.com/science/article/pii/S0888613X11000831

[13]. Kemi O. (2012), "Three Nigerians Suffering from Diabetes" retrieved online from http://nationalmirroronline.net/index.php/health/health-news/42251.html

[14]. Richard S. S. and Andrew G. B. (2011), "Reinforcement learning: an Introduction" retrieved from http://books.google.com/books/about/Reinforcement_l.

[15]. Robert F. (2000) "Introduction to Neuro-Fuzzy Systems: Advances in Soft Computing Series", Springer-Verlag, Berlin/Heidelberg, Germany.

[16]. Sun C.T. and Jang J.S. (1993) "A neuro-fuzzy classifier and its applications", in: Proc. IEEE Int. Conference on Neural Networks, San Francisco, pp.94–98.

[17]. Zadeh L.A. (1965), "Fuzzy sets. Information and Control", Vol.8, pp.338-353.

SOCIETY FOR SCIENCE AND EDUCATION UNITED KINGDOM

JBEMi JOURNAL OF BIOMEDICAL ENGINEERING AND MEDICAL IMAGING

ISSN: 2055-1266
VOLUME 1, ISSUE 5

Automatic Segmentation of cDNA Microarray Images using different methods

Islam Fouad[1], Mai Mabrouk[2] and Amr Sharawy[3]
[1]*College of Applied Medical Sciences, SALMAN Bin ABDUL-AZIZ University, Kharj, KSA*
[2]*Biomedical Engineering, MUST University, 6th of October, Egypt*
[3]*Biomedical Engineering, Cairo University, Giza, Egypt*

ABSTRACT

Due to the vast success of bioengineering techniques, a series of large scale analysis tools has been developed to discover the functional organization of cells. Among them, cDNA microarray has emerged as a powerful technology that enables biologists to cDNA microarray technology has enabled biologists to study thousands of genes simultaneously within an entire organism, and thus obtain a better understanding of the gene interaction and regulation mechanisms involved. The analysis of DNA microarray image consists of several steps; gridding, segmentation, and quantification that can significantly deteriorate the quality of gene expression in formation, and hence decrease our confidence in any derived research results. Thus, microarray data processing steps become critical for performing optimal microarray data analysis and deriving meaningful biological information from microarray images .Segmentation is the process, by which each individual cell in the grid must be selected to determine the spot signal and to estimate the background hybridization. In this paper, four segmentation methods are explored; “fixed circle”, “adaptive circle”, “thresholding”, and “adaptive shape” segmentation. By comparing the results, it was found that the “adaptive shape segmentation method” can segment noisy microarray images correctly, gives high accuracy results and minimal processing time, and can be applied to various types of noisy microarray images.

Keywords: *Noisy Microarray Image, Gene Expression, Analysis of DNA Microarray Image, Segmentation.*

1 Introduction

Microarray technology came on time to cover the need to monitor in parallel all the DNA sequences and to have the adequate sensibility to detect the variation of gene expression. There may be tens of thousands of spots on an array. Each spot contains tens of millions of identical DNA molecules with lengths from tens to hundreds of nucleotides. Afterwards, the microarray slide is exposed to a set of labeled cDNA samples, which are derived from tissue of interest. With the completion of hybridization reaction, the amount of the target that bounds to each sample is measured with the aid of image capturing devices and computer technology. The measurement is based on the intensity of the spot. There are three basic steps in the processing of microarray image [1]; gridding, segmentation, and quantification.

DOI: 10.14738/jbemi.15.476
Publication Date: 29th September 2014
URL: http://dx.doi.org/10.14738/jbemi.15.476

Image segmentation is the process of distinguishing objects from their background [2]. It is usually the first step in vision systems, and is the basis for further processing such as description or recognition. The goal of segmentation is to extract important features from images. Segmentation of an image can also be seen, in practice, as the classification of each image pixel to be assigned to one of the image compositions.

Different segmentation methods have been presented include the dynamic system modeling based approach [3] performs pixel clustering operations in a parallel manner to speed-up the segmentation process. The cellular neural network scheme [4, 5] segments the spots by performing a number of operations such as background clean-up, grid analysis, irregular spot elimination, and intensity analysis. The morphology based approach [6] uses a series of optional steps to segment the microarray image. The combination of Markov random field based grid segmentation and active contour modeling constitutes an approach suitable for spot detection and segmentation [7]. The two-stage clustering based approach [8] is comprised of spots‟ boundaries adjusting and intensity-based partitioning operations. The use of adaptive thresholding and statistical intensity modeling is the base for some segmentation schemes [9], whereas another approach [10] uses a seeded region growing algorithm to identify spots of different shapes and sizes. Histogram and thresholding operations were used to classify microarray image samples into either foreground (spots) or background pixels [11].

One of the key steps in extracting information from a microarray image is the segmentation whose aim is to identify which pixels within an image represent which gene. This task is greatly complicated by noise within the image and a wide degree of variation in the values of the pixels belonging to a typical spot. A comparison between four different segmentation methods are presented on a noisy microarray image, with high accuracy. The paper is organized as follows: a brief introduction is presented in this section, section 2 presents the used materials, section 3 summarizes the proposed segmentation methods for various cDNA microarray noisy images and section 4 discusses the results of the applied algorithms on microarray data set image. Conclusions are presented in section 5.

2 Materials

Different images have been selected from two different data sets, to test the performance of the proposed methods. They have different scanning resolutions, and different noise types, in order to study the flexibility of the proposed methods to detect spots with different sizes and features.

The images are stored in TIFF files with 16-bit gray level depth. A chosen microarray image with various kinds of artifacts or noises is drawn from Princeton University Microarray (PUMA) database [12].

The image includes thirty two sub-grids presenting acute lymphoblastic leukemia tissues (PUMA Experiment ID: 10223). The slide name is (shae082) and it is a cDNA microarrays spotted by a total of 24192 genes.

MATLAB [13] is used for data analysis and technical computing, as it is a high performance and powerful tool. MATLAB version is 6.5 on a windows XP platform. The P.C used has a processor: Intel Core r2 4300 CPU with 2GB of memory.

3 Methods

Once grids have been placed, discrimination between areas that are considered the spot signal and areas that are considered the background signal must be carried out. The process, by which each individual cell in the grid must be selected to determine the spot signal and to estimate the background hybridization, is called segmentation. That information will be put towards a quantitative measurement at each cell. There are four presented approaches for segmentation; fixed circle segmentation, adaptive circle segmentation, thresholding segmentation, and adaptive shape segmentation.

3.1 Fixed Circle Segmentation

Fixed circle segmentation method assigns all the spots the same size and shape. It uses a constant-diameter circle as the shape of all the spots in the image. The proposed fixed circle segmentation technique is presented as in the following steps:

1. *Input the gridded image.*
2. *Get the region of interest (R.O.I.).*
3. *Let: I = i^{th} row in the R.O.I.*
4. *I = 1 to end of R.O.I.*
5. *For each I, we calculate the center of its corresponding boundary box.*
6. *Draw a circle with the obtained center and the obtained estimated period (distance between two adjacent spots).*

3.2 Adaptive Circle Segmentation

Adaptive circle segmentation considers the shape of each spot as a circle, where the center and diameter of the circle are estimated for each spot. It involves two steps. First, the center of each spot needs to be estimated. Second, the diameter of the circle has to be adjusted. Adaptive Circle Segmentation method is shown in figure

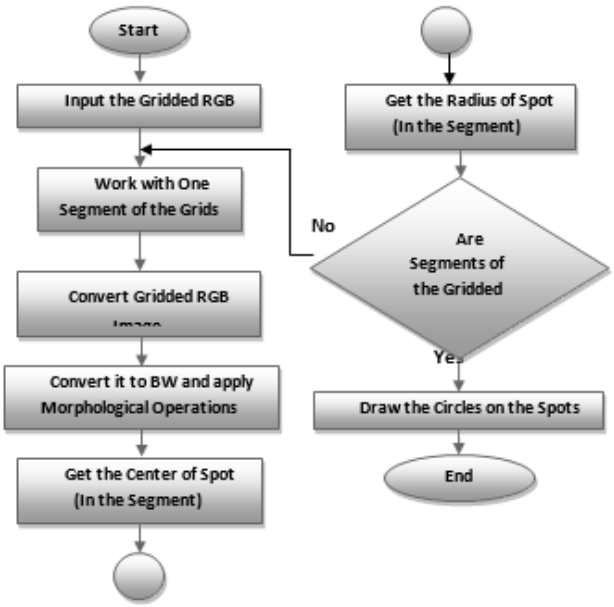

Figure 1 Flowchart of Adaptive Circle Segmentation

3.3 Thresholding Segmentation

The first step to start this technique is to apply a single threshold level to the whole image, so all spots are detected equally. However, it doesn't work so well due to the large differences in the spot brightness. One way to equalize large variations in magnitude is by transforming intensity values to logarithmic space. This works much better, but some weak spots are still missed. Alternatively, the bounding boxes can be used to determine local threshold values for each spot. For an overview of the Thresholding segmentation algorithm the reader is referred to figure 2

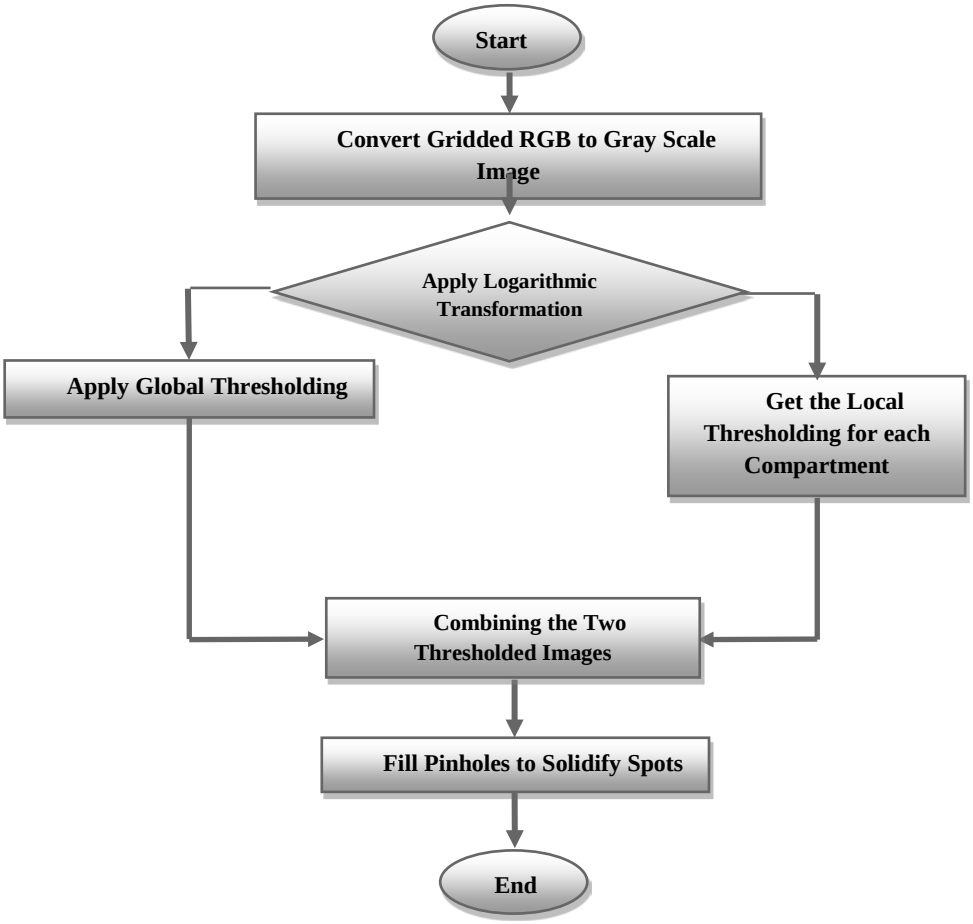

Figure 2 Flowchart of Thresholding Segmentation.

Unfortunately, results reveal that weak spots showed up well but spots with bright perimeters were as bad as the original global threshold before log space transformation. Since each of the local and the global thresholding has a special advantage, we combined the best of both approaches. These spot segmentation results were indeed much better.

The silhouettes of some spots still contained pinholes. The whole image could be filled using image filling operation, but this may not be a good idea. Notice that some spots run together. If four mutually adjacent spots (sharing a common corner) were all joined at their edges then a single function call would incorrectly fill in the common corner as well. To avoid that possibility, it is safer to fill each spot; take each bounding box region at a time by looping. Indeed, the spot segmentation now looks quite good [14].

3.4 Adaptive Shape Segmentation

Seeded region growing (SRG) is a common technique that deals with different shapes in image segmentation. In SRG, the regions grow outwards from the seed points, preferentially, based on the difference between the pixel value and the running mean of values in an adjoining region. This method requires an initial point to be known, which is called the *seed*. After obtaining the seeds, the process is repeated simultaneously for both foreground and background regions until all the pixels are assigned to either foreground or background. Those pixels that are adjacent to a region are assigned first according to its intensity. Figure 3 shows the steps of applying the method.

An important advantage of SRG method is that it can be applied to microarray images containing spots of any shape and size.

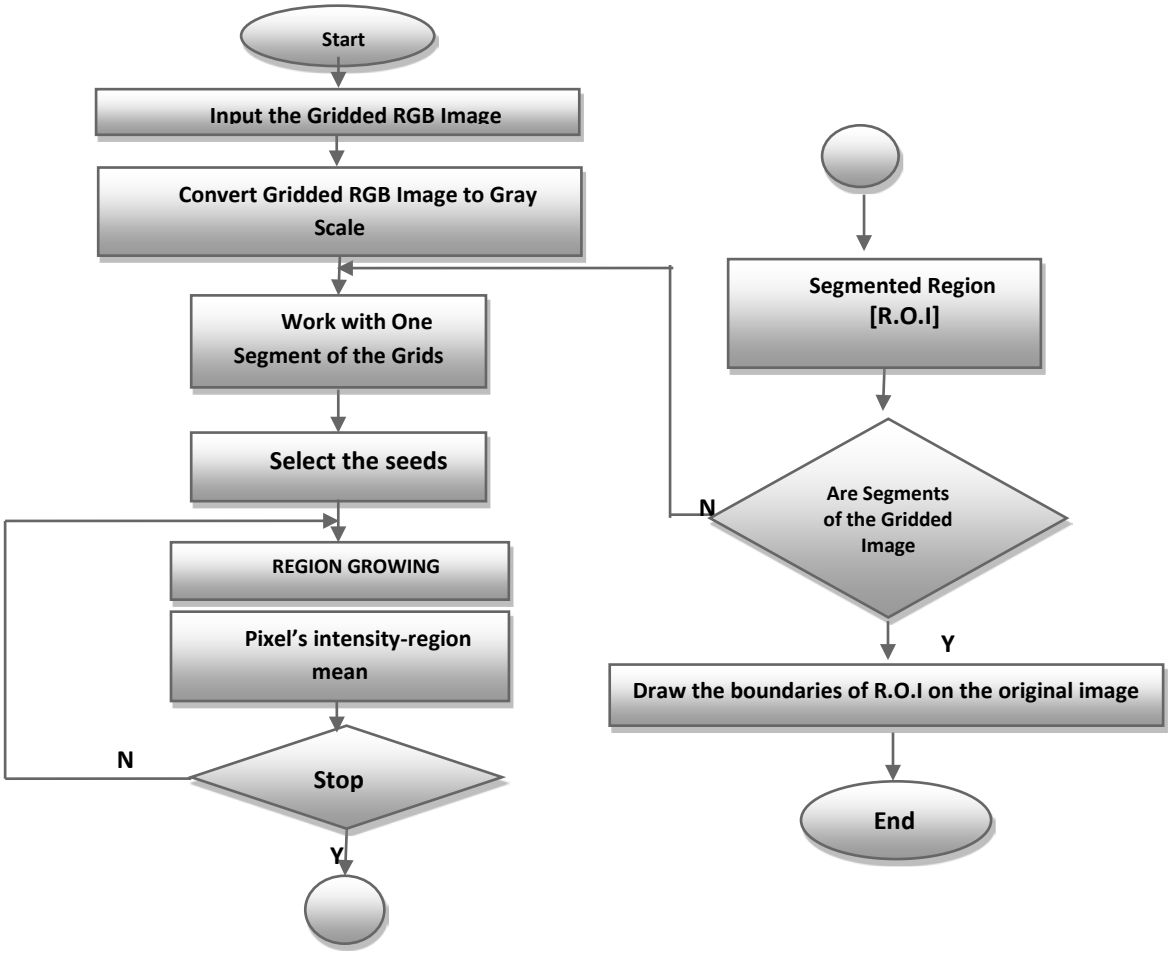

Figure 3 Flowchart of S.R.G. Segmentation

The seed; which is the initial point to start applying the method is determined automatically. The pixel which has the maximum intensity in the spot window: as that point should most probably one pixel of the inspected spot.

4 Results and Discussion

Four different segmentation methods were presented; Fixed Circle, Adaptive Circle, Thresholding, and Adaptive Shape Segmentation.

These presented segmentation methods are tested on a number of noisy microarray images drawn from Princeton University Microarray (PUMA) database. The results of applying these segmentation methods on a microarray image are shown in this section. The chosen noisy microarray image includes thirty two sub-grids (PUMA Experiment ID: 10223) and it is spotted by a total of 24192 genes. To test the efficiency of the proposed methods, a sub-array in the fourth row and the second column was cropped as shown in figure 4.

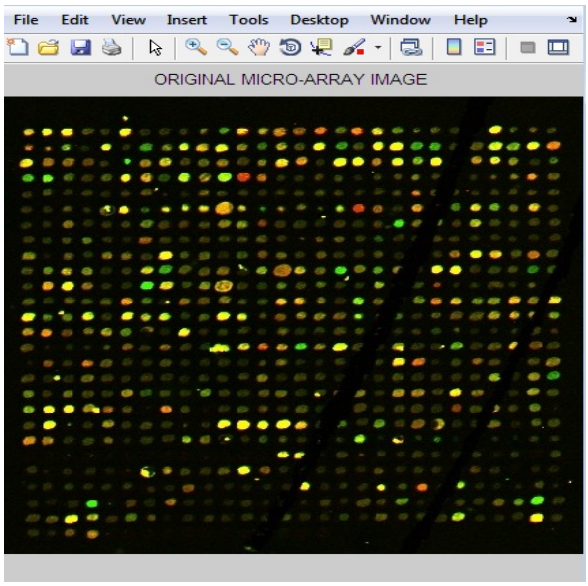

Figure 4: The Original Microarray Image

The accuracy of the proposed segmentation methods were analyzed by means of a statistical analysis [15]. A spot was "very efficiently segmented" if at least 90% of the entire spot area was enclosed in the contour of that spot.

Figure 5 shows the effect of applying the fixed circle segmentation method the microarray image, figure 6 shows the effect of applying the adaptive circle segmentation method on the microarray image, figure 7 to figure 12 show the effect of applying the thresholding segmentation method, and figure 13 shows the effect of applying the adaptive shape segmentation method.

4.1 Fixed Circle Segmentation

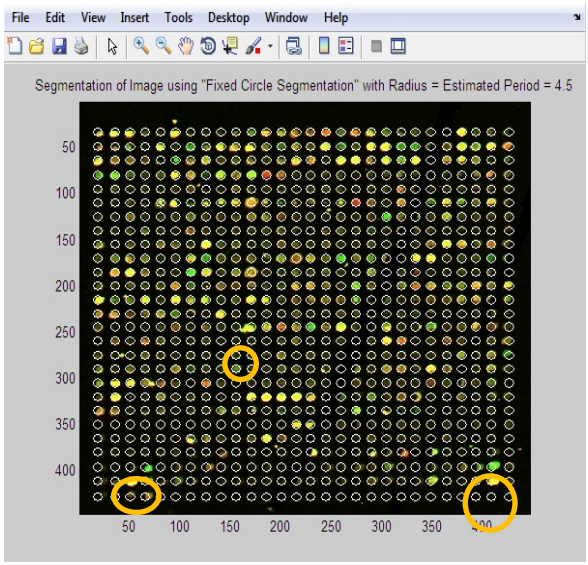

Figure 5: Image after Applying "Fixed Circle Segmentation" Method.

It was obviously shown that the fixed circle method clearly cannot satisfy the needs. Figure 5 shows the resulting image after applying the fixed circle approach. We can see that some regions within the high intensity areas (spots) are left out of the foreground, and some regions within the low intensity areas (background) are included in the foreground regions. That is because of the fixed diameter of all the drawn circles despite the variation in the diameters of the spots in the same image.

4.2 Adaptive Circle Segmentation

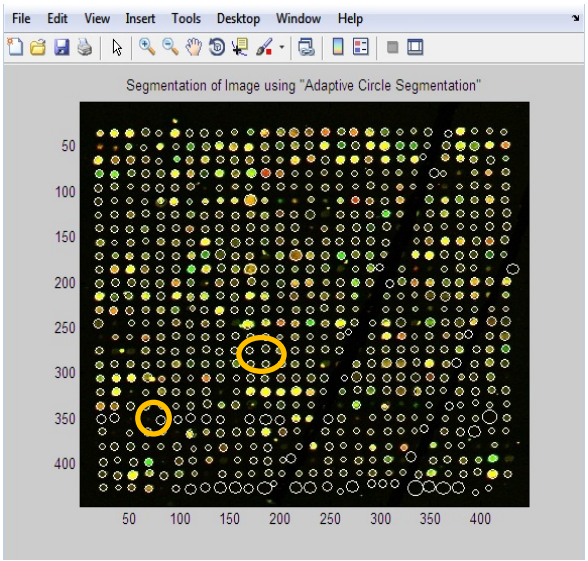

Figure 6: Image after Applying "Adaptive Circle Segmentation" Method.

The adaptive circle segmentation method achieves better results for circle-shaped spots. However, the spots in a microarray image can take shapes including ellipses. That is the main drawback of the adaptive circle segmentation method is that it restricts the shape, it's obvious in figure 6.

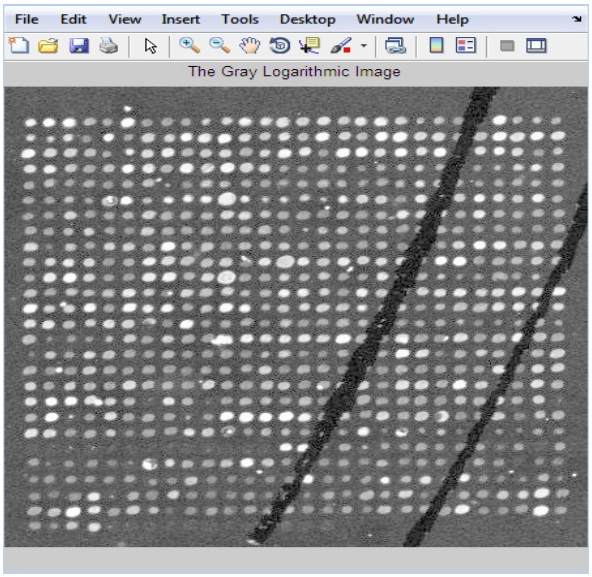

Figure 7: Gray Logarithmic Image

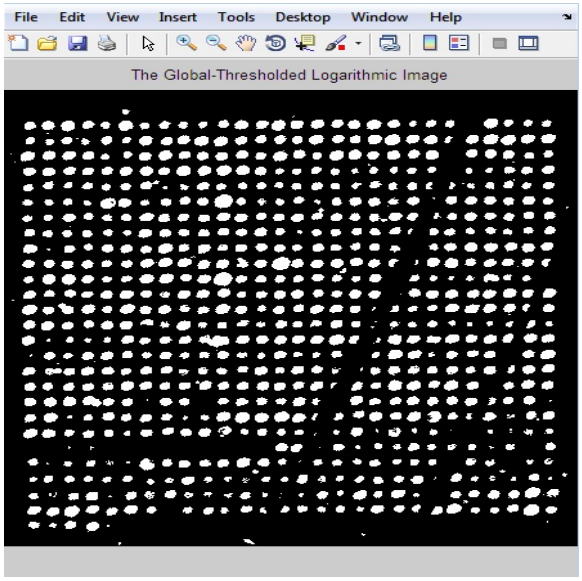

Figure 8: Image after Applying Global Thresholding

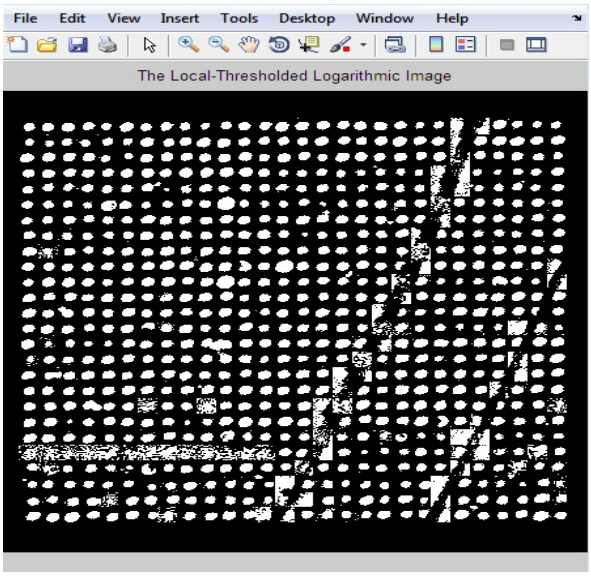

Figure 9: Image after Applying Local Thresholding

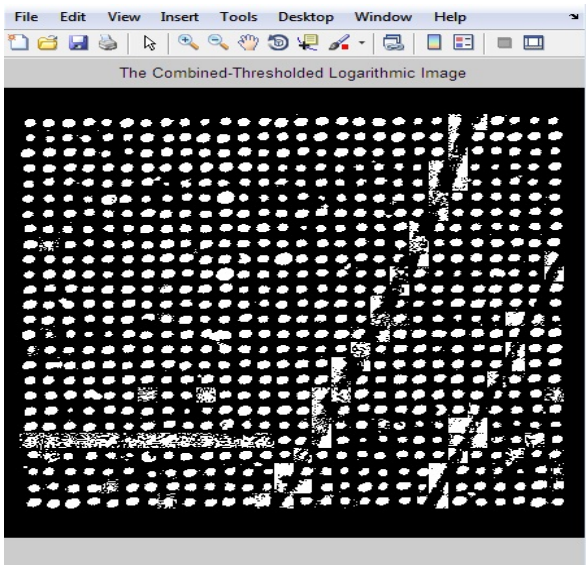

Figure 10: Image after Applying Combined- Thresholding

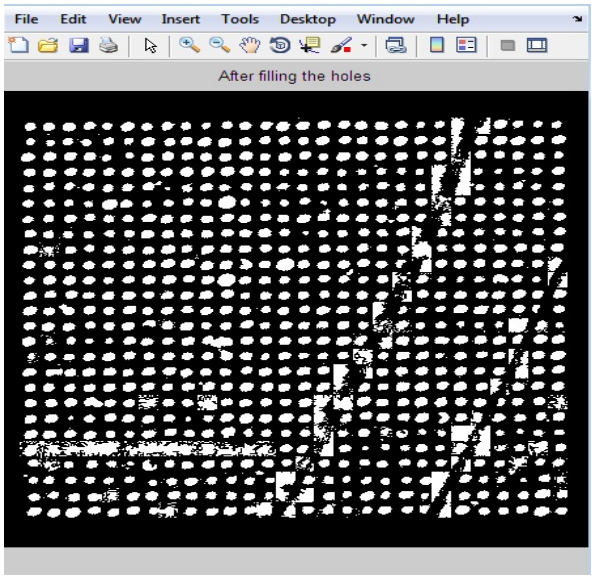

Figure 11: Image after Filling the Pinholes Method

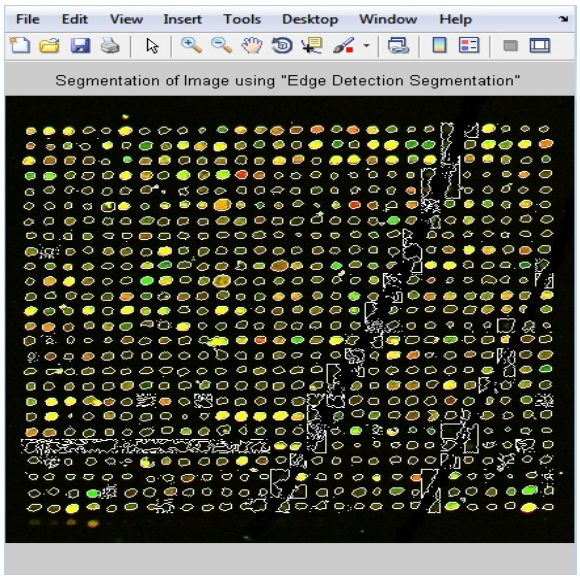

Figure 12: Image after Applying "Thresholding Segmentation" Method

Figure 7 to figure 12 show the results of applying thresholding segmentation on the microarray image. It is clearly observed that when using the current segmentation method to separate background from foreground in microarray images, it gives good results in the images that have clear spots. But it cannot deal well enough with weak spots.

4.3 Adaptive Shape Segmentation

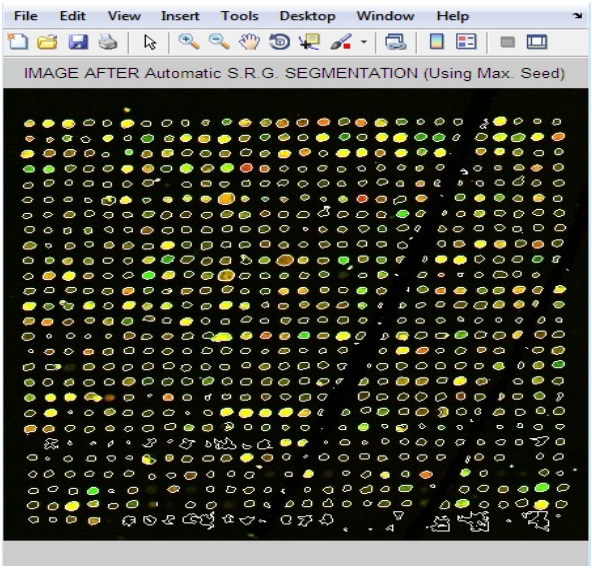

Figure 13: Image after Applying "Adaptive Shape Segmentation" Method.

Figure 13 shows the result of applying the adaptive shape segmentation method using a maximum seed point. This method requires an initial point to be known, which is called the seed. An advantage of using

SRG in microarray image segmentation is that the location of foreground pixels and background pixels can be estimated. It also deals with different shapes and sizes of spots.

The accuracy of the proposed methods was analyzed by means of a statistical analysis. More precisely, using the proposed approach, 91.5% of spots were "very efficiently segmented", and no spurious spot were detected. A spot was "very efficiently segmented" if at least 90% of the entire spot area was enclosed in the contour of that spot [15]. By comparing the results of applying the four presented segmentation methods; Fixed Circle Segmentation, Adaptive Circle Segmentation, Thresholding Segmentation, Adaptive Shape Segmentation methods, It is clearly obvious that the Adaptive Shape Segmentation method can segment noisy microarray images correctly despite of the degree of noise and the shape and size of the spots. That is shown in table 1.

Table 1: Comparison between the Four Proposed Segmentation Methods

Method	Accuracy	Segmented Percentage
Fixed Circle Segmentation	Good	79%
Adaptive Circle Segmentation	Very Good	86%
Thresholding Segmentation	Very Good	90%
Adaptive Shape Segmentation	Excellent	98%

5 Conclusion

The development of biomedical research has been led by the increasing knowledge as well as new advances in technology. Traditionally, researchers were able to investigate a small number of genes at a time by using the available techniques back then. DNA microarray technology has enabled biologists to study all the genes within an entire organism to obtain a global view of genes' interaction and regulation. This technology has a great potential in obtaining a deep understanding of the functional organization of cells. The emergence of this technology allows the researchers to tackle difficult problems and reveal promising solutions in many fields

In this respect, our research based heavily on the requirement for a reliable yet time efficient automated method. One of the key steps in extracting information from a microarray image is the segmentation whose aim is to identify which pixels within an image represent which gene. This task is greatly complicated by noise within the image and a wide degree of variation in the values of the pixels belonging to a typical spot.

This work emphasizes the impact of microarray image segmentation. In the segmentation stage, four segmentation methods have been presented; "fixed circle segmentation", "adaptive circle segmentation", "thresholding segmentation", and "adaptive shape segmentation" methods. When the four proposed methods sere compared, it was found that the first two methods are shape-based segmentation methods. Fixed circle segmentation cannot segment clearly all types of images; when the spots size varies in the image, it will works bad. While the adaptive circle segmentation method achieves better results for circle-shaped spots. The other two segmentation methods; "adaptive shape segmentation" and "thresholding segmentation" gives better results. When using "thresholding segmentation" to separate background from foreground in microarray images, the current methods

cannot deal well enough with weak spots. So, it was very clear that "adaptive shape segmentation" gives better results using a maximum seed.

REFERNCES

[1]. Istepanian, R., Microarray image processing: Current status and future directions. IEEE Tran. Nanobioscience, 2: 4, 2003

[2]. T. Asano, D. Chen, N. Katoh, T. Tokuyama. Polynomial-time solutions to image segmentation, *Proc. of the 7th Ann. SIAM-ACM Conference on Discrete Algorithms*, 104-113, 1996.

[3]. A. P. G. Damiance, L. Zhao, and A. C. P. L. F. Carvalho, A dynamic model with adaptive pixel moving for microarray images segmentation, Real-Time Imaging 10 (2004), 189-195.

[4]. P. Arena, M. Bucolo, L. Fortuna, and L. Occhipinty, Cellular neural networks for real-time DNA microarray analysis, IEEE Eng Med Bio 21 (2002), 17-25.

[5]. X. Y. Zhang, F. Chen, Y. T. Zhang, S. G. Agner, M. Akay, Z. H. Lu, M. M. Y. Waye, and S. K. W. Tsui, Signal Processing techniques in genomic engineering, Proc IEEE 90 (2002), 1822-1833

[6]. R. Hirata Jr, J. Barrera, R. F. Hashimoto, D. O. Dantas, and G. H. Esteves, Segmentation of microarray images by mathematical morphology, Real-Time Imaging 8 (2002), 491-505.

[7]. Katzer, M., Kummert, F. & Sagerer, G. (2003). Methods for automatic microarray image segmentation. IEEE Transactions on Nanobioscience, 2, 202-214.

[8]. R. Nagarajan, Intensity-based segmentation of microarrays images, IEEE Trans Med Imaging 22 (2003), 882-889.

[9]. A. W. C. Liew, H. Yana, and M. Yang, Robust adaptive spot segmentation of DNA microarray images, Pattern Recognit 36 (2003), 1251-1254.

[10]. Yang, Y.H., Buckley, M.J., Dudoit, S. & Speed, T.P. (2002). Comparison of Methods for Image Analysis on cDNA Microarray Data. Journal of Computational & Graphical Statistics, 11, 108-136.v

[11]. Y. Chen, E. Dougherty, and M. Bittner, Ratio-based decisions and the quantitative analysis of cDNA microarray images, J Biomed Opt 2 (1997), 364-374.

[12]. Princeton University Microarray Database (PUMA; http://puma.princeton.edu/)

[13]. Matlab (R2012b) Image Processing Toolbox, Signal Processing Toolbox.

[14]. Islam Fouad, Mai Mabrouk, Amr Sharawy, "A Fully Automated Method for Noisy cDNA Microarray Image Quantification", International Journal of Computers and Technology, Vol.11, No. 3, October 2013.

[15]. Dimitris Maroulis, Eleni Zacharia, Microarray Image Segmentation using Spot Morphological Model, IEEE, July, 2009.

SOCIETY FOR SCIENCE AND EDUCATION UNITED KINGDOM

JBEMi JOURNAL OF BIOMEDICAL ENGINEERING AND MEDICAL IMAGING

ISSN: 2055-1266
VOLUME 1, ISSUE 5

Recent Advances in Acquisition/Reconstruction Algorithms for Undersampled Magnetic Resonance Imaging.

Giuseppe Placidi
A²VI-Lab, c/o Dept. of Life, Health, and Environmental Sciences, University of L'Aquila, Via Vetoio Coppito L'Aquila, ITALY
giuseppe.placidi@univaq.it

ABSTRACT

Several applications of Magnetic Resonance Imaging (MRI), in particular dynamic MRI and functional MRI (fMRI), require rapid acquisition to measure dynamic processes changes. Experimental data are collected in the k-space by following different trajectories to cover the whole space. Complete data acquisition necessitates waiting for a fixed time interval: a reduced number of collected trajectories allows acquisition time reduction but undersampling occurs, often producing artefacts. In what follows, a review of methods for sparse sampling acquisition and reconstruction is presented.

In particular, a differentiation is done between sparse acquisition methods which do not use any restoration algorithm (artefacts are tolerated) and those methods for which a restoration algorithm is essential. The first class contains also methods where spatial information is shared between temporal images to reduce the collected data. In the second class of methods, a differentiation is done between those reconstruction/restoration methods that reduce artefacts independently of the sample shape, and those restoration methods that adapt their action by modifying the acquisition trajectories during the acquisition, i.e. the chosen trajectories (both in number and directions) are dependent on the sample shape. A third emerging class of methods, those including hybrid forms of the second class, are also reported.

1 Introduction

In conventional MRI, the number of collected data is determined by spatial resolution requirements and by the Nyquist criterion for the alias-free field of view (FOV) to obtain an image by fully-sampled k-space set. Recently, MRI has developed considerably into the direction of dynamic imaging opening up several new applications such as monitoring of contrast agent dynamics [[1]-[4]], mapping of human brain neural activity based on blood oxygenation level-dependent (BOLD) imaging contrast [[4]], MR-guidance of biopsies [[6]-[8]], monitoring of ablations [[9]-[11]], guidance of intravascular procedures [[12]-15], and real-time visualization of cardiac motion [16,17]. Although these developments are generally promising their application is limited by the compromise between temporal and spatial resolution. To improve temporal resolution many approaches use "undersampling".

DOI: 10.14738/jbemi.15.499
Publication Date: 29th September 2014
URL: http://dx.doi.org/10.14738/jbemi.15.499

The term undersampling indicates that the Nyquist criterion is not satisfied, at least in some regions of *k*-space, i.e. images are reconstructed by using a number of k-space samples lower than that theoretically required to obtain a fully-sampled image.

Undersampling is used for several reasons, such as reducing acquisition time [17-21] and motion artifacts [22], achieving higher resolution [23-25], and balancing the trade-off between spatial and temporal resolution [26,27]. Normally undersampling implies image artifacts, often in the form of aliasing or streak structures. Parallel imaging methods such as sensitivity encoding (SENSE) [28], simultaneous acquisition with spatial harmonics (SMASH) [29] and generalized auto calibrating partially parallel acquisition (GRAPPA) [30] also can be thought of as undersampling methods in which artifacts are removed by using information obtained from multiple RF coils and receivers. But, at the end of the process, a complete image is reconstructed through the partial information collected by different receivers.

Time required to fully sample 3D Cartesian *k*-space is relatively long. Alternative non-Cartesian trajectories can provide faster *k*-space coverage and more efficient gradients usage. When very fast volume coverage is required, undersampling strategies can be combined with non-Cartesian trajectories for further reduction of the scan time.

Undersampling can influence the resulting image in different ways depending on the k-space covering paths: Cartesian, radial, spiral, 2D, 3D, etc. (see Figures 1-3).

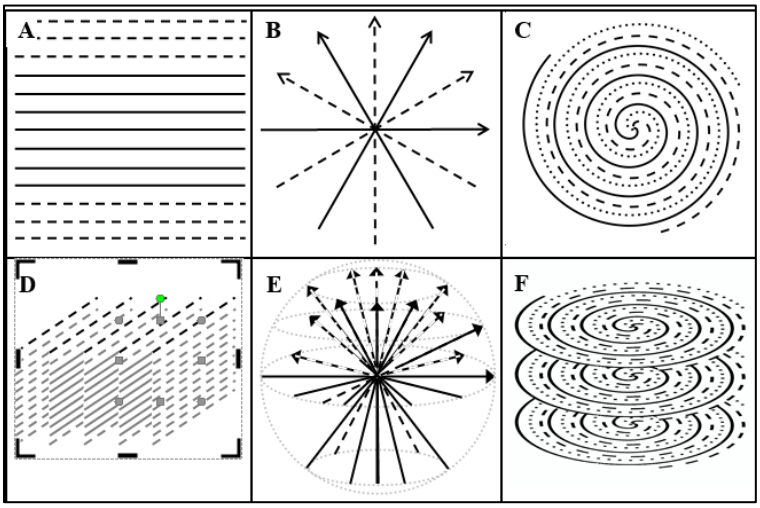

Figure 1. Sparse sampling in 2D (A-C) and 3D (D-F) settings: Cartesian (A, D), Radial (B, E) and Spiral (C, F) samplings. Measured trajectories are represented by continuous lines, missing trajectories are represented by dashed/dotted lines.

This implies that it can occur differently in different k-space regions. For example, when Cartesian sampling is used, undersampling occurs because some rows in the k-space rectangular grid are missing along the phase encoding direction (see Figures 1A and 1D); in case of radial acquisition, i.e. acquisition from projections, undersampling occurs because some radial directions in the k-space are missing (see Figures 1B and 1E). As will be clarified later, each of these cases requires a specific restoration algorithm, but all the methods afford the same problem: to reconstruct an image, suppose a 2D image

$\hat{f}(t_1,t_2)$, starting from some collected sparse samples of its Fourier coefficients, $\hat{f}|_\Omega$ while violating the Nyquist rate. In this paper, a review of the most effective sparse sampling and restoration strategies for solving the previous problem are reported. In particular, a differentiation is done between sparse acquisition methods which do not use any restoration algorithm (artifacts are tolerated) and the sparse acquisition methods for which a restoration algorithm is essential (this differentiation is defined by a temporal transition). The first class of methods contains also those methods that use temporal correlation between dynamic images (when temporal resolution is required) as a sort of restoration algorithm: some k-space coefficients are collected just once and shared by the whole set of dynamic images. The decision to include these methods among those of the first class is that no mathematical strategy is used to estimate the missing coefficients: the missing k-space coefficients are supplied from a reference image to the whole set of dynamic images. In the last class of methods, a differentiation is done between those that adapt their strategy to a given acquisition method, trying to reduce artifacts independently of the sample shape, and those that start their action by modifying the acquisition trajectories during acquisition, i.e. the acquisition trajectories (both in number and in directions) depend on the sample shape. Finally, hybrid methods, that are emerging by those allowing to the second class, are presented.

2 Sparse Methods without Restoration

The method proposed by Liao et al. [22] uses a variable-density stack of spiral trajectories which varies the sampling density both along the *kx-ky* plane and the *kz* direction. The method is shown to preserve reasonable image quality while reducing the acquisition time by approximately half compared to a fully-sampled stack of spirals. Vastly undersampled 3D projections are used to increase temporal resolution and provide better dynamic information for 3D contrast-enhanced angiography (CE)-MRA. Aliasing caused by undersampling in this method often can be tolerated because the vessel-tissue contrast is high. In [32] variable density k-space sampling trajectories are used to restrict the violation of the Nyquist criterion to the outer part of the k-space. Spiniak et al. [20] use an efficient undersampling method for a progressive missile guidance trajectory. The purpose of this work is to examine *k*-space undersampling in conjunction with the shells trajectory. The shells method is a non-Cartesian 3D *k*-space trajectory [33]: fully sampled concentric spherical shells are used for 3D selective RF pulse design [34]. The same sampling strategy is used for a single *k*-space shell acquisition that acts as a spherical navigator echo for motion tracking [35]. A full 3D *k*-space shells acquisition is implemented in [36] and it is demonstrated to have motion correction properties in [37].

Because the shells trajectory does not acquire data on the “corners” of *k*-space, it offers a volume coverage reduction compared to a fully-sampled 3D Cartesian acquisition. This is substantially larger than the *k*-space volume coverage reduction obtained by skipping views in the phase encoded corners of a Cartesian 3D acquisition. The shells trajectory samples *k*-space on the surfaces of a series of concentric spheres. In reference [38] interleaved helical spirals sweep on the surface of each shell from one pole to another (see Figure 2).

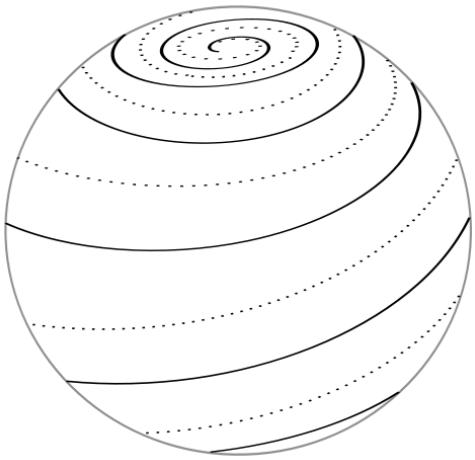

Figure 2. Shells *k*-space trajectories. Spiral interleaves, coded by continuous and dotted lines respectively, sweep from one pole to the other of a spherical surface. In an undersampling scheme, some interleaves are skipped, for example that represented by a dotted line.

The shells acquisition method is a true center-out trajectory in 3D *k*-space, in that it starts from the origin of the *k*-space and extends progressively to the periphery. An important property of the shells trajectory is that a large number of interleaves exclusively collect data from the periphery without crossing the center of *k*-space. Because the number of interleaves varies on a per-shell basis, there is flexibility in controlling the sampling density as a function of the *k*-space radius. These properties suggest that the shells trajectory is well suited for undersampling design. The way used to implement undersampling for the shells trajectory method is to remove selected interleaves within a shell. This method is proven to be an optimal balance between acquisition time reduction, undersampling artifacts reduction and edges preservation.

In PROPELLER (periodically rotated overlapping parallel lines with enhanced reconstruction) [39,40], data acquisitions consist in a multiple-shot fast spin-echo approach in which several parallel k-space lines are collected in each time of repetition (TR), forming a blade that is then rotated around its center and acquisition is repeated to cover the k-space (see Figure 3).

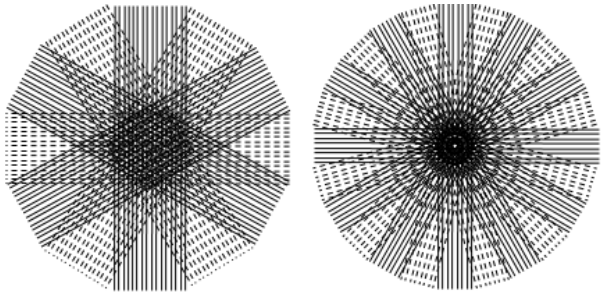

Figure 3. Different PROPELLER k-space sampling patterns. In particular: (A) shows a 6 blades scheme, each blade composed by 16 lines; (B) shows a 12 blades scheme, each blade composed by 8 lines. Undersampling is realized by skipping dotted blades.

The acquisition is radial. PROPELLER imaging is an MRI data acquisition and reconstruction that is attracting due to its greatly reduced sensitivity to various source of image artifacts (first of all motion artifacts). In ref. [41] PROPELLER is used in undersampled form and the resulting artifacts are studied.

Other methods utilize information redundancy from temporal correlations of dynamic images as a sort of restoration. Keyhole methods [42,43], selective acquisitions [44, 45] and reduced-encoding MR imaging by generalized series reconstruction (RIGR) [46] assume temporal variation is primarily from the central portion of k-space. In the keyhole fMRI technique [47,48], a full k-space reference image is acquired for each cycle and for each activation state. To reduce acquisition time, the strategy for the other images in each cycle consists of sampling only a central fraction of the k-space (low k-space data). The missing peripheral lines in the k-space (high k-space data) are supplied from the reference images. In this way, an approximately 60% in acquisition time per image can be saved for T_2^*-weighted gradient-echo schemes. The resultant keyhole fMRI images retain nearly all the functional information of the original high spatial resolution images while substantially reducing the acquisition time [48]. However, two potential problems, associated with the keyhole technique, may affect the reconstructed images: noise correlation between different images and discontinuities. Because of data sharing, high k-space data are the same for all the keyhole images. Therefore, noise between images is correlated. When statistical analysis is performed across a series of images to assess significant activations, the shared k-space data will decrease the effective sampling size and result in a higher noise level.

Regarding discontinuities, the basic principle of the keyhole technique is to combine the dynamic low k-space data with the reference high k-space data. Due to the “image to image” signal fluctuation, amplitude and phase discontinuities may exist at the junction of the high k-space and the low k-space data. These discontinuities may result in artifacts and spatial resolution reduction. A detailed description of the effects of the key-hole method can be found in [49].

Clinical practice shows that a high spatial resolution is essential for most dynamic imaging applications. To this purpose, some technique increases temporal and/or spatial resolution by directly exciting the region of interest, such as the zoomed imaging technique [50]. Beyond finding the optimal compromise between temporal resolution, spatial resolution and SNR for a specific application, it is desirable to find ways to introduce some *additional* information into the imaging process and so to truly enlarge the amount of information available without spending additional measuring time. In this sense, reduced field-of-view (rFOV) reconstruction utilizes the fact that only a limited region of an image undergoes substantial variation over time [51,52]. The idea of rFOV is to exploit the fact that dynamic changes in an image series may be confined to a certain area (rFOV) within the full FOV. This information can be used to increase temporal resolution in fluoroscopic imaging without sacrificing spatial resolution. Having been demonstrated first for Cartesian sequences [[51]] it is applicable to any segmented k-space acquisition scheme as radial [53-55] or spiral imaging [56]. The principal limitation of such a technique is that erroneous results will be produced if some of the additional information is wrong or the required conditions are not filled, e.g., if dynamic changes of the object *outside* the rFOV do occur. Because in clinical practice it will generally be difficult to strictly satisfy such conditions, it is important to evaluate the respective robustness of the different implementations of the rFOV technique. The projection-reconstruction rFOV approach (PR rFOV) has been demonstrated to be more robust than the other rFOV

approaches. The greater robustness is a consequence of the special aliasing properties of projection-reconstruction imaging and is considered to be crucial for clinical applications.

Both Keyhole and rFOV methods are based on the fact that the information from relatively stationary regions in object space is considered to be redundant.

The method UNFOLD (UNaliasing by Fourier-encoding the Overlaps using the temporaL Dimension) [57,58] supposes that data have to be collected both in spatial and in temporal directions: the same image has to be reconstructed more times to reproduce temporal variations occurring inside it. UNFOLD uses the t axis of k–t space to resolve information normally encoded along the k axes. In some dynamic applications in which the time axis is not efficiently exploited by conventional encoding, such a reorganization of k–t space can lead to a significant decrease in acquisition time for the temporal frames. In this case, spatial aliased versions of the same image (each image having a determined phase shift offset) are collected: spatial aliasing is eliminated by separating overlapped information through the temporal Fourier transform. This can lead to a temporal resolution improvements by nearly a factor of two in cardiac-triggered imaging, and by as much as a factor of eight in fMRI. Image reconstruction process requires aliasing elimination (through temporal Fourier transform) before the spatial Fast Fourier Transform. Depending on the situation, the acquisition time reduction of a temporal frame can be translated into a reduction of the total imaging time, into an improvement of the spatial or temporal resolution, or into an increase in the spatial coverage. The reduction can also be used to allow a faster pulse sequence to be replaced by a slower one while preserving time resolution. This method cannot be used to improve spatial resolution when temporal data are not necessary or not available.

Temporal acceleration can be achieved with the k-t broad-use linear acquisition speed-up technique (k–t BLAST), which uses training data as prior information along with the interleaved sampling function [59]. Conceptually, UNFOLD and k-t BLAST reduce the information redundancy by economically using k–t space (the combination of k-space with a time axis [60]). Originally, k-t BLAST has been used with Cartesian k-space trajectories [59,60], due to the simplicity of describing and correcting for the aliasing produced by rectilinear sampling patterns. After that, it has been also presented as a non-Cartesian sampling/reconstruction method [61]. However, spiral readouts are appropriate for certain applications [62] because they have good flow properties and are time efficient, which enables further increases in spatial and/or temporal resolution when combined with under sampling techniques. Shin et al. [63] solve elegantly the problem for spiral trajectories. An improvement to the UNFOLD method is proposed in [64] where UNFOLD is combined with the under sampled 3D stack of spirals acquisition [65] to increase spatial coverage for high resolution fMRI.

3 Sparse Methods with Restoration

3.1 Sample Independent Acquisition/Restoration Methods

A first group includes those methods where the redundancy sources are inherent properties of the image but the image properties (for example sparseness or symmetries) are not used while performing data acquisition.

Placidi et al. [66] describe an algorithm which is effective in reducing truncation artifacts due to missing k-space samples in MRI. The algorithm works first by filling the incomplete matrix of coefficients with

zeroes and then adjusting, through an iterative process, the missing coefficients by performing a reduction of the undersampling artifacts before the image reconstruction through a Fourier Transform method [67]. Then, this set of coefficients is used as a basis for a superresolution algorithm that estimates the missing coefficients by modeling data as a linear combination of increasing and decreasing exponential functions, through the Prony's method. The Prony's method consists on the interpolation of a given data set with a sum of exponential functions: the MRI signals can be well represented as a sum of exponential functions and the missing data can be extrapolated by this representation. The algorithm performs very well, both for Cartesian missing rows scheme (phase-frequency acquisitions) and for radial-missing angle (acquisition from projections) undersampling, but it requires some computational overhead. A simpler variation of this method is reported in [68] where a simple constraint for iterative reconstruction, capable to deal with any sparse acquisition method, is used. The methodology herein suggested is based on the attempt to fill in the missing complex k-space values iteratively, making the assumption that the image has to be zero outside a compact support. This approach transforms the original problem into an interpolation problem in the complex domain. The novelty is that it deals with iterative interpolation in the k-space based on the elimination of the artifacts from an extended support of the reconstructed image. The results, simulating different sparse acquisition strategies (Cartesian, radial, and spiral sampling), are not significantly different from those obtained from other, more complicated, iterative methods [66]. Residual artifacts are reduced by using the method reported in [69].

During the last few years, the emerging theory of compressive (or compressed) sensing (CS) [70-74] has offered great insight into both when and how a signal may be recovered to high accuracy (or, for some instances, exactly) even when sampled significantly below the Nyquist rate.

CS requires the measurement of a relatively small number of "random" linear combinations of the signal values (much smaller than the number of signal samples nominally defining it). However, because the underlying signal is compressible, the nominal number of signal samples is a gross overestimate of the "effective" number of "degrees of freedom" of the signal. As a result, the signal can be reconstructed with good accuracy from relatively few measurements by a convex constrained optimization procedure. In MRI the sampled linear combinations are simply individual Fourier coefficients (k-space samples) and CS can be used. In that setting, CS is claimed to be able to make accurate reconstructions from a small subset of k-space, rather than an entire k-space grid. The original paper by Candès et al. [70] is dedicated at random undersampling of Fourier coefficients that is the practical situation of MRI. In order to reconstruct a complete image from the undersampled problem, the simpler strategy assumes that the Fourier coefficients at all of the unobserved frequencies are zero (thus reconstructing the image of "minimal energy" under the observation constraints). This method does not perform very well because the reconstructed image, has severe non local artifacts caused by angular undersampling [70]. A good reconstruction algorithm, it seems, would have to guess the values of the missing Fourier coefficients, i.e. to interpolate $\hat{f}\left(\omega_1,\omega_2\right)$. However, the prediction of Fourier coefficients from their neighbours are very delicate, due to the global and highly oscillatory nature of the Fourier transform. The prediction can be more efficiently done through convex optimization. To recover f from partial Fourier samples, a solution f^* is found for the optimization problem

$$\min \|g\|_{TV} \text{ subject to } \hat{g}(\boldsymbol{\omega}) = \hat{f}(\boldsymbol{\omega}) \text{ for all } \boldsymbol{\omega} \in \Omega \quad (1)$$

Where $\|g\|_{TV}$ represents the total-variation norm of a 2D object g that, for discrete data $g(t_1, t_2)$, 0 $\leq t_1, t_2 \leq$ N-1, has the following form

$$\|g\|_{TV} = \sum_{t_1,t_2} \sqrt{|D_1 g(t_1,t_2)|^2 + |D_2 g(t_1,t_2)|^2} \quad (2)$$

and

$$D_1 g = g(t_1,t_2) - g(t_1 - 1, t_2), \; D_2 g = g(t_1,t_2) - g(t_1, t_2 - 1)$$

As it is, this technique allows just to reduce artifacts with respect to zero filling of the missing Fourier coefficients (with the exception of the first example reported in [70]). To allow an accurate reconstruction, though in presence of a certain undersampling degree, it is necessary to fill three requirements:

Transform sparsity: the desired image should have a sparse representation in a known transform domain (i.e., it must be compressible by a transform coding).

Incoherence of undersampling artifacts: the artifacts in linear reconstruction caused by *k*-space undersampling should be incoherent (noise like) in the sparsifying transform domain.

Nonlinear reconstruction: the image should be reconstructed with a nonlinear method that enforces both sparsity of the image representation and consistency of the reconstruction with the acquired samples.

The first condition ensures the unknown image can be represented with a lower number of coefficients than that required by Nyquist criterion. MR images meet the first condition. The second condition ensures the position of the sampled coefficients is casual, i.e. they are collected without a specific, deterministic, pattern: this allow the undersampling artifacts have to be distributed as uncorrelated noise. Incoherence is important: MR acquisition can be designed to achieve incoherent undersampling. The third condition is ensured by the presented non-linear reconstruction method. More details on this very promising method applied to MRI can be found elsewhere [73,74]. Though very promising, CS can be efficiently applied if the undersampling is not too different from the Nyquist's rate. In fact, most CS applications, especially within medical imaging, have centred on the l_1-minimization problem due to the fact that the corresponding l_0-minimization problem is untractable. An interesting recent improvement of CS regards the proposal of an innovative Homotopic l_0-Minimization [75]. In this paper [75], Trzarsko et al. describe a method for reconstructing MR images at sampling rates even further below that which are achievable using l_1-based CS methods by directly attacking the ideal l_0-minimization problem. The l_0-minimization problem is described along with both its applied and theoretical implications. Moreover, a practical scheme is presented for addressing the l_0 quasi-norm based on homotopic approximation using a wide class of deformable sparse priors, and an efficient semi-implicit numerical scheme for computation is described. The authors demonstrate both the problem tractability and the goodness of

their results, when compared to the classical l_1-based CS methods, in spite of a reduction of the used samples for reconstruction.

Knopp et al. [76] present interesting results about the iterative reconstruction from non-uniform k-space sampled data though data sparsity is not reflecting CS requirements. In particular, they discuss about the effectiveness of using non-equispaced FFT to reconstruct images directly from radial or spiral directions, through a generalization of the gridding process [77]. Very accurate results are obtained by using an iterative method to estimate density compensation weights, taking the result of gridding as a starting point. The best gridding results are obtained using the more expensive Voronoi weights. However, substantial improvement of the reconstruction quality is achieved during a small number of iterations for all used trajectories and weights. It should be very interesting to use the method they proposed for image reconstruction from severely undersampled data.

Also Block et al [78] afford the problem of severely undersampled radial data in an iterative way with the usage of a total variation (TV) constraint for the final image to reduce the strike artifacts produced by radial undersampling: also in this case the sparse samples do not fill the CS requirements. The reconstruction is obtained as a non-linear optimization problem, solved through the conjugate gradient method. The conjugate gradient method is an iterative two-step scheme, which is repeated until a satisfying solution has been found. First, a search direction is estimated and, second, a line search into that direction is performed until the minimum of the functional in this direction has been identified. The search direction is obtained by calculating the gradient at the actual estimate and by superposing it with the prior search direction scaled by a factor that guarantees the conjugacy of successive search directions. At every step of the algorithm, the actual image estimate is mapped to the frequency domain. It is then compared how well the estimate fits to the measured data by calculating the difference. If the estimate is good enough, then the residuum vector contains only small entries, otherwise it contains large entries. In this case, the algorithm needs to know how to modify the image estimate in order to improve the match of the samples in the frequency domain. This information is obtained by mapping the residuum back to the image space. The reconstruction of an undersampled radial image through optimization still leads to streaking artifacts: the procedure does not measure the accuracy of the estimate at any other position in k-space than at the positions of the measured k-space coefficients. Being an underdetermined problem, more than one solution exist. To overcome this limitation, a penalty function is introduced into the optimization problem, based on the total variation constraint. The basic assumption of this idea is that the object consists of areas with constant (or only mildly varying) intensity, which applies quite well to medical tomographic images. If the object is piecewise constant, then the best representation of all image estimates that match at the spoke positions should be given by the one with the lowest derivatives at all pixel positions, that is the one minimizing the total variation, represented as the summation of the modules of the image second order derivatives (as discussed by the authors, the choice for the best derivative order still remain a debated argumentation). The obtained results are quite good regarding artifacts reduction, but some blurring occurs.

3.2 Sample Adaptive Acquisition/Restoration Methods

Different approaches are based on driving the acquisition process in order to adapt the collected signals to the sample shape. As first example of these methods, Contreras et al. [79] propose a sparse sampling

method for MRI non-destructive analysis of woods logs, taking advantage of the log cylindrical symmetry by acquiring transverse 1-D projections with a helical and undersampled pattern. Linear interpolation is used to estimate the skipped data and slice images are reconstructed by filtered back-projection. The sequence is improved using selective multi-pass scanning, without major variations of the scan time. The technique is particularly useful for tree logs, since they present several characteristics that can be used to reduce the long scan time, but similar techniques can be also studied for MRI in humans.

Placidi et al. [80-82] present an adaptive acquisition technique for MRI from projections, first defined in the image space [80] and then in the k-space [81,82], to reduce the total acquisition time by collecting just the most informative projections, without any a-priori information about the sample, but using information about the sample collected while acquisition proceeds. This is possible through the calculation of a function, called the entropy of a projection, which is able to measure the information content of the projections during the acquisition process, useful to discover sample internal symmetries, smooth or regular shape. In the k-space method [82] the entropy function is defined on the power spectrum of the projections. The process starts by measuring the projections at four regular orientations: 0°, 45°, 90°, and 135°. Then the evaluation of the information content of these four initial projections is performed, followed by the selection of new angles where the information content is maximum. The entropy of the power spectrum of each of these starting projections is evaluated and the next projection is measured between the two where the entropy function has a maximum. The procedure is repeated until the difference in entropy remained above a given threshold. The method makes it possible to reduce the total acquisition time, with little degradation of the reconstructed image, adapting itself to the arbitrary shape of the sample (being able to catch eventual internal symmetries, low dynamic range and regular shape). The choice of, approximately, the most informative projections is made during the acquisition process, taking into account the information content of the previous projections. The method allows the acquisition of a near optimal set of projections, close to the most informative set of projections composed by the minimum number of projections, but not the optimal one. In fact, though very effective in reducing the acquisition time and undersampling artifacts, this method suffers from the following limitations: some important projections can be excluded from the acquired set, especially in the proximity of entropy function minima or maxima; some redundant projections can be collected, especially in the proximity of entropy function sharp variations. An effective application of the previous adaptive acquisition method has been also presented as a medical image compression strategy [83].

The method described in [84] considers the problem of measuring exactly the most informative set of projections by collecting a-priori information about the sample through the preliminary measurement of two circular paths at different distances from the k-space centre. The idea behind the algorithm is that the power spectrum of a standard MR image is mainly distributed along particular radial k-space directions. These directions often terminate before the k-space border has been reached. Some of them do not start from the k-space centre and extend to the k-space border. In order to take into account these opposite situations, a set of preliminary circular trajectories are collected. The circular trajectories allows the interception of the most important projections. By analyzing the collected data, it is possible to establish the desired set of projections before the image acquisition starts. For this reason, the acquisition process consists of the preliminarily collection of two concentric circular trajectories having

the centre in the image k-space centre. The directions of the most informative projections can then be set by using the information acquired from the power spectra of these paths of coefficients. In particular, from the logarithm (used to reduce differences in scale) of the power spectra of the collected trajectories, the mean values are calculated and maxima above the mean value, in both curves, are used to indicate the presence of the most informative radial directions. The set of these angular directions is considered to be the optimal, most informative, set of projections to be collected in a standard way. Thought they require some preliminary time to collect the necessary information about the optimal angle set before the acquisition of radial projections started and, in some case, specialized hardware, the adaptive algorithms allow both the improvement in image quality and the reduction of the number of k-space coefficients with respect to other, non-adaptive, methods. Near optimal acquisition parameters are priory studied and set by using a numerical MRI simulation algorithm [85]. The adaptive methods proposed in [80-84] use a restoration/reconstruction method based on FFT and nearest neighbor interpolation [86]. Nearest neighbor interpolation is justified by the fact that close measured projections are very similar because of the used adaptive acquisition methods.

In principle, both sampling/reconstruction strategies, CS and the adaptive, appear reasonably, but it seems that they have to be considered separately. The question arising in the last period is to verify the possibility of using the characteristics of CS in an adaptive way. The advantage would be twofold. Classical CS, being a completely random sampling strategy that not uses information about the sample shape, needs that a minimum, fixed, number of samples is collected in order to avoid undersampling artifacts: the use of information about the sample shape furnished by an adaptive acquisition technique could reduce the number of necessary samples and to reach a near optimal, image dependent, value. On the other side, by verifying that for the adaptively collected samples the previously reported CS requirements (constraints) are satisfied, a CS non-linear reconstruction procedure could be used on these samples in order to obtain otimal image reconstruction. The possibility of using an hybrid, adaptive-CS, sampling strategy is, for the first time, proposed in [87], where it has been verified that the adaptively, radially collected, samples verify the CS constraints and a L1-norm based non-linear reconstruction can be used to obtain very accurate image reconstruction. After that, in [88,89], an alternative adaptive-CS method is presented that combines random sampling of Cartesian trajectories with an adaptive 2D acquisition of radial projections. It is based on the evaluation of the information content of a small percentage of the k-space data collected randomly to identify radial blades (similar to those used in PROPELLER [39,40]) of k-space coefficients having maxi-mum information content. The information content of each direction is evaluated by calculating an entropy function defined on the power spectrum of the projections. Besides that, the images are obtained by using a non linear reconstruction strategy, based on the homotopic L0-norm [75], on the sparse data. The method overcomes classical weighted CS in image quality, though a lower number of collected samples is used. The use of homotopic L0-norm minimization makes possible to obtain better reconstructions than by simple L1-norm. The same method is also applied on cardiac MRI data in [90] and very impressive results are obtained. Though the adaptive-CS method is capable to reduce the number of necessary samples below that required by classical CS, this number is still far to be optimal and can be further reduced. Work is currently in progress in order to verify how to reduce this number and how to apply the adaptive CS also to other sampling strategies (for example, pure cartesian, or spiral).

4 Conclusions

Recently MRI has developed considerably into the directions of dynamic imaging and fMRI opening up several new fields of application, in particular referring to real-time imaging. Although these developments are generally promising their application can be limited by the compromise between temporal and spatial resolution. In order to improve temporal resolution, many sampling approaches use undersampling.

A review of the most effective methods for sparse sampling acquisition and reconstruction, with the aim of reducing the undersampling artifacts, have been presented. In particular, methods have been classified in two classes: those acquisition methods which do not use any restoration algorithm and those methods for which a restoration algorithm is essential.

A first consideration which can be made is that methods allowing to the second class are more complicated than those allowing to the first class but, in general, they perform better. Further considerations regard the last class of methods. In fact, it has been divided in two sub-classes: those reconstruction/restoration methods that reduce artifacts independently of the sample shape, and those acquisition/reconstruction/restoration methods that adapt their action by modifying the trajectories during the acquisition, i.e. the chosen trajectories (both in number and directions) are dependent on the sample shape. To the first subclass of methods allows also Compressed Sensing, a very breakthrough technique which, for some extends, appears as counterintuitive: images can be almost exactly reconstructed by a sparse set of its Fourier coefficients, below the Nyquist requirements, if they are compressible and the collected coefficients are casually collected in the k-space plane. The second subclass contains some adaptive methods: they allow a strong reduction of the collected data if the k-space paths are collected through the most informative directions (coefficients with maximum energy). Both CS and Adaptive methods require the images to be compressible, but they are completely different regarding the acquisition directions: in the first data are collected casually, in the second data are collected along the “most informative” directions, where energy is maximum. Hybrid methods, adaptive-CS strategies, are currently under investigation in order to obtain near optimal image reconstruction (as ensured by CS) with a reduced number of collected samples (as ensured by an adaptive sampling strategy).

REFERENCES

[1]. B.R.Rosen, J.W.Belliveau, D.Chien, “Perfusion imaging by nuclear magnetic resonance”. *Magn. Reson. Q*. 5:263–281; (1989).

[2]. N.Wilke, C.Simm, J.Zhang, J.Ellermann, X.Ya, H.Merkle, G.Path, H.Ludemann, R.J.Bache, K.Ugurbil, “Contrast-enhanced first pass myocardial perfusion imaging: Correlation between myocardial blood flow in dogs at rest and during hyperemia”, *Magn. Reson. Med.* 29:485– 497; (1993).

[3]. V.M.Runge, J.F.Timoney, N.M.Williams, “Magnetic resonance imaging of experimental pyelonephritis in rabbits”, *Invest. Radiol.*, 32,696 –704; (1997).

[4]. A.H.Wilman, S.J.Riederer, B.F.King, J.P.Debbins, P.J.Rossman, R.L.Ehman, "Fluoroscopically triggered contrast-enhanced three-dimensional MR angiography with elliptical centric view order: Application to the renal arteries". *Radiol.* 205:137–146; (1997).

[5]. K.K.Kwong, J.W.Belliveau, D.A.Chesler, I.E.Goldberg, R.M.Weisskoff, B.P.Poncelet, D.N. Kennedy, B.E.Hoppel, M.S.Cohen, R.Turner, "Dynamic magnetic resonance imaging of human brain activity during primary sensory stimulation". *Proc. Natl. Acad. Sci. USA*. 89:5675–5679; (1992).

[6]. R.Lufkin, L.Teresi, L.Chiu, W.Hanafee, "A technique for MR guided needle placement". *Am. J. Roentgenol*. 151:193–196; (1988).

[7]. D.A.Leung, J.F.Debatin, S.Wildermuth, N.Heske, C.L.Dumoulin, "Real-time biplanar tracking for interventional MR imaging procedures". *Radiology* 197:485– 488; (1995).

[8]. G.Adam, J.M.Neuerburg, A.Bucker, A.Glowinski, D.Vorwerk, a.Stargardt, J.Jvan Vaals, R.W.Gunther, "Interventional MR: First clinical experiments on a 1.5T system combined with C-arm fluoroscopy". *Invest. Radiol.* 32:191–197; (1997).

[9]. F.A.Jolesz, A.R.Bleier, P.Jakab, P.W.Ruenzel, K.Huttl, G.J.Jako, "MR imaging of laser tissue interaction". *Radiology* 168:249 –253; (1988).

[10]. R.Matsumoto, A.M.Selig, V.M.Colucci, F.A.Jolesz, "MR monitoring during cryotherapy in the liver: Predictability of histologic outcome". *J. Magn. Reson. Imag.* 3:770 –776; (1993).

[11]. J.Kettenbach, S.G.Silverman, K.Kuroda, Y.Nakajima, G.P.Zientara, P.Saiviroonporn, N. Hata, P.R.Morrison, S.G.Hushek, D.Gering, P.McL.Black, R.Kikinis, F.A.Jolesz, "Real-time monitoring and quantitative analysis of MR-guided laser ablations". In: Book of abstracts: Fifth Annual Scientific Meeting and Exhibition. ISMRM; 523, (1997).

[12]. C.L.Dumoulin, S.P.Souza, R.D.Darrow, "Real-time positioning of invasive devices using magnetic resonance". *Magn. Reson. Med.* 29:411– 415; (1993).

[13]. A.Glowinski, G.Adam, A.Bucker, J.M.Neuerburg, J.J.van Vaals, R.W.Gunther, "Catheter visualization using locally induced actively controlled field inhomogeneities". *Magn. Reson. Med*. 38:253–258; (1997).

[14]. G.Placidi, D.Franchi, L.Marsili, P.Gallo, "Development of an auxiliary system for the execution of vascular catheter interventions with a reduced radiological risk; system description and first experimental results", Comp. Meth. Progr. Biomed. 88 (2), 144-151, (2007).

[15]. G.Placidi, D.Franchi, A.Maurizi, A.Sotgiu, "Review on Patents about Magnetic Localisation Systems for in vivo Catheterizations", Recent Patents on Biomedical Engineering 2 (1), 58-64, (2009).

[16]. A.B.Kerr, J.M.Pauly, B.S.Hu, K.C.Li, C.J.Hardy, C.H.Meyer, A.Macovski, D.G.Nishimura, "Real-time interactive MRI on a conventional scanner". *Magn. Reson. Med.* 38:355–367; (1997).

[17]. V.Rasche, D.Holz, R.Proksa, "MR Fluoroscopy Using Projection Reconstruction Multi-Gradient-Echo (prMGE) MRI". *Magn. Reson. Med.* 42:324–334; (1999)

[18]. J.H.Lee, B.A.Hargreaves, B.S.Hu, D.G.Nishimura, "Fast 3D imaging using variable-density spiral trajectories with applications to limb perfusion". *Magn Reson Med*; 50:1276–1285, (2003).

[19]. G.J.Marseille, R.de Beer, M.Fuderer, A.F.Mehlkopf, D.van Ormondt, "Nonuniform phase-encode distributions for MRI scan time reduction". *J. Magn Reson B*; 111:70–75, (1996).

[20]. J.Spiniak, A.Guesalaga, R.Mir, M.Guarini, P.Irarrazaval, "Undersampling k-space using fast progressive 3D trajectories". *Magn Reson Med*; 54:886–892, (2005).

[21]. K.Scheffler, J.Hennig, "Reduced circular field-of-view imaging", *Magn Reson Med*; 40:474–480, (1998).

[22]. J.R.Liao, J.M.Pauly, T.J.Brosnan, N.J.Pelc, "Reduction of motion artifacts in cine MRI using variable-density spiral trajectories". *Magn Reson Med*; 37:569–575, (1997).

[23]. D.C.Peters, F.R.Korosec, T.M.Grist, W.F.Block, J.E.Holden, K.KVigen, C.A.Mistretta, "Undersampled projection reconstruction applied to MR angiography". *Magn Reson Med*; 43:91–101, (2000).

[24]. D.M.Spielman, J.M.Pauly, C.H.Meyer. "Magnetic resonance fluoroscopy using spirals with variable sampling densities". *Magn Reson Med*;34:388–394, (1995).

[25]. J.H.Gao, J.Xiong, S.Lai, E.M.Haacke, M.G.Woldorff, J.Li, P.T.Fox. "Improving the temporal resolution of functional MR imaging using keyhole techniques". *Magn Reson Med*; 35:854–860 (1996).

[26]. K.K.Vigen, D.C.Peters, T.M.Grist, W.F.Block, C.A.Mistretta "Undersampled projection-reconstruction imaging for time-resolved contrast-enhanced imaging". *Magn Reson Med*; 43:170–176, (2000).

[27]. A.V.Barger, W.F.Block, Y.Toropov, T.M.Grist, C.A.Mistretta, "Time resolved contrast-enhanced imaging with isotropic resolution and broad coverage using an undersampled 3D projection trajectory". *Magn Reson Med*; 48:297–305, (2002).

[28]. K.P.Pruessmann, M.Weiger, M.B.Scheidegger, P.Boesiger. "SENSE: sensitivity encoding for fast MRI". *Magn Reson Med*;42:952–962, (1999).

[29]. D.K.Sodickson, W.J.Manning, "Simultaneous acquisition of spatial harmonics (SMASH): fast imaging with radiofrequency coil arrays". *Magn Reson Med*;38:591–603, (1997).

[30]. M.A.Griswold, P.M.Jakob, R.M.Heidemann, M.Nittka, V.Jellus, J.Wang, B.Kiefer, A.Haase, "Generalized autocalibrating partially parallel acquisitions (GRAPPA)," *Magn. Reson. Med.*, 47, 1202–1210, (2002).

[31]. D.R.Thedens, P.Irarrazaval, T.S.Sachs, C.H.Meyer, D.G.Nishimura, "Fast magnetic resonance coronary angiography with a three-dimensional stack of spirals trajectory". *Magn Reson Med*;41:1170–1179, (1999).

[32]. C.M.Tsai, D.G.Nishimura, "Reduced aliasing artifacts using variable density k-space sampling trajectories", *Magn Reson Med*;43:452– 458, (2000).

[33]. P.Irarrazaval, J.M.Santos, M.Guarini, D.Nishimura, "Flow properties of fast three-dimensional sequences for MR angiography". *Magn Reson Imag.*;17:1469–1479 (1999)

[34]. S.T.Wong, M.S.Roos, "A strategy for sampling on a sphere applied to 3D selective RF pulse design", *Magn Reson Med*;32:778–784, (1994).

[35]. E.B.Welch, A.Manduca, R.C.Grimm, H.A.Ward, Jr.C.R. Jack, "Spherical navigator echoes for full 3D rigid body motion measurement in MRI", *Magn Reson Med*;47:32–41 (2002).

[36]. Y.Shu, A.M.Elliott, S.J.Riederer, M.A.Bernstein, "3D RINGLET: spherical shells trajectory for self-navigated 3D MRI". In: Proceedings of the 13th Annual Meeting of ISMRM, Miami Beach, FL, USA, 2693, (2005).

[37]. Y.Shu, S.J.Riederer, M.A.Bernstein, "Motion correction properties of the shells k-space trajectory". *Magn Reson Imag.*, 24:739–749, 2006.

[38]. Y.Shu, S.J.Riederer, M.A.Bernstein, "Three-Dimensional MRI with an Undersampled Spherical Shells Trajectory", *Magn. Reson. Med.* 56:553–562 (2006)

[39]. J.G.Pipe, "Motion correction with PROPELLER MRI: Application to head motion and free-breathing cardiac imaging". *Magn Reson Med*, 42, 963–969 (1999)

[40]. J.G.Pipe, V.G.Farthing, K.P.Forbes, "Multishot diffusion-weighted FSE using PROPELLER MRI". *Magn Reson Med*, 47, 42–52 (2002).

[41]. K.Arfanakis, A.A.Tamhane, J.G.Pipe, M.A.Anastasio, "k-Space Undersampling in PROPELLER Imaging", *Magn. Reson. Med.*, 53, 675–683 (2005)

[42]. J.J.van Vaals, M.E.Brummer, W.T.Dixon, H.H.Tuithof, H.Engels, R.C.Nelson, B.M.Gerety, J.L.Chezmar, J.A.den Boer, "Keyhole method for accelerating imaging of contrast agent uptake," *J. Magn. Reson. Imag.*, 3, 671–675, (1993).

[43]. R.A.Jones, O.Haraldseth, T.B.Muller, P.A.Rinck, A.N.Oksendal, "K-space substitution: A novel dynamic imaging technique," *Magn. Reson. Med.*, 29, 830–834, (1993).

[44]. S.Di Giuseppe, G.Placidi, J.Brivati, M.Alecci, A.Sotgiu, "Pulsed EPR imaging: image reconstruction using selective acquisition sequences", Phys. Med. Biol., 44, N137-N144, (1999).

[45]. D.Franchi, A.Sotgiu, G.Placidi, "A novel acquisition–reconstruction algorithm for surface magnetic resonance imaging", Magn. Reson. Imag, 26 (9), 1303-1309, (2008).

[46]. A.G.Webb, Z.P.Liang, R.L.Magin, P.C.Lauterbur, "Applications of reduced-encoding MR imaging with generalized-series reconstruction (RIGR)," *J. Magn. Reson. Imag.*, 3, 925–928, (1993).

[47]. J.Tintera, G.Schaub, J.Gawehn, P.Stoeter, "Functional MRI with keyhole technique". *Human Brain Mapping* s1: 124; (1995).

[48]. J.H.Gao, J.Xiong,; S.Lai,; E.M.Haacke, M.G.Woldorff, "Improving the temporal resolution of functional MR imaging using keyhole techniques". *Magn. Reson. Med.* 35:854–860; (1996).

[49]. J.Xiong, P.T.Fox, J.H.Gao, "The effects of k-space data undersampling and discontinuities in keyhole functional MRI". *Magn. Reson. Imag.*, 17, 109–119, (1999)

[50]. J.J.van Vaals, G.H.van Yperen,; R.W.de Boer, "Real-time MR imaging using the LoLo (Local Look) method for interactive and interventional MR at 0.5T and 1.5T". In: Book of abstracts: Second Annual Meeting of the Society of Magnetic Resonance Imaging. SMR; 421, (1994).

[51]. X.Hu, T.Parrish, "Reduction of field of view imaging". *Magn. Reson. Med.* 31:691– 694; (1994).

[52]. M.E.Brummer, D.Moratal-Perez, C.Y.Hong, R.I.Pettigrew, J.Millet-Roig, W.T.Dixon, "Noquist: Reduced field-of-view imaging by direct Fourier inversion," *Magn. Reson. Med.*, 51, 331–342, (2004).

[53]. K.Scheffler, J. Hennig, "Reduced Circular Field-of-View Imaging." In: Book of abstracts: Sixth Annual Scientific Meeting and Exhibition. ISMRM; 180, 1998.

[54]. S.Weiß, V.Rasche, "Projection-Reconstruction Reduces FOV Imaging", *Magn. Reson. Imag.*, 17, 517–525, (1999)

[55]. D.C.Peters, M.A.Guttman, A.J.Dick, V.K.Raman, R.J.Lederman, E.R.McVeigh, "Reduced Field of View and Undersampled PR Combined for Interventional Imaging of a Fully Dynamic Field of View", *Magn. Reson. Med.*, 51, 761–767 (2004).

[56]. H.Sedarat, A.B.Kerr, J.M.Pauly, D.G.Nishimura, "Partial-FOV reconstruction in dynamic spiral imaging," *Magn. Reson. Med.*, 43, 429–439, (2000).

[57]. B.Madore, G.H.Glover, N.J.Pelc, "Unaliasing by Fourier-encoding the overlaps using the temporal dimension (UNFOLD), applied to cardiac imaging and fMRI", *Magn. Reson. Med.*, 42, 813–828, (1999).

[58]. J.Tsao, "On the UNFOLD method," *Magn. Reson. Med.*, 47, 202–207, (2002).

[59]. J.Tsao, P.Boesiger, K.P.Pruessmann, "k-t BLAST and k-t SENSE: dynamic MRI with high frame rate exploiting spatiotemporal correlations," *Magn. Reson. Med.*, 50, 1031–1042, (2003).

[60]. Q.S.Xiang R.M.Henkelman, "K-space description for MR imaging of dynamic objects," *Magn. Reson. Med.*, 29, 422–428 (1993).

[61]. M.S.Hansen, C.Baltes, J.Tsao, S.Kozerke, K.P.Pruessmann, H.Eggers, "k–t BLAST reconstruction from non-Cartesian k–t space sampling," *Magn. Reson. Med.*, 55, 85–91, (2006).

[62]. C.H.Meyer, B.S.Hu, D.G.Nishimura, A. Macovski, "Fast spiral coronary artery imaging," *Magn. Reson. Med.*, 28, 202–213, (1992).

[63]. T.Shin, J.F.Nielsen, K.S.Nayak, "Accelerating Dynamic Spiral MRI by Algebraic Reconstruction From Undersampled k–t Space", *IEEE Trans. Med. Imag.*, 26, 917-924, (2007)

[64]. Y.Hu, G.H.Glover, "Increasing Spatial Coverage for High-Resolution Functional MRI", *Magn Reson Med*, 61:716–722 (2009)

[65]. Y. Hu, G.H.Glover, "Three-dimensional spiral technique for high-resolution functional MRI", *Magn Reson Med*;58:947–951, (2007).

[66]. G.Placidi, A.Sotgiu, "A novel restoration algorithm for reduction of undersampling artifacts from Magnetic Resonance Images", *Magn. Reson. Imag.*, 22, 1279-1287, (2004).

[67]. G.Placidi, M.Alecci, S.Colacicchi, A.Sotgiu, "Fourier reconstruction as a valid alternative to filtered back projection in iterative applications: implementation of Fourier spectral spatial EPR imaging", *J. Magn. Reson.*, 134, 280-286, (1998).

[68]. G.Placidi, **"**Constrained Reconstruction for Sparse Magnetic Resonance Imaging", *Proc. WC2009*, September 7-12, Munich, Germany (2009).

[69]. G.Placidi, M.Alecci, A.Sotgiu, "Post-processing noise removal algorithm for magnetic resonance imaging based on edge detection and wavelet analysis", Phys. Med. Biol., 48 (13), 1987-1995, (2003).

[70]. E.Candès, J.Romberg, T.Tao, "Robust uncertainty principles: Exact signal reconstruction from highly incomplete frequency information". *IEEE Trans Inf Theory*, 52, 489–509, (2006).

[71]. D.Donoho, "Compressed sensing". *IEEE Trans Inf Theory*, 52, 1289–1306, (2006)

[72]. E.Candès and T.Tao, "Near optimal signal recovery from random projections: Universal encoding strategies?" *IEEE Trans. Inform. Theory,* 52, pp.5406–5425, (2006).

[73]. M.Lustig, D.Donoho, J.M. Pauly, "Sparse MRI: The Application of Compressed Sensing for Rapid MR Imaging", *Magn Reson Med*, 58, 1182–1195 (2007)

[74]. M.Lustig, D.L.Donoho, J.M.Santos, J.M.Pauly, "Compressed Sensing MRI", *IEEE Sign. Proc. Magazine*, 72-82, (2008)

[75]. J.Trzasko, A.Manduca, "Highly Undersampled Magnetic Resonance Image Reconstruction via Homotopic l_0-Minimization", *IEEE Trans. Med. Imag.*, 28, 106-121, (2009)

[76]. T.Knopp, S.Kunis, D.Potts, "A Note on the Iterative MRI Reconstruction from Nonuniform *k*-Space Data", *Intern. J. Biomed. Imag.*, 2007, 1-9, (2007).

[77]. J.D.O'Sullivan, "A fast sinc function gridding algorithm for Fourier inversion in computer tomography," *IEEE Trans. Med. Imag.*, 4, 200–207, (1985).

[78]. K.T.Block, M.Uecker, J.Frah, "Undersampled Radial MRI with Multiple Coils. Iterative Image Reconstruction Using a Total Variation Constraint", *Magn Reson Med*, 57, 1086–1098, (2007)

[79]. I.Contreras, A.Guesalga, M.P.Fernandez, M.Guarini, P.Irarrazaval, MRI fast tree log scanning with helical undersampled projection acquisitions, *Magn. Reson. Imag.*, 20, 781–787, (2002)

[80]. G.Placidi, M.Alecci, A.Sotgiu, "Theory of Adaptive Acquisition Method for Image Reconstruction from Projections and Application to EPR Imaging", *J. Magn. Reson., Series B*, 108, 50-57, (1995).

[81]. G.Placidi, M.Alecci, A.Sotgiu, "Metodo perfezionato di acquisizione di dati nel dominio della frequenza spaziale per la ricostruzione di immagini bidimensionali, in particolare di risonanza magnetica nucleare, e relativo apparato", Italian Patent No. RM98A000217, Issued April 3, (1998).

[82]. G.Placidi, M.Alecci, and A.Sotgiu, "ω-Space adaptive Acquisition Technique for Magnetic Resonance Imaging from Projections", *J. Magn. Reson.*, 143, 197-207, (2000).

[83]. G.Placidi, "Adaptive compression algorithm from projections: Application on medical greyscale images", Comp. Biol. Med., 39 (11), 993-999, (2009).

[84]. G.Placidi "Circular Acquisition to Define the Minimum Set of Projections for Optimal MRI Reconstruction" *Lecture Notes in Computer Science*, 6026, 254-262 (2010).

[85]. G Placidi, M Alecci, A Sotgiu, "A general Algorithm for Magnetic Resonance Imaging Simulation: a Versatile Tool to Collect Information about Imaging Artefacts and New Acquisition Techniques", Studies in health technology and informatics, 13-17, (2002).

[86]. G.Placidi, M.Alecci, A.Sotgiu, "Angular Space-Domain Interpolation for Filtered Back Projection Applied to Regular and Adaptively Measured Projections". *J. Magn. Reson., Series B*, (110), 75-79, (1996).

[87]. G.Placidi, "MRI: Essentials for Innovative Technologies", *CRC Press*, (2012).

[88]. L.Ciancarella, D.Avola, E.Marcucci, G.Placidi, A hybrid sampling strategy for Sparse Magnetic Resonance Imaging, Di Giamberardino et al. Editors, CRC Press, 285-289, (2012).

[89]. L.Ciancarella, D.Avola, G.Placidi, "Adaptive Sampling and Reconstruction for Sparse Magnetic Resonance Imaging", Computational Modeling of Objects Presented in Images, Lecture Notes in Computational Vision and Biomechanics, Springer, 15, 115-130, (2014).

[90]. G.Placidi, D.Avola, L.Cinque, G.Macchiarelli, A.Petracca, M.Spezialetti, "Adaptive Sampling and Non Linear Reconstruction for Cardiac Magnetic Resonance Imaging", Computational Modeling of Objects Presented in Images. Fundamentals, Methods, and Applications, Lecture Notes in Computer Science, 8641, 24-35, (2014).

SOCIETY FOR SCIENCE AND EDUCATION UNITED KINGDOM

JBEMi JOURNAL OF BIOMEDICAL ENGINEERING AND MEDICAL IMAGING

ISSN: 2055-1266
VOLUME 1, ISSUE 5

Role of Trace Elements in Duchenne Muscular Dystrophy

Sanjeev Kumar[1], Reena Mittal[2], Sweety[1] and D. C. Jain[3]

[1]Department of Physics, Central Medical Physics Research Laboratory,D.A.V. (P.G.) College, Muzaffar Nagar, U.P. (India).

[2]Deptt. of Mathematics, Shri.K.K.JAIN. College, Khatauli, Distt. Muzaffarnagar,U.P.India

[3]Department of Neurology, Safdarganj Hospital, New Delhi,

sanjeev1962kumar@yahoo.co.in; drdcjain@gmail.com; reena_math@rediffmail.com

ABSTRACT

Atomic absorption analysis involves measuring the absorption of light by vaporized ground state atoms and relating the absorption to concentration. The incident beam of light is attenuated by atomic vapour absorption according to Beer's Law. The estimation of trace elements show a colorful presentation of different metals. It has been seen and found that the levels of zinc and selenium were lower in DMD cases in comparison to healthy controls. The elements such as copper, calcium, iron, magnesium, potassium, sodium were found higher than controls. On the basis of statistical analysis we have measured regression and correlation coefficients including multiple correlation coefficients between different trace elements like Na, K, Ca, Mg, Zn, Cu, Fe and Selenium in normal samples. A trend has been found in coefficient of correlation such as $r_{\mathrm{CuZn}} > r_{\mathrm{NaK}} > r_{\mathrm{Zn.Se}} > r_{\mathrm{CuFe}}$ with positive correlation and $r_{\mathrm{ZnFe}} > r_{\mathrm{Fe.Se}} > r_{\mathrm{Cu.Se}} > r_{\mathrm{CaMg}}$ with negative correlation. Coefficient of partial correlation is also calculated and found that a trend has been set up between trace elements and given here as $r_{\mathrm{ZnFe.Cu}} > r_{\mathrm{ZnCu.Fe}} > r_{\mathrm{CuFe.Zn}} > r_{\mathrm{NaK.Ca}} > r_{\mathrm{CaNa.K}} > r_{\mathrm{CaK.Na}} > r_{\mathrm{NaK.Mg}}$ with positive correlation and we have found also a negative correlation between some of the elements and a trend is given here as $r_{\mathrm{ZnFe.Se}} > r_{\mathrm{MgK.Na}} > r_{\mathrm{MgNa.K}}$

Multiple correlation coefficient in normal healthy person has been estimated and found that a trend, which is given here as

$$R_{\mathrm{Zn.FeCu}} > R_{\mathrm{Fe.CuZn}} > R_{\mathrm{Cu.FeZn}} > R_{\mathrm{Zn.FeSe}} > R_{\mathrm{K.MgNa}} > R_{\mathrm{Mg.NaK}} > R_{\mathrm{Na.MgK}} > R_{\mathrm{K.NaCa}} > R_{\mathrm{K.NaCa}} > R_{\mathrm{Ca.KNa}}.$$

We have also measured correlation coefficients including multiple correlation coefficients between different types of trace elements like Na, K, Ca, Mg, Zn, Cu, Fe and Selenium in DMD samples. A trend has been found in coefficient of correlation such as $r_{\mathrm{CaMg}} > r_{\mathrm{FeZn}} > r_{\mathrm{NaK}} > r_{\mathrm{Cu.Se}}$ with positive correlation

DOI: 10.14738/jbemi.15.480
Publication Date: 28th October 2014
URL: http://dx.doi.org/10.14738/jbemi.15.480

and $r_{Fe.Se} > r_{CuFe} > r_{Zn.Se} > r_{CuZn}$ with negative correlation. Coefficient of partial correlation is also calculated and found that a trend has been set up between trace elements and given here as $r_{CuFe.Zn} > r_{CaNa.K} > r_{MgK.Na}$ with negative correlation and also found a trend of positive correlation as $r_{ZnFe.Cu} > r_{NaK.Ca} > r_{ZnFe.Se} > r_{NaK.Mg} > r_{CaK.Na} > r_{MgNa.K}$.

Multiple correlation coefficient in DMD patients has been estimated and found that a trend, which is given here as $R_{Fe.CuZn} > R_{K.NaCa} > R_{Zn.FeCu} > R_{Na.KCa} > R_{Zn.FeSe} > R_{K.MgNa} > R_{Cu.FeZn} > R_{Na.MgK} > R_{Ca.KNa} > R_{Mg.NaK}$.

Our findings suggest that the values of higher levels of trace elements should be adjusted such that these levels must slight below or equal to the normal limits of the particular element. The levels of zinc and selenium should be maintained within the normal limits for DMD cases in comparison to healthy controls. The elements such as copper, calcium, iron, magnesium, potassium, sodium may be reduced up to the normal limits in comparison to healthy persons.

Key Words: Duchenne muscular dystrophy, Trace elements, Flame atomic absorption, Multiple and partial correlation coefficiments and regression equations

1 Introduction

Humans are able to freely move their bodies about muscles, which is a precious, complex physiology that should not taken for granted. There are so many types of muscles in human body like voluntary and involuntary muscles and smooth and strained muscle fibers that all function in a tight realm with the nervous system and different chemical reactions.

Muscles are composed of protein in a highly organized system from large groups to small fibers. Muscle units are separated from other muscle groups by plasma membranes called sarcolemma and the cytoplasm, which is called sarcoplasm. There are long protein bundles within the sarcoplasm called myofibrils. There are so many ATP producing mitochondria, as well as glycogen and myoglobin. Bundles of paralled myofilaments make up the myofibrils where most of the action takes place. There are contractile proteins in the myofilaments, called myosin, and action. The myosin are thic filaments and actin thin filaments, when signald, the action and myosin interlock and slide over each other to stretch or slide into one another for contraction. They are signaled from the nervous system followed by a series of chemical reactions involving ATP, calcium, sodium and potassium ions.

There are many other proteins involved in the process. Abide from the contractile proteins, there are regulatory proteins called tropomyosin and troponin where act like a switch to determine when to contract and where to relax. On the muscle fiber the 'I band' is the space between the myosin (thick) filaments, where lies only the thin filaments. There is a dark disc in the middle of each 'I' band called 'Z disc'. This disc is made of titan. This is connected to sarcolemma by the cytoskeleton. As the muscle contracts the "I band' shrinks and the sarcomere shortens and as the Z disc's come closer together pulling on the sarcolemma shortening the cell. This is how the muscle contracts?

One of the most clinically important accessory proteins is dystrophin. This is located just under the sarcolemma in the cytoplasm in the area of the 'I band'. It is produced by specific genes and links the actin filaments to the protein extracellular matrix in the membrane known as the dystrophin associated protein complex.

Elements of the dystrophin gene and the protein structure have been completely identified. The exact functional role is still a bit unclear. It is thought that its primary function is to provide mechanical reinforcement to the structure of the sarcolemma and thereby protecting the membrane from the stress or tearing during contraction. If dystrophin is defective or absent, the membrane breaks down, which then substances and molecules like proteins and enzyme leak out the fibre into circulation. These enzymes and chemicals that leak out are responsible for certain chemical reactions and necessary to produce for muscle contraction. At the same time the extracellular substances leak into the fiber through the broken down membrane damaging the fiber and disrupting the process of muscle contraction and may cause irreparable damage. The absence or abnormality of dystrophin results in a condition known as muscular dystrophy (MD). Muscular dystrophny is a crippling disease resulting from mutated genes, which showly wastes away muscle tissue. It has been seen that without dystrophin to help to protect the fiber membrane keeping it intact, and assisting to create energy, the muscles begin to degenerate and atrophy, being replaced by fat and fibrous scar tissue creating fascia adhesions throughout the body. It is thought that the major determinate of the membrane damage would be the level of stress associated with contraction rather than the number of muscle actions. Petrof, B. *et. al.* [1] have given their thoughts to explain why it primarily affects the peripheral limbs? Muscular dystrophies most commonly involve in a genetic mutation in the dystrophin genes preventing the production of dystrophin or limiting the amount in subnormal levels. Generally in muscle tissue it has a normal value for small tares on the sarcolemma to occur as the muscle undergoes excessive strain and there are small molecules that enhance the natural repair process.

However in the absence of dystrophin, the sarcolemma is left unprotected tearing more frequently and more easily therefore muscle degeneration greatly out weights muscle regeneration eventually leading to death and adhesion of the tissue.

Emery, A.E. [2] has given his thought regarding muscular dystrophies, which are characterized by progressive irreversible degeneration process, which results in weakness and wasting of muscle tissue. The muscular dystrophies share clinical symptoms. These differ largely in severity, age of onset, and distribution of affected muscle tissue.

The mechanisms responsible for this divergence in pathology are still not identified in detail. It is useful to understand the basic anatomy of the nerve and muscle disorders. The nerve cells have bodies that contain a nucleus. The nucleus contains a genetic material, projection called dendrites that receive information from other nerves, and axons that transmit information to other nerves, ultimately, to muscles. Whether it be the limb, eyes, bladder, bowel, lungs, or heart, all body movements depend on or regulated by the action of nerves on muscle. The brain is made up of billions of nerve cells that communicate with each other by sending information across interconnecting axons and dendrites, i.e., by synapsing. Some nerve cells in the brain have long axons that leave the brain and descend in the spiral cord to synapse with the cell bodies of other nerves, the anterior horn cells, in the spinal cord. These cell bodies are found at each level of the spine. After receiving the information from the brain,

they send these informations down their axons (peripheral nerves) to communicate synapse with muscles in the limb, head and diaphragm. The axons of limbs peripheral nerves synapse with muscle cells across meet at a junction called myoneural junction.

By definition, neuropathies are diseases of nerves and myopathies are diseases of muscle. After cystic fibrosis, myopathies are the most commonly inherited diseases. Muscular dystrophies are myopathies and tend to progressive, with ongoing degeneration and regeneration of muscle fibers. Spinal muscular atrophy (SMA), amyotrophic lateral sclerosis (ALS) and polio myelitis are essentially diseases of the anterior horn cells of the spine. Bach, R .J.[3] has given views that people with SMA are born with fewer-than normal anterior horn cells of the spine. Neuromuscular diseases are diseases of the peripheral nerves (neuropathies and anterior horn cell diseases), the myoneural junctions (myasthenia gravis), or the muscles (myopathies) themselves can be understood with the detailing of these diseases. These conditions cause muscle weakness but do not affect sensory functions such as the ability to feel objects, see, hear, or smell, nor do they affect the autonomic nervous system that controls bladder and bowl function.

Every cell in the human body has forty eight chromosomes. Forty six chromosomes are autosomes and two are X or Y sex chromosomes. Forty six autosomes are twenty three pairs of chromosomes; one in each pair is inherited from each parent. Our entire genetic make-up is determined by the deoxyribonucleic acid (DNA) content of the hundreds of thousands of genes in each of the chromosomes. Defective genes result in many of the neuromuscular diseases.

Recessive diseases require that the abnormal gene by inherited from both parents. When an abnormal gene needs to be present on the autosome inherited from one parent only, the disorder is called autosomal dominant. Thus, neuromuscular diseases inherited from defective genes on autosomes are either autosomal recessive or autosomal dominant disorders. One of about every 40 – 60 adults carries the defective gene for SMA on one of his or her two number 5 chromosomes. For a child to inherit SMA, an autosomal recessive disorder, both mother or father must carry the defective gene and transmit it to the child. There is one out of four chance that a child of parent carriers of SMS will inherit the abnormal gene from both parents and develop SMA. There is a fifty percent chance that the child will be a carrier but not develop SMA. There will be twenty five percent chance that the child will neither be a carrier nor develop SMA. Children with SMA must inherit defective genes from both parents. For an autosomal dominant condition like facioscapulohumeral muscular dystrophy, on the other hand, only one parent's affected gene needs to be transmitted. Each patient must have one affected parent, and there is a fifty percent chance of each child inheriting the disease. Neuromuscular disease can also be inherited from defects on the X (Sex) chromosome. Children with sex-linked recessive disorders, such as Duchenne, Becker, and Emery-Dreifus muscular dystrophies, inherit a single defective gene on the X chromosome from the mother and a normal Y chromosome from the father. Because Y chromosome does not have the genetic material to offset the presence of the defect on the X-chromosome, the child inherits the disease. This is called sex-linked recessive disorder.

A female child with a defective X-chromosome from the mother and a normal X chromosome from the father does not develop the disease. She is a disease carrier who can transmit it to her own male children. When the mother is a carrier, her sons will have a fifty percent chance of being affected, while

her daughters will have the same chance of being heterozygous carriers. Mother's male relatives may be affected. A survey has been made and it has been reported in the literature that 70% of the carriers of the abnormal gene for Duchenne muscular dystrophy (DMD) actually have some degree of muscle weakness.

There are nine kinds of muscular dystrophies. These are classified by the depending on distribution of affected muscle groups, severity and prognosis, genetic defects and the means of inheritance. Duchenne muscular dystrophy is the most common and most severe. It affects not just all the voluntary muscles but also the heart and respiratory muscles as well shortening one's life span drastically. This type of dystrophy is due to genetic mutations on the twenty third chromosome, the sex determining chromosome, being an X linked recessive or sex-linked recessive trait. Therefore the males are affected from the gene passed down by their mothers. Mother was only a carrier.

Other types of dystrophies are those inherited through X-linked recessive trait are Becker and Emery-Dreifuss muscular dystrophy. Becker muscular dystrophy is a different mutuated gene. It is located on the same gene locus as Duchenne. This type of dystrophy affects the heart tissue in general. It is less severe. It has a longer life expectancy. Autosomal dominate trait may inherit in some different types of dystrophies. These are facioscapulohumeral, distal and occulopharyngeal muscular dystrophies as well as myotonic dystrophy. Facioscapulohumeral muscular dystrophy is caused by a missing piece of DNA on chromosome 4. This type of dystrophy affects the face, shoulders and upper arms but later affects certain muscles of the legs, the abdominal and pelvic girdle leading to extreme lordosis which may require a wheel chair. This type of dystrophy rarely affects the heart and respiratory muscles. It cannot short the span of life. The most of this type begins at the age of 20 years. It spreads very slowly due to rapid bursts of muscle deterioration.

Neuropathies and myopathies such as polymyositis and mysthania gravis are due to inflammatory or immunologic disorders that affect muscle. They can also appear in childhood and in many ways resemble inherited neuromuscular diseases. They are acquired rather than inherited conditions. There is no defect in the genes or chromosomes of patient of polymyosis or myasthenia gravis.

We are giving the details of Duchenne muscular dystrophy only because the exact theme of the work is to carry research as the approved and ethically committee cleared topic. We have chosen this topic to study different aspects of the DMD with spectroscopic tools of Science.

Duchenne muscular dystrophy is the most common neuromuscular disease.. A case of DMD was first reported in 1836 in Italy. It was recognized and described as an inherited disorder of boys by the English physician Meryan, E. [4] in 1852. The condition was in appropriately named after 'Duchenne'. Duchenne, G.B.A. [5] was a senior neurologist practicing in Paris. Duchenne was disparaged Meryan's work and first wrote about the condition in 1868. Duchenne at first confused it with cerebral palsy, poliomyelitis, and other conditions.

Although muscle strength may be slightly decreased from birth. Infants with DMD are thought to have no physical problems. It has been reported in the literature that the children with DMD begin to walk at the age of one and half years. Thirty percent children can walk independently before fifteen months of age. Some children can begin to walk only when they are three years old. There is no correlation found between the late walking and rapid progression or severity.

Muscle weakness is generally first recognized between ages of three and five years. It progress symmetrically and in a predictable pattern. Children tend to walk on their toes. Some children walk up on their toes from outset and are never able to walk with their feet flat. They also tend to waddle and have to climb up their legs, thighs, and hips when getting up from the floor or from the chair. The ability to run, which is generally achieved by two years of age, is not attained.

If the children of DMD are not properly treated they develop an imbalance in muscle strength at every joint. Hip flexors remain stronger than hip extensors. Knee flexors remain stronger than knee extensors. The ankle plantar flexors remain stronger than ankle dorsiflexors. The imbalance in strength at any joint leads to contracture of the joints muscle and soft tissues.

The stronger muscles are shorten. The muscles and their surrounding connective tissues become tight. The joint's range of motion is decreased. The stronger muscles on one side of the joint stretch the weaker muscles on the other side of the joint. This not only causes contracture of the stronger muscles but also makes the weaker muscles get weaker even faster, because they are stretched and no longer at their ideal length for contracting. Severe muscle weakness can prevent ambulation. It has been seen that the children with DMD and other neuromuscular diseases lose the ability to walk prematurely because of joint contractures.

Moser, H. [6] has studied Duchenne muscular dystrophy: Pathogenic aspects and genetic prevention. The author has put forward his views before the medical science as the patients are an wheel chair bound at the age of eight to ten years. The die before the age of twenty years generally. The mutation rate is in the order of 7×10^{-5}. This rate is higher than for any other X-linked genetic disease. There is no structurally or functionally abnormal protein known that might represent the primary gene product. It has no any pathogenic mechanism leading to the observed biochemical and histochemical alterations been elucidated. The functional defect of the muscular plasma membrane is still most attractive. It would be able to explain both the excess of muscular constituents found in serum of patients and carriers such as creating kinase (CK), as well as the excessive calcium uptake by dystrophic muscle fibres, which, prior to necrosis, could lead to hyper contractions rupture of myofilaments in adjacent sarcomas and by excessive calcium uptake to mitochondrial damage causing crucial energy loss.

Eemery, A. E. [7] and Abood, E. A. *et. al.* [8] have studied and given their thought as the incidence of DMD is approximately 1 in every 3000.

The first symptoms of DMD are characterized by frequent falling, difficulty of getting up from a standing or lying position and a waddling gait. The calf musculature is significantly enlarged by hypertrophy, fat, infiltration, and accumulation of connective tissue. It has been seen that twenty percent patients of DMD has a mental impairment. Affected skeletal musculature is mainly proximal, and results in wheel chair dependence during the early teenage. Patients die with cardiae failure as an adolescent. Simands, A. K. *et. al.* [9] have studied DMD and found that infections, leading to pneumonia as a result of lack of ventilation are the cause of death. The care of respiration may increase the survivals. Somer,H. *et. al.* [10] have studied DMD and found that a major characteristic of DMD and other muscular dystrophies is displayed of muscle necrosis, which results in high serum levels of the isoenzyme creatine kinase (CK). The leaks of CK from affected degeneration myofibers to the blood stream in addition to other enzymes such as perovative Kinase.

Mokri, B. *et. al.* [11] have found that plasma membrane defects are early and basic pathologic alterations and are represented by lesions of various sizes. He also found that there are some ultra-structural abnormalities of the membrane. Engel, J. *et. al.* [12] have studied regions near small lesions contain dilated endocytotic vesicles, whereas large lesions harbor dilated SR Vesicles, irregularly positioned sarcotubular components depending mitochondria, and small clusters of glycogen.Gillis, T. N. [13] has studied and found that **extracellular calcium** can enter the myobiber and cause as imbalance of the **calcium homeostasis**, which results in myofiber degeneration. The imbalance of calcium homeostasis might be that degeneration preludes the extracellular calcium influx. Sandri, M.[14], Tidball J. G.et.al.[15] and Matsuda, R.et.al[16] have studied the degeneration leading to myofiber necrosis, which was initiated via other mechanisms. The detection of apoptotic nuclei demonstrating DNA fragmentation in muscle biopsies from DMD patients. The absence of the DGC leads to sarcolemmal rupture and subsequent leaking of intracellular proteins, which are **unknown to the immune system.**

Spencer, M. J. *et. al.* [17] have studied DMD and found that the leaking of intracellular proteins attracts and activates cytotoxic lymphocytes and helper T-cells, which initiate the apoptotic program in ruptures myofibers.

Bradley, W. G. *et. al.* [18] have studied dystrophin deficiency and found that this deficiency leads to irreversible myofiber cell death or necrosis. The first necrotic myofiber can be demonstrated in the neonatal period. The myobiber at this stage is single. The necrotic myobibers appear in groups of 2-15 myofibers with the increase of age of the patient.

Bowman, W. [19] has studied muscular dystrophy and found that myofiber necrosis is segmental, which means that not the entire myofiber is affected by necrosis. The basal lomina surrounding the necrotic myofiber is not affected. It remains empty shell. **The affected myofibers contain membrane attack complexes, which are the result of complement activation**. The insertion of this in the sarcolemma creates holes and causes cell-lysis.

The interests of brevity and accuracy are both properly served by a simple statement that we do not know the etiology of DMD. There has been so much discussion in the last few years challenging the traditional concept of muscular dystrophy as a primary illness of the muscle. Murphy, D. L. *et. al.* [20] have given their views regarding the search for abnormalities in catecholamine metabolism and it was accelerated by the findings that there was a reduced initial rate of accumulation of serotonin in platelets from the DMD patients.

Paulson, O. F. *et. al.* [21] have studied blood flow in muscle of DMD patients and could not find any abnormality. Jerusalem, F. *et. al.* [22] have studied electron microscopic and morphometric studies of the capillaries in muscle from patients with the disease have been unrevealing.

Mc Comas, A. J. *et. al.* [23] have suggested that the muscle fibers in Duchenne muscular dystrophy were not being lost in a random fashion but disappearing in groups associated with the loss of motor units. They also proposed that DMD might have its origin in the malign influence of a sick motor neuron upon the muscle fibers.

Panayiotopoulos, C. P. *et. al.* [24] and Ballantyne, J. P. *et. al.* [25] have studied DMD and could not find any abnormality in the muscle fibers. The disease may be associated with an abnormal **neural influence**.

Matheson, D. W. *et. al.* [26] have studied the changes in the behaviour of different cell membranes and critically described the DMD and concluded that an abnormal surface deformation of erythrocytes produced by washing the red blood cells of DMD patients in saline.

Miale, T. D. *et. al.* [27] and Miller, S. E. *et. al.* [28] have studied DMD patients and could not attain the results of Matheson, D. W. *et. al.* [26] and proposed that it may be a non-specific outcome of Matheson, D. W. *et. al.* [26] work.

The behaviour of some of the enzymes, which are associated with sarcolemmal or erythrocyte membranes are anomalous.

Brown, H. D. *et. al.* [29] have studied the activity of Na, K, ATPase of erythrocyte membranes in DMD found that this is stimulated by ouabain, rather than being inhibited as in the normal situation.

Peter, J. B. *et. al.* [30] have shown that a factor present in the serum of DMD patients may contribute to the alteration given by Brown, H. D. *et. al.* [29]. Roses, A. D. *et. al.* [31] have studied endogenoces phospnorylation of a group of membrane proteins. This protein activity is called as protein Kinase activity and it is found abnormal high in erythrocyte membranes.

Mawatari, S. *et. al.* [32] have studied adenyl cyclase which is an enzyme and it is found to be abnormal. It is associated with sarcolemmal membranes. The enzyme is stimulated by epinephrine and sodium fluoride but in DMD patients this stimulation is less than normal .Most of the efforts in carrier detection have been directed to the detection of subclinical abnormalities. Muscle biopsy can be done. Pearce, G. W. *et. al.* [33] and Roy, S. *et. al.* [34] have studied muscle biopsies in DMD patients and one may see foci of necrotic fibers, moth eaten and whorled changes in intermyfibrillar network pattern. The internal nuclei are in abnormal number. These changes were also found in normal healthy persons. These patients are not carriers and the gastro enemius muscle is biopsied. Their changes are found in patients who are at the risk. This is the strong presumptive evidence of the carrier state.

Ionasescu, V. *et. al.* [35] have found an abnormality in ribosomal protein synthesis of DMD patients and found that isolated ribosomes were synthesized and are in increased amounts of collagen. Ionasescu, V. *et. al.* [36] have also found similar situations in the carriers of DMD patients. Ribosomes were found to synthesize abnormally higher amounts of noncollagenous protein as well as collagen. Roses, A. D. *et. al.* [37] have studied and concluded that the increased ability of the erythrocyte membrane to phosphorylate protein is found in carriers of the illness. The mean values for groups of definite, probable and possible carriers were found to be similar and different from the mean value for matched healthy controls. The mutation rate must be very low. If there were non-carrier mothers in the possible and probable groups, their normal values of protein Kinase should have reduced the mean value of these two groups compared to the definite carriers.

Hobbins, J. C. *et. al.* [38] have studied an interesting concept of the detection of DMD patients. They have performed amneucontesis at the fifteen weeks of pregnancy and a determination of the sex of the fetus. If the fetus is female, the child will not suffer the clinical symptoms of DMD. If the fetus of the examination uterus is male, then mother may elect to have the pregnancy terminated. It is the question of emotional aspects of the mother and can be left to decide what should be done? Analysis of amniotic

fluid CPK is not a useful test to detect whether a male fetus has the illness or not. It has become feasible to obtain fetal blood at the eighteen weeks during fetuscopy prenatal diagnosis of the illness.

Bodensteiner, J. B. *et. al.* [39] have studied calcium in muscle of DMD patients and found that there is a tendency of calcium level to be on the higher side. Bertorini, T. E. *et. al.* [40] have studied calcium and magnesium content in muscle of DMD patients and found that the levels of calcium were higher and levels of magnesium were lower. Some of the researchers have applied Freeze fracture technique (FFT) to study the muscle membrane and splits the surface membrane, peeling the outer surface away from the inner surface along a line, which passes through the interior of the membrane. Both the faces can be looked at under the electron microscope and these faces are found to be covered with particles of various types, some of which are arranged with a rectangular distribution. These are called square or orthogonal arrays.

Schotland, D. L. *et. al.* [41and 42] applied FFT to the DMD patients and found that there is a significant diminution in the number of orthogonal arrays. Peluchetti, D. *et. al.* [43] have studied this technique and suggested that there may be a decrease in the intermembranous particles on both surfaces.

The cell surface membrane is not homogenous. There are so many proteins and other compounds embedded in cell membrane, which serving different aspects of membrane activity. The glycoproteins and glycolipids of cell membranes perform important functions including a role in the receptor sites. There are some probes to identify these constituents by virtue of the selective binding of the probe to a specific compound. One such probe is Concanavalin A. This probe is a member of group of plant proteins called lections which have a specific affinity for sugar residues. Concanavalin A binds specifically with mannose, glucose, and fructose residues. Heimann-Patterson, T. D. *et. al.* [44] have studied the pattern of Concanavalin A binding in DMD patients and found that it was patchy and irregular. It was regular and have a good pattern in normal muscle. They have also found an abnormality in the cell membrane.

Brooke, M. H. [45] has written in his book on muscular dystrophy as if DMD is a primary abnormality in the muscle, then we would suppose to the change might be reproduced by culturing muscles cells from patients with the illness. Ionasescu, V.et.al.[46] and Thompson, E. Jet.al.[47] have studied DMD patients and found some abnormalities in the growth pattern which are able to change in the isoenzyme pattern of CK in the myotubes. It has also been noticed that this growth pattern is suspiciously normal in the cultured muscle. FFt does not reveal any abnormality in the inter membranous particles.

Rottman, S. M. *et. al.* [48] and Mawatri, S. *et. al.* [49] have found that the cultured cells seem to behave normally electro-physiologically. Cerri, C.A. *et. al.* [50] have found that there is abnormality in adenyl cyelase. It was not the same as that found in the dystrophic muscle itself.

It is believed that the possibility of hypothetical membrane abnormality might affect other tissues then muscle alone has been raised. DMD is a genetic disease and different cell surface membranes share many similar properties. Rowland, L. P. [51] has studied the relatively in exhaustible supply of membrane in the red blood cell and this has led to a legion of studies.

Falk, R. S.et.al.[52], Fischer, S. et.al.[53], Roses, A. D et.al.[54], Mabry, M. E. et.al.[55]and Roses, A. D. et.al[56] have studied the red cell membranes have been both inculpated and exculpated of all of the following such as changes in size, shape, deformability and other physical properties, abnormalities in

different ATPases, changes in **Calcium transport**, abnormalities of electrolyte content and permeability, abnormal phospnorylation of protein, abnormalities of adenyl cyelase.

Arthur, H. *et. al.* [57] have found that there is an abnormality in **low density lipoproteins in the plasma in DMD children** leading to a suggestion that there transport capacity was impaired. Fibroblasts cultured from the skin of patients with the illness have also been harvested in an attempt to detect abnormalities. A decreased adhesiveness between fibroblasts has been described using a technique in which the cells are encouraged to collide with each other and the stickiness is measured in such collisions. The adhesiveness has been found to be reduced in the fibroblasts from Duchenne patients. There is an overlap between the normal healthy controls and the DMD patients. Cultured skin fibroblasts also contain CK, which might make this a useful tool for studying the enzyme in disease states.

Minerals are important to our health. These are inorganic, chemical is elements not attached with carbon atom. Minerals and trace minerals can be differentiated easily. These trace minerals are called trace elements. If the cellular body requires less than 100 mg of eleven minerals is labeled a trace element and if accepts more than this level is labeled a mineral.

Trace elements are required in quantities of few milligrams or micrograms per day. A study of relationships of minerals with human health is very necessary and important. A balance of the level for minerals in every organ, tissue and cell of the human body may lead to a good health.

Minerals comprise only a fraction of total body weight. These are crucial for many functions of the human body. These include transporting oxygen, normalizing the central nervous system (CNS) and simulating growth, maintenance and repair of tissues and bones [58].

Romeyn, M.[59] has given a statement that the regulation of trace elements balance in the body is essential to survival. Every cell is a living organism and we must try to maintain its internal environment. The mobility of trace elements across cell membranes, between the extra-cellular and intra-cellular fluid forms the basis for the body's most primary functions. The electrical activity may be initiated; heart beats, nerve cells signal, muscles may respond, blood vessels may tighten or relax. Water balance should be maintained.

Most of the trace elements found in the tissues and body fluids are also present in the blood. Some of the metallic elements have a specific metabolic function and the presence of these is not merely the result of contamination from our environment. The trace elements, which are biologically active produce their effects through enzyme systems. Metalloenzymes and metal protein complexes are two systems. The former has a fixed amount of specific metallic ion per molecule of protein addition of an agent, which binds the metal inactivates the enzymes and the later is a larger group of proteins loosely bound to metal. The metals may substitute for each other with fluctuating degrees of affinity and can be taken out from the body by the process of dialysis. Some of these complexes may have enzymatic activity only. Rests of these are concerned with transportation process only. Herring,W.B.et.al. [60] have shown that chelation affects the activity of enzymes . Khurshid, S.J.et.al.[61] and Suhaila,R. et.al.[62] have shown that the essential metals at trace levels play a role in the human body and can cause some diseases when present beyond the limit of normal concentration .

It has been seen that the trace elements occur in the tissue of animals, plants and micro-organisms in very low concentrations. The concentration of these elements change highly among many elements. Their concentrations are also different among various living organisms and their parts. These differences are seen in nutritionally essential elements and also in those elements, which are associated with no vital function.

The trace elements have divergent roles to play depending upon their chemical form or combination and their position in the body fluids and tissues. The functional forms of the trace elements and their characteristic concentrations ought to be maintained with narrow limits if the functional and structural integrity of the tissues is to be safeguard and the growth, health and fertility of the individual have to be unaffected. Continued ingestion of diets that are deficient, imbalanced, or excessively high in a particular trace element invariably induces changes in the functioning forms activities, or amount of these elements in the tissue or fluids, so that they fall below, or rise above the normal and permissible limits or ranges. Biochemical disturbances in these situations develop along with physiological functions, which are influenced and structural disorders may arise due to the change with elements. Kumar, S.[63] has reported in his Ph. D thesis that the degree and duration of the dietary deficiency or toxicity, age, sex and species are important factors associated with the trace elements .

It has been seen that food is the basic need of life of a living organism. Everybody eats food whether it is vegetarian or non-vegetarian. Scientists were very curious about the food they consumed. Food passes in the body and affects the body. Food is the substance taken into the body that will help to meet the body's need for energy. It helps in maintaining good health, health growth, growth and reproduction.

Proteins are important and vital to any living creature. These are the important constituents of cells and tissues of the human body. Proteins form the important component of muscles and other tissues and vital body fluids like blood, cerebrospinal fluid (CSF) and synovial fluid in human joints. The proteins in the form of enzymes and hormones are concerned with a wide range of vital metabolic mechanisms in the body. They supply the body building material and make good the loss which occurs due to wear and tear. Proteins as antibodies may help the body to defend against infections. Proteins are one of the most important nutrients required by the body has to be supplied through the diet we consume. The dietary proteins are broken down into amino acids and absorbed and are used by the body for various functions like tissues building, replacement of proteins depleted, etc. Amino acids are used for providing energy to the body.

Fat is an important component of our diet. It serves a number of functions in the body. Fat is a concentrated source of energy and it supplies, per unit weight more than twice of energy furnished by either proteins or carbohydrates. Fat also imparts palatability to a diet and retards stomach emptying time. Fat in the diet can be of two categories, the visible and invisible. The visible fats are those derived from animal fats like butter, ghee which are solid fats and those derived from vegetable fats like groundnut, mustard, coconut, sunflower oil, till, which are liquid fats. Hydrogenated vegetable oil known as Vanaspati is a solid fat. These fats are triglyceride of fatty acids, both saturated and unsaturated. Animal fats like ghee and butter contain Vitamin A and D. These vitamins are not present in vegetable oils.

Some amount of fat is present in other foods like cereals, pulses, oil seeds, milk, egg, meat, etc. This type of fat contributes to the total fat and essential fatty acids content of diet depending upon the foodstuff present in the diet. Nuts, oilseeds, soyabean, avocado, pear and animal foods have a higher amount of invisible fat.

Minerals and trace elements are circulating in the human body. Some of these elements form part of body structural component and some others act as catalytic agents in different body reactions. Bones and skeleton are made up of calcium, magnesium and phosphorus and iron, which is a component of blood. Minerals like zinc, molybdenum, copper, manganese and magnesium are either a structural part or activate a large number of enzyme systems. Iodine is a part of hormone, thyroxin. Sodium, potassium are important elements present in fluids within the outside the cells and along with ions like chloride, bicarbonate and carbonate keep water and acid base balance.

Every individual absorbs minerals in a slightly different way, called biochemical individuality. Those nutrients that have not been transferred through the intestinal mucosal cell to enter the circulation have no meaning regarding the study of the elements. The variety of nutrients from organism's environment that have been made available by absorption must be transported through the circulatory system to the aqueous microenvironment of the cells. They may serve the purpose of participation in different metabolic processes in the cells on which the life of the total organism depends.

The absorption of minerals is dependent on many different factors related to the mechanism of human body. Mary, R.L.A. et.al [64] have reported that the addition of vitamins and minerals to food can be effective public health intervention to correct inadequate intake of nutrients in both the general society.

1.1 Different types of Trace Elements circulating in Human system:

There are ninety two elements found in nature. We have some additional twenty two elements also. It has been reported in the literature that there are hundreds of isotopes of the elements exist. We may say the any one of which may play an undiscovered role in human health.

Alaxander,G.S. [65] reported that through geophysical forces, mixing of the earth's crust with water may provide virtually every mineral for our body, which requires to maintain health. The water is compatable with more substances that any known solvent . It is an ideal medium for transporting nutrients in the cells for the chemical reactions of cellular metabolism to take place. Human body contains lot of element out of 25 are divided into mainly three categories such as major, minor components and trace elements.

Pike, R.L.et.al.[66] have given a statement that the major components, which make up 96% of human body are composed of oxygen, nitrogen, carbon and hydrogen. Major elements found in the biological molecules such as proteins, nucleic acids, fats and carbohydrates and are capable to make-up the body. Hydrogen ions are very important for our cells to make ATP or energy. Water is also a medium for all the chemical reactions taken place in the human body. Water is a mixture of oxygen and hydrogen atoms .

Minor components make up 4% of our body. They may include calcium, phosphorus, potassium, sulfur, sodium, chlorine and magnesium. Some of these are necessary for chemical processes to run correctly. Our muscles need calcium in order for them to twitch properly. Enough calcium is required to our body.

Trace elements make up 0.1% of our body. They include copper, zinc, selenium, molybdenum, fluorine, iodine, manganese, cobalt, iron, lithium, strontium, aluminum, silicon, lead, vanadium, arsenic and bromine. These elements are essential for our body to function properly.

Zumkley, H. [67] stated that clinical experimental and epidemiological studies indicate that a large number of trace elements may be involved in the etiology of different human body disorders. Both increased levels of any trace element or reverse of this can influence the development of disease.

2 Trace Elemental Effects on Human Health

A very high concentration of the trace elements may prove toxic. Depletion in the concentration of essential trace elements may lead to create so many different metabolic instabilities due to dysfunction of enzyme. Different types of metabolic changes in human body are accompanied by changes made in the concentration of one or more trace elements in some body fluids, such as blood serum or plasma.

The trace elemental analysis from human hair, nails, and body fluids such as plasma, serum and cerebrospinal fluid has been stated in the literature as the best predicator.

2.1 Trace elemental role in human Body:

We are giving the description of some of the important trace elements here as

2.1.1 Copper:

The presence of copper in animals and plants is very necessary. Copper is most abundant trace element in human beings. This element is carried mostly in the bloodstream on a plasma protein. We may call it is ceruloplasmin. This element is firstly absorbed in the gut and transported to the liver bound to albumin. It is found in a variety of enzymes, including the copper centre of cytochrome C oxidase.

Human body needs copper for normal growth and health. It is said that copper is required to help body use iron. This element is very important for nerve function, bone growth and to help body use sugar and it is a component of a cofactor for different enzymes, approximately. Fifty enzymes are required copper to function properly. Davis, I.J.J. [68] has given a statement that a young person requires one hundred to one hundred fifty milligram of copper daily. Copper in higher concentration is found in liver, hair, muscle and lung.

2.1.2 Zinc:

Zinc Zn) is a necessary trace metal of suitable importance in the dietary management of many human body complex disorders. A young person has 3 gm of zinc. This trace element is found in all our cells. This element is essential for all forms of life. Many proteins contain structures called zinc fingers may help to regulate genes. The distribution of zinc in human tissues is well documented in the literature. Liver, kidney, bone, retina, prostate and muscle appear to be very rich in zinc. Burns, R.R. et.al.[69] have studied and found that most of the red cells zinc is tightly bound to enzyme carbonic anhydrase. It is exchangeable with plasma zinc. Whole of plasma zinc is found with proteins. Sixty percent zinc is bound to albumin and thirty percent has binding with alpha 2 macroglobulin and the remainder with low molecular weight proteins including amino acids.

Prasad, A. S. *et. al.* [70] have shown that zinc is bound to amino acids and serum proteins. Histidine, glutamine, threonine, cystine and lysine showed the most markable effects. The amino-acid-bound

fraction of zinc may have an important role in biological transport of zinc. The stable zinc content is higher in albumin fraction. Similar concentrations of zinc were found in the α, β and γ-globulins. These are fraction of immunoglobulin G.

Kelin, D. *et. al.* [71] have shown the first demonstration of a specific biological function critically dependent on the presence of zinc. They have also shown that carbonic anhydrase contains zinc and it is essential to the mechanism of action.

Riordan, J. F. *et. al.* [72] have reported in the literature that there are more than seventy zinc metalloenzymes. Zinc metalloenzymes exhibit diversity both of catalytic function and of the role played by the metal atom.

It is evident that zinc in small quantities is present in various cell membranes. Most of the membrane-bound zinc is linked to a distinct macromolecule constituent lipoprotein fraction. Chavapil, M.et.al.[73] have shown that the effect of zinc and other metals on aggregation of platelets and release of H^3 serotonin activated either by collagen or epinephrine .

Prasad, A. S. *et. al.* [74] have shown that a syndrome of iron deficiency anaemia, hepatosplenomegaly and dwarfism has been found to be associated with malfunctioning of zinc metabolism . Walravens, P.A. et.al.[75] have studied and found that the orthopedic and CNS have relatively slow zinc uptake. This element remains tightly attached for a lengthy span of time. The deficiency of zinc leads to growth retardation or failure, lesions of the skin and its appendages, and impaired reproductive development and function. Psychological disturbances are reported in individuals suffering from acrodermatitis enteropathic . Henkin, R.I. et.al.[76] have studied zinc induced deficiencies in human beings and these are associated with neurological symptoms such as depression, poor concentration, nervousness and moodiness . Dresti, I.E. [77] has studied the hippocampus, which is rich in zinc. Zinc deficiency is associated with learning and memory defects similar to behaviour syndromes resulting from destruction of the hippocampus. Acute oral zinc toxicity has been reported to produce drowsiness and somnolence.

2.1.3 Iron:

Fairbanks, V. E. F. *et. al.* [78] have reported that the therapeutic indications for iron during the Roman era included alopecia, acne, dermatitis, wounds, hemorrhoids, gout, pulmonary diseases, diarrhoea, vomiting, weakness, edema, fever and cystitis . McCance, *et. al.* [79] have reported that once the iron was absorbed by the human body, its excretion was very minimal and was not controlled either by gastrointestinal tract or by the kidneys. The plasma iron was in equilibrium with tissue iron. The level of plasma iron influenced the rate of iron absorption. The intestine regulates the rate of iron absorption.

Granick, S. [80 adopted and extended the hypothesis of ferritin as the mucosal regulator of iron absorption. This hypothesis was used and named as mucosal block theory. Moore, C. V. *et. al.* [81 have shown that the plasma iron as the major form of transport iron. Flavoprotein enzymes of iron were discovered by Mahler, H. R. *et. al.* [82] and Richert, D. A. *et. al.* [83]. Fisher, H.et.al. [84] have synthesized four ferroprotoporphyrin (heme) moieties.

Ingram, D. J. E. *et. al.* [85] have extablished a three-dimensional picture of molecule with its four attached hemes. They have studied the nature of the bond between iron and globin. Now iron is

stabilized in the ferrous state completely, which allows it to be reversibly bonded to oxygen. Due to this mechanism, hemoglobin works as an oxygen carrier.

The iron in human serum was studied by Holmberg, G. C. *et. al.* [88] Schade, *et. al.* [87] have shown that the trace element iron may be bounded completely to transferrin.

Lipschitz, D.A. et.al.[88] and Simes, M.A.et.al.[89] have established a correlation between serum ferritin, concentration and storage iron.

2.1.4 Magnesium:

Aikawa, J. K. [90 and 91] showed in the studies related to magnesium and found that magnesium is associated with so many different biological processes.

Magnesium is present in a small concentration in all cells and it is necessary for cellular metabolism. This trace element is also present in bone along with calcium. It shares so many properties of calcium so far as absorption and metabolism and tissue distribution are concerned. Widdowson, E. M. *et. al.* [92] have studied the magnesium content in human body and found a range of magnesium, which stated from 22.7 to 35.0 meq/kg weight of tissues. Magnesium reaches us in many forms. These are magnesium amino acid chelate, magnesium carbonate, magnesium oxide, magnesium oxide dolomite and magnesium sulfate. Seventy percent of human body magnesium resides in bones and teeth .This element is essential to the functioning of human body because it transmits nerve impulses, causes contraction of muscles and integral to healthy development of bones and teeth. Waterlow, J.C.[93], Clasen,H.G.[94] and AL-Ghamadi,S.M. et.al.[95] have shown that the human body contains about 760mg of magnesium at the time of birth. It goes upto 5 gm at the age of 4-5months and it reaches upto 25 g when a body attains an age of adult. About 30 to 40% magnesium is found in muscles and soft tissues. One percent is found in extracellular fluid, and the remainder is in skeleton. If we are going to consider the particular importance with respect to the pathological effects of magnesium depletion. We have to take into account the role of this element in regulating potassium fluxes and its involvement in the metabolism of calcium . Wester,P.[96] has shown that

about 1% of magnesium is found in the extracellular fluid, inside cells, magnesium may be bound to phospholipids. It is very important to note that increasing dietary protein intake may increase magnesium requirements because high protein intake may decline magnesium retention .It is advisable that to completely understand magnesium function, it is very important to explore magnesium's relationship with calcium and potassium. Magnesium and potassium also have a close relationship. Magnesium is required for the function of sodium and potassium pump. If a magnesium deficiency occurs, then pumping of sodium out of the cell and pumping potassium into the cell may be impaired. Krasner,B.[97] ,Furukawa,Y.et.al.[98],Stark,G. et.al.[99] and Haigney,M.C.P. et.al.[100] have studied and shown an effect of the level of magnesium regarding heart attack.

Alcoholism, renal disease, diabetes mellitus may all cause a deficiency of magnesium. Nausea, vomiting, anorexia, muscle weakness, muscle weakness, muscle spasms and tremors are the few symptoms and signs related to deficiency of magnesium.

Magnesium has an effect on CNS. It is used for a better sleep. This element may be used to calm irritated and over excited nerves. This is useful with epileptic attacks, convulsions in pregnant women

and shakes with tremors in alocholism. If the level of magnesium is very low, the nerves lose control over muscle activity, respiration and mental processes. Nervous fatigue, ties and twitches, tremors, irritability, hypersensitivity, muscle spasms, restlessness, anxiety, confusion, disorientation and irregular heartbeat all respond to higher levels of magnesium.

2.1.5 Calcium:

We know that 99% of calcium is found in the bones and teeth of a human body. Rest of the element resides in the soft tissues and blood of the body. Calcium is most important element of the body and human body structure is made up calcium and other minerals. We shall lie on the ground without calcium and not able to stand.

Ireland,P.et.al.[101]. Heaney,R.P.et.al.[102] ,Wilkinson,R.et.al.[103] and Marshall,D.H.et.al.[104]have studied the ingested calcium mixes with digestive juice calcium in the proximal small intestine from where it is absorbed by a mechanism. This process has an active saturable component and diffusion component .Calcium is absorbed by active transport during the low calcium intake mainly. This active transport is called trans cellular transport. High intake of calcium lead to increasing proportion of calcium, which may be absorbed by paracellular diffusion. The unabsorbed component appears in the faeces together with the unabsorbed component of digestive juice calcium. This is called as endogeneous faecal calcium. The faeces contain unabsorbed dietary calcium and un reabsorbed digestive juice calcium. Urinary and endogenous faecal calcium are not the only forms of calcium for excretion. The calcium looses from skin,hair, nails must taken into account. The deficiency of calcium causes osteoporosis. Morris ,H. et.al.[105] ,Ebeling, P.R.et.al.[106] , Need,A.G. et.al.[107] have shown that the calcium absorption decreases with the increase of age in both males and females .

Nordin, B.E.C.et.al.[108] shown that the calcium content of human milk is 36 mg per 100 ml. A lactating lady may produce 750 ml of milk daily. It has been reported that 280 mg of calcium can be fed to a new born child. Kent, G.N. et.al.[109] and Lopez, J.M. et.al. [110] have shown that the bone is lost during lactation and restored after weaning. Chan. G.M.et.al. [111] have shown that the loss of calcium may be prevented by the supplementation of calcium. Calcium deficiency is very serious. Researchers have shown a low bone density. Due to low density, the fracture rate is very high in developing countries. The intake of calcium is also low. Rickets has not been reported in developing countries.

2.1.6 Sodium:

Sodium was isolated in the year 1807 by passing an electric current through molten sodium hydroxide. The sodium quickly oxidizes in air and is reactive. The free metal is used for chemical synthesis, analysis and heat transfer applications. Sodium ion is soluble in water. Most of the sodium in the human body is found in blood and lymph fluid. Aldosterone hormone controlled partly the levels of sodium in human system. Adrenal glands are responsible for the hormone. The level of aldosterone in human body tells about the kidneys when to hold the sodium element in the body instead of passing it in urine. Small amounts of sodium may last through the skin during the process of sweating. The ability of the kidney to both conserve sodium in response to sodium deprivation and to excrete sodium in response to sodium loading are impaired with the aging factor. Blood pressure in the body has to be maintained at the

prescribed and standard rates. If the standards of the pressure are failed, the system leads to serious damage of the blood vessels and results might be lethal.

2.1.7 Potassium:

This element is very important for the proper function of all cells, tissues and organs in the human system. This is an electrolyte able to conduct electricity in the body, along with sodium, chloride, calcium and magnesium. It is very crucial element to proper heart function and plays an important role in skeletal and smooth muscle contraction, making it very useful for normal digestive and muscular function. This element acts as a conductor for energy impulses throughout the body. It triggers chemical reactions in the body.

Potassium ion diffusion is a key mechanism in nerve transmission, and potassium depletion in human. There are some neurological dysfunctions such as epilepsy, headache, migraine, muscular dystrophy and Alzheimer's disease developed by the fluctuations in levels of potassium in the blood.

2.1.8 Hyperkalemia:

If we found the levels of potassium in the blood higher than normal value then a disease may occur, which is called hyperkalemia. This may be related to an increase in total body potassium or the excess release of potassium from the cells into the blood stream. Kidneys remove excees potassium from the body. It has been found in most of the cases that hyperkalemia is caused by disorders which reduce the ability to get rid of potassium. These disorders are such as acute kidney failure, chronic kidney failure, glomerulonephritis, obstructive uropathy and rejection of a kidney transplant.

2.1.9 Hypokalemia:

Hypokalemia means serum or plasma levels of potassium below the normal value. There are two causes for hypokalemia defined here, one is related to overall depletion in body's potassium and the next is related to excessive uptake of potassium by the muscle from the surrounding fluids. It is well reported in the literature that need have potassium is to control muscle action. Hypokalemia can cause the heart to stop breathing.

Mild hypokalemia does not show any symptom understandable position is missing. If a person has moderate hypokalemia which is very important to diagnose easily by the help of some understandable symptoms such as confusion, disorientation, weakness and discomfort of muscles, discomfort in the legs. Severe hypokalemia may produce extreme weakness of the body, paralysis. Different types of paralysis such as flaccid, limpness, lung muscles are common. This type of hypokalemia may cause abnormal heart beat. Abnormal heart beat is dangerous for our heart and it is the sign of cardiac arrest. Hypokalemia does not show any symptom in healthy subjects because of the rich percentage of potassium is found in healthy persons.

2.2 Trace elemental role in relation to immunity:

Nutrition and health both are linked each other but the importance of trace elements on immune system is also a field of research, which was established in the last two decades. It is a field of understanding of adequate trace elements supplementation may be a good path to design a better nutrition, which protects human beings against infections.

Cell biology and molecular genetics are the branches of science have been facilitated main efforts to determine specific cellular and molecular functions of trace elements in maturation, activation and functions of host defense mechanisms.

Immune cells require a proper supply of trace metals to express and preserve the structure and function metalloproteinase. These cells may also participate in energy production. Trace element levels can affect the immune function not only in a direct process but also by modulating plasma levels of hormones which are used to regulate the development and function of host deference cells. The trace elements may influence some mechanisms of non-specific immunity by modulating inflammatory cell function.

It has been seen that the effect of mineral deficiency on acquired immune system can be demonstrated by examining the response of lymphocytes to T cells mitogens. The levels of trace elements may also affects the synthesis and secretion of cytokines and chemokines which modulate the activities of immune and other cells.

A good application of micronutrient which is also called as trace elements interventions is probably related to vaccine response in older stage in human beings. Mortality associated with influenza is more likely to appear in this population.

A significant physiological role of many trace elements in the development, maturation, and sustenance of the morphologic integrity and function of the lymphoid organs concerned with immunity has been well established.

The immune system plays a key role in the body's ability to fight against infections and reduce the risk of developing tumors autoimmune and degenerative disease. Nutritional deficiencies and excesses influence different components of the immune system.

3 Review of the Literature

Katz, M. [112] and Suskind, R. M. [113] have studied the influence of nutrition upon host immune compertence. Correlations of protein and energy nutriture and their role in immuno responsiveness have been studied by- Bongiorni, I. B. *et. al.* [114] and Malave, I. *et. al.* [115]. Many trace elements are critical for mammalian survival and reproduction. High consumption of highly refined and heavily processed food items reflect that the trace element content may be reduced significantly. Gershwin, M.et.al.[116] have shown that the value of level of zinc may affect the phagocytic cell function the complement system and mast cell mediator release which can be seen at the efferent arm of immune response .

Rigas, *et. al.* [117] have reported that an additional process due to which copper acts in altering immune response may involve an interaction at the level of the plasma membrance.

Calcium ion are involved intimately is so many aspects of lymphocyte activation such as blast transformation in response to mitogens. Calcium is known to complete in a number of biological systems. Walton, W. S. *et. al.* [118] have suggested regarding elements metabolism and body composition and found that life in its very early stage surely included the conjunction of mineral ions with the simplest organic compounds and with subsequent nucleic acids and proteins to determine the

form and function of cellular components and processes. A separation of many cations and anions accompanied the creation of membranes and the development of the cell. Electro chemical and electromotive forces were already established with selective, often linked, passage of organic and inorganic molecules through channels or pores in membranes. A bioenergetics system developed and the fundamental, unique nature of intracellular life was also determined. Disturbances or breakdowns in the dynamic system development on location, movement and functions of mineral ions underlie many diseases of CNS and other different types of diseases.

Malcolm, J. J. *et. al.* [119] have measured calcium and other elements in muscle biopsy samples from patients of Duchenne muscular dystrophy (DMD) and found that the calcium content of muscle of DMD patients was significantly elevated compared to normal healthy controls.

Allen, D. G. *et. al.* [120] have studied calcium and the damage pathways in muscular dystrophy and found that the stretched contractions activate ROS production, which activates src kinase. Activity of such type of kinase causes opening of SACNSC and allows Ca^{++}entry. This pathway may be a possible cause of muscle damage.

Imbert, N. *et. al.* [121] have studied abnormal calcium homeostasis in DMD myotubes contracting in vitro and found that the resting intracellular calcium level was significantly higher in contracting DMD cells and it was (107 ± 8 n M). The level of calcium in controls was (66 ± 6 n M). It was (56 ± 6 n M) in FSM cells. They have also reported that contraction is a dominant factor contributing to Ca^{++} abnormalities in DMD cells. Contracting dystrophin-deficient cells have defective calcium handling mechanics during electrical events which involve sarcolemma.

Rena, Y. *et. al.* [122] have studied elements in muscle measured in vivo and vitro with X-ray spectrometry. They have found that muscles of myopathic animals had pathologic changes. The tongue and myocardium are composed of red fibers showed excessive calcium accumulation. This suggest that the basic genetic aberration is not directly related to the oxidative metabolism, white muscles have a more efficient system for dealing with calcium overload.

Caroline, A. M. *et. al.* [123] have studied elemental analysis of skeletal muscle in DMD using X-ray fluorescence spectrometry. They have found that levels of calcium and copper were significantly elevated in DMD compared to controls. X-ray fluorescence spectrometries provide further evidence for the involvement of calcium in dystrophic processes.

Hisao, K. *et. al.* [124] have studied Manganese, Copper, Zinc and Iron concentrations and subcellulor distribution in two types of skeletal muscle and found that the iron, zinc, copper and manganese concentrations of red muscle were 1.83, 4.31, 2.05 and 1.67 times higher than those of white muscle respectively. They have also reported that in skeletal muscle subcellulor distribution of iron, zinc and copper were different. The distribution of manganese does not have any deviation from the liver. They have also suggested that the differences between subsarcolemmal and interfibrillar mitrochondria were ascertained by the distribution of the trace elements.

Turner, P. R. *et. al.* [125] have studied increased calcium influx in dystrophic muscle and found that increased calcium influx or decreased efflux could lead to elevated $[Ca^{++}]_i$ levels. The calcium sequestering mechanisms were not altered in dystrophic muscle but were slowed by higher resting. They have also suggested that the agents increased leak channel activity due to this activity there is also

increment of $[Ca^{++}]_i$ in fibers and myotubes. The increased calcium influx could result in elevated $[Ca^{++}]_i$ in dystrophic muscle.

Arthur, J. R. *et. al.* [126] have studied free radicals and trace elements in muscle disorders and sport. They have suggested that trace elements and free radical activity can be associated with the pathogenesis of some skeletal and cardiac myopathies. They have also concluded that the deficiency of vitamin E may be a causative factor of the disease.

Baharch, M. *et. al.* [127] have studied nutritional inadequacy in adults with muscular dystrophy. They have reported that patients with DMD may be prone to nutrient deficiency due to mobility limitations or orophayngeal weakness. Patients with myotonic muscular dystrophy may be prone to nutritional deficiencies from associated dysmotility of the entire gastrointestinal tract. Many patients in both groups of dystrophies demonstrated in adequate nutrient intake of protein, energy, vitamins, water, fat, calcium and magnesium. They have also spot out the current dietary intake recommendations could not be properly maintained in adults of DMD.

Kando, H. *et. al.* [128] have studied trace element movement and oxidative stress in skeletal muscle atrophied by immobilization. They have measured Fe, Zn, Mn and Cu concentrations and the levels of thiobarbituric acid-reactive substance and glutathione. The rate of atrophy increased rapidly. Fe concentration has a tendency of elevation. Zinc and Manganese were also elevated. Their sub cellular distributions were also changed.

Gage, V. H. *et. al.* [129] have studied hypokalemic myopathy and elevation of serum enzymes. They have found and observed that there was an alteration in serum enzymes specially CPK. Altered potassium metabolism has already been associated with muscle dysfunction. There is a link between hypokalemia, myopathy and serum enzyme elevation, which has already reviewed and lot of literature available to have a better attainment regarding the disease.

Howard, M. K. *et. al.* [130] have studied malignant hyperthermia in a child with DMD. They have reported that patients with DMD are susceptible to different adverse intraoperative and postoperative side effects of anesthetic agents. These include hyperthermia and hyperkalemia, systemic acidosis, cordiac abnormalities rhabdomyolysis as well as death. They have concluded that response to testing of a muscle biopsy specimen was consistent with the diagnosis of malignant hyperthermia.

William, B. *et. al.* [131] have studied body potassium content in patients with muscular dystrophy. The significance of potassium metabolism in muscle disease has been the subject of investigation and speculation for the last about more than fifty years. The essential nature of potassium in the synthesis of muscle protein is well established. Potassium has also been implicated in the physiochemical interaction associated with muscle contraction, Role of potassium and determination of this element is very necessary in the diseases of muscle.

Serum potassium levels in primary muscle disease are consistently within the normalcy. Ninety five percent of the body potassium is intracellular. Serum values of potassium cannot reflect intracellular derangements of potassium metabolism. A method which can measure total body exchangeable potassium is isotope dilution that does not depend on serum potassium levels.

Authors have studied potassium by means of radioactive method and found that patients with primary muscle disease have a diminution in total body potassium, which was correlated in large measure with the severity of muscle involvement. This study was done in the case of relatives of the patients and found a similar decrease in body potassium. Authors have also investigated that the relationship of body water with primary muscle disease. A consistent relationship between body potassium and a fundamental component of body composition has been established.

Kossmann, R. J. *et. al.* [132] have studied neuromuscular diseases. They have given their views on the importance of potassium in biological functions. Potassium plays a role of protein synthesis in muscle. It plays a role in creatine phosphorylation, which is necessary to energy transfer. Potassium maintains the membrane potential too. Abnormalities of potassium distribution in the human body become manifest as muscle dysfunction in disease such as cardio renal failure, diabetic acidosis, and periodic paralysis. The disturbance in potassium has been also reported in the many neuromuscular diseases. Authors have tried method of natural radioactivity to study the whole body potassium up to the accuracy of 2% in less than two hundred seconds. Authors have determined the potassium in muscular dystrophy and found that significance of the measured values were uncertain. It is very hard to say that whether this is a fundamental pathogenesis or a consequence of loss of muscle in bulk.

Hull, K. L. *et. al.* [133] have studied stoichiometry of sodium and potassium transport in erythrocytes from patients with myotonic muscular dystrophy. They have used ^{22}Na and ^{42}K radioisotopes to measure Na efflux and K efflux in identical suspensions of fresh erythrocytes from patients of myotonic dystrophy and controls. Each flux was measured in the presence and absence of ouabain. The mean ouabain-sensitive Na efflux rate in controls was found to be significantly greater than the corresponding rate in myotonic dystrophy.

Edmands C. J. *et. al.* [134] have studied total body potassium and water, and exchangeable sodium in muscular dystrophy. They have found that total body potassium was reduced even in the youngest patients and was slightly higher in the older boys. Total body water was also reduced. The total body water measurements indicated that many of the affected boys were obese.

William, H. B. *et. al.* [135] have studied the significance of decreased body potassium concentrations in patients with muscular dystrophy and non dystrophic relatives and found that diminished total body potassium concentrations appear to correlate with the severity of muscle involvement. They have also provided a logical explanation for the loss of body potassium level. It is related to the gradual replacement of normal muscle tissue by potassium poor fat.

Rowland, L. P. *et. al.* [136] have studied lack of some muscle proteins in serum of patients with Duchenne dystrophy. They have studied phosphofructokinase (PFK), phosphorylase (PPL) and myoglobin in normal human muscle diseases. The PFK and myoglobin were absent at all. The activities of PPL were very slow. The abnormal increase in the activity of several serum enzymes is one clue to the nature of the biochemical abnormality in the cases of DMD. The increased serum enzyme activity may occur because enzyme protein molecules are released from muscle. This is the fundamental disorder of an abnormality of the muscle membrane. This abnormality permits pathological leakage of large molecules.

Hopf, E. W. *et. al.* [137] have studied calcium misregulation and the pathogenesis of muscular dystrophy. The exact nature of the relationship between calcium and pathogenesis of DMD is still an

open question. It is very difficult to understand the cellular basis of DMD. The absence or low level of dystrophin, a cytoskeleton protein may slow the necrosis of the muscle fibers with progression of the disease. Loss of cytoskeletal and sarcolemmal integrity results from the absence of dystrophin. It plays a role in the pathogenesis of DMD. A number of calcium-permeable channels have been identified ,which can exhibit greater activity in dystrophic muscle cells.

Neve, J. [138] has studied quite different element selenium (Se) and put forward basic views regarding this element. Selenium has been appreciated in nutrition and therapeutics for the last three decades. Selenium constituting the active centre of about 20 eukaryotic proteins. It has been considered as highly relevant in Biochemistry. It can be used as radox state regulating properties. Besides well characterized selenium deficiency symptoms appear in pronounced deficiency states and are associated with different and various cofactors. The deficiency of this element causes significant adverse effects. It can increase the susceptibility of cancer, cardiovascular diseases or some other chronic degenerated pathologies such as DMD. Dietary recommendations of selenium not defined very much and are inadequate.

Westermarck, T. *et. al.* [139] have studied the trace element Se and reported the importance of this element as nutrition in protecting against so many degenerative and chronic neurological diseases. The nutritional antioxidants may be effective in preventing or retarding the process of the disease. It has been reported that a clinical response is also effective in the treatment of the DMD patients.

Alain, L. *et. al.* [140] have studied selenoprotein function in muscle disease. The crucial role of the trace element Se in livestock and human health in striated muscle function has been well established. There are two proteins discovered till date and these are Sel W and Sel M. Some of the recent findings on the functional consequence of the mutations suggest and an important contribution of Sel M to the regulation of oxidative stress and calcium homeostasis.

Zunkley, H. [141] has studied the clinical aspects of selenium metabolism. Selenium deficiency has been recognized to play secondary role in different human diseases. Many of these diseases can be prevented or treated by means of selenium supplementation. Importances of selenium with other trace elements are also of clinical significance.

Harris, L. S. *et. al* [142] have studied magnesium and calcium in human muscular dystrophy. They have mentioned that new impetus has been given the study of distribution and utilization of metallic ions in DMD by increasing recognition of their influences upon activities of enzymes. There are so many abnormal activities of different types of glycogenolytic enzymes, transminase, nueleotidase and creative phosphokinase in DMD have very much studied earlier. They have also reported that all of the enzymes catalyze the transfer of phosphate from adenosine triphosphate (ATP) to a phosphate receptor, or from a phosphorylased compound to adenosine diphosphate (ADP) are activated by magnesium ATP is necessary in such diverse functions as muscle contraction.

Samuel, W. B. *et. al.* [143] have studied plasma and erythrocyte magnesium in muscular dystrophy. They have reported that magnesium in serum is tightly bound in dystrophic patients. It has different value in normal persons. Studies of magnesium metabolism in pseudo hypertrophic muscular dystrophy are appropriate. Magnesium works as a metal cofactor in many reactions of muscle metabolism. There is a necessity of optimum levels of magnesium in muscle fibers for contraction and relaxation of muscle.

Tulio, E. B. *et. al.* [144] have studied muscle calcium and magnesium content in Duchenne muscular dystrophy. They have found that muscle calcium levels were fifty percent higher in comparison to normal healthy persons. The levels of magnesium were decreased by forty four percent in DMD persons in comparison to healthy controls. Authors have given their arguments for the role of calcium in DMD, which were very authentic and may implicate magnesium depletion as secondary pathogenic factor.

Csenkér, E. *et. al.* [145] have studied ion concentrations in serum and cerebrospinal fluid of patients with neuromuscular diseases. Authors have studied Na^{+}, Ca^{+2}, K^{+}, Ce^{-} , Mg^{2+} and Pi concentrations in serum and lumber CSF with neuromuscular diseases. They have measured pi concentration, which was remarkable point of diagnosis in DMD. On the basis of ion content with possible alterations of serum of CSF may guide us in the diagnosis of various neuromuscular diseases.

Carlier, L. *et. al.* [146] have studied nutritional assessment in Duchenne muscular dystrophy. Authors confirmed the accuracy of the DMD ideal-weight chart of earlier scientists. Obesity may occur from the age of seven years. Obese boys show a centralized body-fat distribution. They have also concluded that a specific weight chart and simple clinical tools are sufficient to obtain on accurate diagnosis of nutrition or obesity among DMD patients

4 Basic Theory of Flame Atomic Absorption Spectroscopy

The phenomenon of atomic absorption was first observed in 1802. Walsh proposed the atomic absorption spectroscopy for the quantitative analysis of elements [147]. Skoog *et. al.* [148] have supplied relevant information about this technique in detail. Atomic absorption analysis involves measuring the absorption of light by vaporized ground state atoms and relating the absorption to concentration. The incident beam of light is attenuated by atomic vapor absorption according to Beer's Law. The instrumental and chemical parameters of the system must be geared towards the production of neutral ground state atoms of the proposed element for study. The conversion of sample from its native state to the atomic state can be achieved by using a method called flame atomic absorption spectroscopy (AAS) or an electric furnace. The sample undergoes a number of pretreatment steps prior to analysis in the furnace. The sample is dried by evaporating the solvent in the first step. The organic matrix is decomposed by heating the sample in the second step. The heating temperature may go up to 1000^{o}C. Ultimately the furnace is rapidly heated to a temperature around 2400^{o}C to produce vaporized neutral atoms with as many as possible in their electronic ground states. Block diagram of a flame spectrophotometer is given in Figure 4. 1.

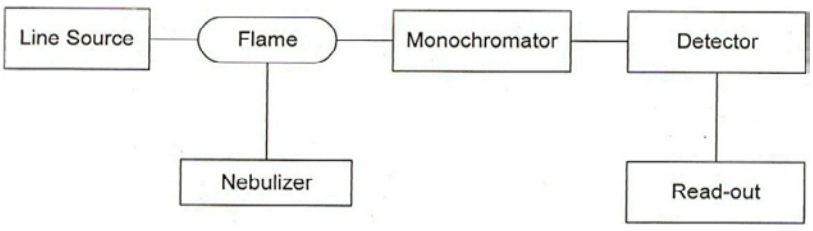

Fig. 4. 1 : Block diagram of a flame spectrophotometer.

Optical arrangement of atomic absorption spectrophotometer is given in Figure 4. 2.

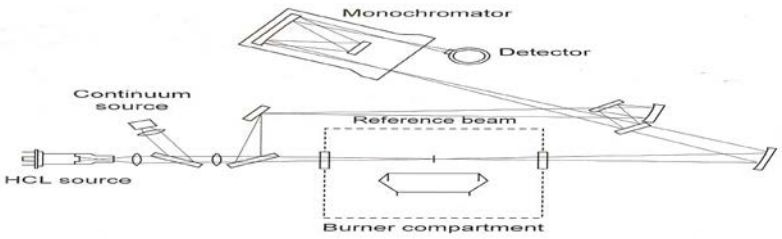

Fig. 4. 2: Optical arrangement of atomic absorption spectrophotometer

5 Materials and Methods

Blood sample of Duchenne muscular dystrophic patients along with normal healthy control were collected from the Department of Neurology, Safdarjang Hospital, New Delhi-110016 after the approval of ethical committee of the hospital. 10 ml freshly drawn blood from each patient was collected in clean and dry test tube without any anti-coagulant. The test tube was kept for 45 minutes at room temperature (22 ± 2^{o}C) for the formation of clot. Sera of different patients were separated by centrifugation at 1500 r.p.m. upto 15 minutes and were collected in screw capped test tubes.

The atomic absorption spectral estimation of the serum samples from normal persons and epileptic patients were carried out on atomic absorption spectrophotometer Model No. AA- 6300 of Shimadzu Japan, at Deptt. of Environmental study University of Delhi 110007.

6 RESULTS

We have measured the values of trace elements such as Cu, Fe, Zn, Na, K, Ca, Se and Mg, in Duchenne muscular dystrophic patients and healthy normal control given in Table No. 1 along with the latest availability of the literature.

Table 6.1 : Results along with work carried out by researchers on different mode of analysis using different types of samples and diseases.

S. No.	Trace elemental parameters	Types of Samples	Mean±S.D Unit	Disease/Control	Reference
1	Calcium	Serum	(9.0 ± 0)mg/100ml	Epileptic	John, H. *et. al.*[149]
2	Calcium	Serum	(10.47 ± 1.16) µg/dl		Prasad, R. *et.al.* [150]
3	Calcium	Serum	(10.76 ± 3.29) µg/dl	Controls	
4	Calcium	Hair	(906 ± 796) µg/g		Lech, T. *et.al.* [151]
5	Calcium	Hair	(520 ± 436) µg/g	Neurological disorders	
6	Calcium	Hair	(960 ± 419) µg/g	Controls	Avci *et.al.* [152]
7	Calcium	Hair	(1162 ± 533) µg/g		
8	Calcium	Hair	(947 ± 850) µg/g	Epileptic	
9	Calcium	Hair	(1143 ± 437) µg/g		
10	Calcium	CSF	(6.47 ± 0.87) µg/dl	Controls	Prasad, R. *et.al.*[150]
11	Calcium	CSF	(5.85 ± 2.49) µg/dl	Epileptic	
12	Calcium	Serum	(2.46 ± 0.09) µg/dl	Controls	Barlow, P. J. *et.al.* [153]
13	Calcium	Serum	(2.41 ± 0.08) µg/dl	Hyperactive children	
14	Calcium	Hair	(430 ± 200) µg/g		
15	Calcium	Hair	(694 ± 349) µg/g	Controls	
16	Copper	Serum	(38.119 ± 2.68) µg/dl	Birth Asphyxia	Khanna, R. S. *et.al.* [154]
17	Copper	Serum	(29.677 ± 1.611) µg/dl	Controls	

18	Copper	Serum	(2.328 ± 0) mg/dl	Smokers	Adnan, M. *et.al.* [155]
19	Copper	Serum	(11.28 ± 0) µmol	Neurotoxic	Guidotti, T. L. *et.al* [156]
20	Copper	Serum	(112.9 ± 41.88) µg/dl	Epileptic	Prasad, R. *et.al.*[150]
21	Copper	Serum	(66.46 ± 9.76) µg/dl	Controls	
22	Copper	Serum	(111.22 ± 13.06)mg/l		Denitz, T. *et. al.* [157]
23	Copper	Serum	(112.65 ± 9.33) mg/l		
24	Copper	Serum	(114.55 ± 7.38) mg/l	Epileptic	Denitz, T. *et. al.* [100]
25	Copper	Serum	(111.45 ± 5.97) mg/l		
26	Copper	Serum	(0.86 ± 0.24) mg/l	Controls	Soylak, M. *et.al.* [158]
27	Copper	Hair	(19 ± 7) µg/g		Avci *et.al.* [152]
28	Copper	Hair	(16 ± 8) µg/g		
29	Copper	Hair	(14 ± 9) µg/g	Epileptic	
30	Copper	Hair	(10 ± 2) µg/g		
31	Copper	Serum	(97.9 ± 0) µg/100ml	Control	Delvis, H.T. *et. al.* [159]
32	Copper	Serum	(2.328 ± 0) mg/dl	Neurological disorders	
33	Copper	Serum	(2.328 ± 0) mg/dl	Control	Kumar, S. *et.al.* [160]
34	Copper	Serum	(2.328 ± 0) mg/dl	GMF	
35	Copper	Serum	(2.328 ± 0) mg/dl	Epileptic	Smith and Bone [161]
36	Copper	Serum	(2.328 ± 0) mg/dl	Control	
37	Copper	CSF	(66.46 ± 9.76) µg/dl		Prasad, R. *et. al.* [150]
38	Copper	CSF	(66.46 ± 9.76) µg/dl	Epileptic	
39	Copper	Serum	(66.46 ± 9.76) µg/dl		Kaji, H. *et. al.* [162]
40	Copper	Serum	(66.46 ± 9.76) µg/dl	Control	
41	Copper	Hair	(14 ± 9) µg/g	Hyperactive children	Barlow, P. J. *et. al.* [153]
42	Copper	Hair	(14 ± 9) µg/g	Control	
43	Iron	Serum	(108.636 ± 13.03) µg/dl	Birth Asphyxia	Khanna, R. S. *et.al.* [154]
44	Iron	Serum	(91.469 ± 2.42) µg/dl	Controls	
45	Iron	Hair	(9 ± 2) µg/g		Avci *et.al.* [152]
46	Iron	Hair	(15 ± 9) µg/g		
47	Iron	Hair	(6 ± 4) µg/g	Epileptic	
48	Iron	Hair	(7 ± 5) µg/g		
49	Iron	Serum	(386.0 ± 0) µg/100ml	Controls	Delvis, H.T. *et. al.* [159]
50	Iron	Serum	(373.4 ± 0) µg/100ml	Neurological disorders	
51	Iron	Serum	(20 ± 8) mg/dl	Control	Kumar, S. *et.al.* [160]
52	Iron	Serum	(29 ± 15) mg/dl	GMF	
53	Iron	Hair	(8.8 ± 3.0) µg/g	Hyperactive children	Barlow, P. J. *et.al.* [153]
54	Iron	Hair	(15.7 ± 10.6) µg/g	Controls	
55	Magnesium	Serum	(0.87 ± 0.34) µg/dl	Epileptic	Prasad, R. *et. al.* [150]
56	Magnesium	Serum	(0.93 ± 0.18) µg/dl	Controls	
57	Magnesium	Serum	(24.13 ± 0.81) mg/l	Epileptic	Denitz, T. *et. al.* [157]
58	Magnesium	Serum	(19.44 ± .53) mg/l		
59	Magnesium	Serum	(24.33 ± 2.74) mg/l	Controls	
60	Magnesium	Serum	(19.50 ± 0.64) mg/l		
61	Magnesium	Hair	(40.5 ± 32.9) µg/g		Lech, T. *et.al.* [51]
62	Magnesium	Hair	(29.3 ± 25.3) µg/g	Neurological disorders	
63	Magnesium	Hair	(259 ± 76) µg/g	Controls	Avci *et.al.* [152]
64	Magnesium	Hair	(505 ± 219) µg/g		
65	Magnesium	Hair	(329 ± 285) µg/g	Epileptic	
66	Magnesium	Hair	(444 ± 203) µg/g		
67	Magnesium	CSF	(1.31 ± 0.18) µg/dl	Controls	Prasad, R. *et. al.* [150]
68	Magnesium	CSF	(1.03 ± 0.58) µg/dl	Epileptic	
69	Magnesium	Serum	(0.80 ± 0.04) µmol/l	Controls	Smith and Bone [161]
70	Magnesium	Serum	(0.80 ± 0.06) µmol/l	Epileptic	
71	Magnesium	Hair	(53.9 ± 36.9) µg/g	Hyperactive children	Barlow, P. J. *et. al.* [153]
72	Magnesium	Hair	(67.5 ± 47.4) µg/g	Controls	
73	Zinc	Serum	(99.523 ± 7.44) µg/dl	Birth Asphyxia	Khanna, R. S. *et.al.* [154]

74	Zinc	Serum	(91.497 ± 2.44) µg/dl	Controls	
75	Zinc	Serum	(3.214 ± 0) mg/l	Smokers	Adnan, M. *et.al.* [155]
76	Zinc	Serum	(8.20 ± 0) µmol	Neurotoxic	Guidotti, T. L. *et.al* [156]
77	Zinc	Serum	(64.82 ± 18.44) µg/dl	Epileptic	Prasad, R. *et. al.* [150]
78	Zinc	Serum	(99.0 ± 8.0) mg/l	Controls	Denitz, T. *et. al.* [157]
79	Zinc	Serum	(85.90 ± 2.79) mg/l		
80	Zinc	Serum	(56.65 ± 4.62) mg/l	Epileptic	
81	Zinc	Serum	(69.75 ± 3.07) mg/l		
82	Zinc	Hair	(134.0 ± 9.41) µg/g	Controls	
83	Zinc	Hair	(136.59 ± 8.56) µg/g		
84	Zinc	Hair	(130.5 ± 7.9) µg/g	Epileptic	
85	Zinc	Hair	(134.0 ± 7.1) µg/g		
86	Zinc	Serum	(0.54 ± 0.21) mg/l	Controls	Soylak, M. *et.al.* [158]
87	Zinc	Hair	(200 ± 61) µg/g	Controls	Avci *et.al.* [152]
88	Zinc	Hair	(218 ± 87) µg/g		
89	Zinc	Hair	(211 ± 63) µg/g	Epileptic	
90	Zinc	Hair	(218 ± 127) µg/g		
91	Zinc	Serum	(510 ± 0) µg/100ml	Controls	Delvis, H.T. *et. al.* [159]
92	Zinc	Serum	(617.9 ± 0) µg/100ml	Neurological disorders	
93	Zinc	Serum	(16 ± 9) mg/dl	GME	Kumar, S. *et.al.* [160]
94	Zinc	Serum	(13 ± 2) mg/dl	Epilepsy	Smith and Bone [161]
95	Zinc	Serum	(14 ± 2) mg/dl	Controls	
96	Zinc	CSF	(5.61 ± 2.02) µg/dl		Prasad, R. *et. al.* [150]
97	Zinc	CSF	(6.64 ± 4.40) µg/dl	Epilepsy	
98	Zinc	Serum	(83.2 ± 11.8) µg/dl	Hyperactive children	Barlow, P. J. *et. al.* [153]
99	Zinc	Serum	(87.6 ± 12.4) µg/dl	Controls	
100	Zinc	Hair	(97.5 ± 14.7) µg/g	Hyperactive children	
101	Zinc	Hair	(123.0 ± 12.6) µg/g	Controls	
102	Zinc	Serum	(1.6875 ± 1.8156) mg/l	Epilepsy	Kumar, S. *et.al.* [163]
103	Zinc	Serum	(1.0267 ± 0.6347) mg/l	Controls	
104	Calcium	Serum	(4.0285 ± 1.0521) mg/l	Epilepsy	
105	Calcium	Serum	(0.0483 ± 0.0284) mg/l	Controls	
106	Copper	Serum	(0.1767 ± 0.1087) mg/l	Epilepsy	
107	Copper	Serum	(0.1329 ± 0.0380) mg/l	Controls	
108	Iron	Serum	(1.8483 ± 1.8079) mg/l	Epilepsy	
109	Iron	Serum	(1.1826 ± 1.7671) mg/l	Controls	
110	Magnesium	Serum	(4.7017 ± 0.9548) mg/l	Epilepsy	
111	Magnesium	Serum	(0.1098 ± 0.0310) mg/l	Controls	
112	Potassium	Serum	(0.1572 ± 0.0098) mg/l	Epilepsy	
113	Potassium	Serum	(0.1443 ± 0.0043) mg/l	Controls	
114	Sodium	Serum	(3.2271 ± 0.0956) mg/l	Epilepsy	
115	Sodium	Serum	(3.1203 ± 0.0708) mg/l	Controls	
116	Zinc	Serum	(0.325 ± 0.155) mg/l	DMD	1.1 Present work
117	Zinc	Serum	(1.072 ± 0.616) mg/l	Control	Present work
118	Calcium	Serum	(0.154 ± 0.032) ml/l	DMD	Present work
119	Calcium	Serum	(0.044 ± 0.027) ml/l	Controls	Present work
120	Copper	Serum	(2.485 ± 1.668) mg/l	DMD	Present work
121	Copper	Serum	(0.139 ± 0.042) mg/l	Control	Present work
122	Iron	Serum	(11.086 ± 6.628) mg/l	DMD	1.2 Present work
123	Iron	Serum	(1.122 ± 1.177) mg/l	Control	Present work
124	Magnesium	Serum	(1.243 ± 0.371) mg/l	DMD	Present work

125	Magnesium	Serum	(0.109 ± 0.0309) mg/l	Control	Present work
126	Potassium	Serum	(0.2097 ± 0.0310)mg/l	DMD	Present work
127	Potassium	Serum	(0.1371 ± 0.0068)mg/l	Control	Present work
128	Sodium	Serum	(3.359 ± 0.242) mg/l	DMD	Present work
129	Sodium	Serum	(3.1096 ± 0.0931)mg/l	Control	Present work
130	Selenium	Serum	(0.1395 ± 0.0931)mg/l	DMD	Present work
131	Selenium	Serum	(0.198 ± 0.119) mg/l	Control	Present work

Regression coefficient and multiple correlation coefficients were also given is the Table 6.2 and Table 6.3

Table 6.2: Regression and correlation coefficient studies on Na, K, Ca, Mg, Zn, Cu , Fe and Selenium in normal samples.

Diagnosis	Regression coefficients	Regression equations	Coefficient of correlation	Coefficient of partial correlation	Multiple correlation coefficient
Normal	b_{NaK} = 1.577 b_{KNa} = 8.414	Na = 1.577K + 2.8934 K =8.414Na – 2.1874	r_{NaK} = 0.1152	r_{CaNaK} = 0.0585 r_{CaKNa} = 0.0167	$R_{Na.KCa}$ = 0.0166 $R_{K.NaCa}$ = 0.0135
	$b_{Ca.Mg}$ = 0.0332 $b_{Mg.Ca}$ = 0.0436	Ca =0.0332Mg – 0.0403 Mg =0.0436Ca + 0.1071	r_{CaMg} = – 0.0381	$r_{NaK.Ca}$ = 0.1161 r_{MgNaK} = – 0.0687	$R_{Ca.KNa}$ = 0.0035 $R_{Mg.NaK}$ = 0.0740
	$b_{Cu.Fe}$ = 3.3043 $b_{Fe.Cu}$ = 2.5950	Cu =3.3043Fe – 3.568 Fe = 2.5950Cu + 0.7612	r_{CuFe} = 0.0926	$r_{MgK.Na}$ = – 0.2755 $r_{NaK.Mg}$ = 0.0935	$R_{Na.MgK}$ = 0.0179 $R_{K.MgNa}$ = 0.0777
	$b_{Cu.Zn}$ = 0.0204 $b_{Zn.Cu}$ = 4.4029	Cu = 0.0204Zn+ 0.1132 Zn =4.4029Cu + 0.4599	r_{ZnFe} = – 0.4914	r_{ZnCuFe} = 0.3629 r_{ZnFeCu} = 0.4881	$R_{Cu.FeZn}$ = 0.2416 $R_{Fe.CuZn}$ = 0.2447
	b_{FeZn} = – 0.938 b_{ZnFe} = – 0.2571	Fe = -0.938Zn + 2.1275 Zn = -0.2571Fe + 13604	r_{CuZn} = 0.3002	r_{CuFeZn} = 0.2890	$R_{Zn.FeCu}$ = 0.3620
	$b_{Zn.Se}$ = 0.7293 b_{SeZn} = 0.0272	Zn = 0.7293Se + 0.9275 Se = 0.0272Zn + 1.018	$r_{Zn.Se}$ = 0.1409	$r_{ZnFe.Se}$ = – 0.4757	R_{ZnFeSe} = 0.1661
			r_{FeSe} = – 0.3130		
			$r_{Cu.Se}$ = – 0.1300		

Table 6.3 : Regression and correlation coefficient studies on Na, K, Ca, Mg, Zn, Cu , Fe and Selenium in DMD samples.

Diagnosis	Regression coefficients	Regression equations	Coefficient of correlation	Coefficient of partial correlation	Multiple correlation coefficient
DMD	$b_{Na.K}$ = 3.0509 $b_{K.Na}$ = 0.06319	Na = 3.8509K + 2.5514 K = 0.6319Na –1.9128	r_{NaK} = 0.4933	$r_{CaNa.K}$ = –0.3099 $r_{CaK.Na}$ = 0.3577	$R_{Na.KCa}$ = 0.3160 $R_{K.NaCa}$ = 0.3401
	$b_{Ca.Mg}$ = 0.0611 $b_{Mg.Ca}$ = 8.2130	Ca =0.0611Mg + 0.0780 Mg = 8.2130Ca – 0.0218	r_{CaMg} = 0.7084	$r_{NaK.Ca}$ = 0.5182 $r_{MgNa.K}$ = 0.1690	$R_{Ca.KNa}$ = 0.1464 $R_{Mg.NaK}$ = 0.0334
	$b_{Cu.Fe}$ = – 0.1272 $b_{Fe.Cu}$ = – 2.0094	Cu = – 0.1272Fe + 3.8951 Fe = – 2.0094Cu + 16.0793	r_{CuFe} = – 0.5057	$r_{MgK.Na}$ = –0.0219 $r_{NaK.Mg}$ = 0.4897	$R_{Na.MgK}$ = 0.2437 $R_{K.MgNa}$ = 0.2649
	$b_{Cu.Zn}$ = – 1.0944 $b_{Zn.Cu}$ = – 9.4505	Cu = – 1.0944Zn + 2.8406 Zn = – 9.4505Cu + 23.8094	r_{FeZn} = 0.5365	$r_{ZnCu.Fe}$ = 0.2329 $r_{ZnFe.Cu}$ = 0.5651	$R_{Cu.FeZn}$ = 0.2961 $R_{Fe.CuZn}$ = 0.2447
	$b_{Fe.Zn}$ = 22.9414 $b_{Zn.Fe}$ = 0.0125	Fe = 22.9414Zn + 3.6300 Zn = 0.0125Fe + 0.1864	r_{CuZn} = – 0.1017	$r_{CuFe.Zn}$ = – 0.6673	$R_{Zn.FeCu}$ = 0.3265
	$b_{Zn.Se}$ = – 0.3576 $b_{Se.Zn}$ = – 0.1561	Zn = – 0.3576Se + 0.3748 Se = – 0.1561Zn + 0.1887	$r_{Zn.Se}$ = – .2363	$r_{ZnFe.Se}$ = 0.5021	$R_{Zn.FeSe}$ = 0.2939
			$r_{Fe.Se}$ = – 0.5607		
			$r_{Cu.Se}$ = 0.1631		

7 Discussion

The estimation of trace elements show a colorful presentation of different metals .It has been seen and found that the levels of zinc and selenium were lower in DMD cases in comparison to healthy controls. The elements such as copper, calcium, iron, magnesium, potassium, sodium were found higher than controls.

On the basis of statistical analysis we have measured regression and correlation coefficients including multiple correlation coefficients between different trace elements like Na, K, Ca, Mg, Zn, Cu, Fe and Selenium in normal samples. A trend has been found in coefficient of correlation such as

$r_{CuZn} > r_{NaK} > r_{Zn.Se} > r_{CuFe}$ with positive correlation and $r_{ZnFe} > r_{Fe.Se} > r_{Cu.Se} > r_{CaMg}$ with negative correlation. Coefficient of partial correlation is also calculated and found that a trend has been set up between trace elements and given here as $r_{ZnFe.Cu} > r_{ZnCu.Fe} > r_{CuFe.Zn} > r_{NaK.Ca} > r_{CaNa.K} > r_{CaK.Na} > r_{NaK.Mg}$ with positive correlation and we have found also a negative correlation between some of the elements and a trend is given here as $r_{ZnFe.Se} > r_{MgK.Na} > r_{MgNa.K}$ Multiple correlation coefficient in normal healthy person has been estimated and found that a trend , which is given here as

$$R_{Zn.FeCu} > R_{Fe.CuZn} > R_{Cu.FeZn} > R_{Zn.FeSe} > R_{K.MgNa} > R_{Mg.NaK} > R_{Na.MgK} > R_{K.NaCa} > R_{K.NaCa} > R_{Ca.KNa}$$

We have also measured correlation coefficients including multiple correlation coefficients between different types of trace elements like Na, K, Ca, Mg, Zn, Cu, Fe and Selenium in DMD samples.

A trend has been found in coefficient of correlation such as $r_{CaMg} > r_{FeZn} > r_{NaK} > r_{Cu.Se}$ with positive correlation and $r_{Fe.Se} > r_{CuFe} > r_{Zn.Se} > r_{CuZn}$ with negative correlation. Coefficient of partial correlation is also calculated and found that a trend has been set up between trace elements and given here as $r_{CuFe.Zn} > r_{CaNa.K} > r_{MgK.Na}$ with negative correlation and also found a trend of positive correlation as $r_{ZnFe.Cu} > r_{NaK.Ca} > r_{ZnFe.Se} > r_{NaK.Mg} > r_{CaK.Na} > r_{MgNa.K}$.

Multiple correlation coefficient in DMD patients has been estimated and found that a trend, which is given here as $R_{Fe.CuZn} > R_{K.NaCa} > R_{Zn.FeCu} > R_{Na.KCa} > R_{Zn.FeSe} > R_{K.MgNa} > R_{Cu.FeZn} > R_{Na.MgK} > R_{Ca.KNa} > R_{Mg.NaK}$.Many of the essential elements are required for human health and occasionally the margin between minimum needs and maximum tolerance of is very feeble. The chemical form of the trace element and the interactions between different trace elements included in the diet are also important in deciding between health and hazard. If we are able to monitor foods and environment for the effects of pollution therefore demands subtly and an awareness of the complexity. It has been apparent that many trace elements play an important role in the maintenance of human health and that an imbalance in trace elements may be a significant factor in a number of physical and neurological conditions. The imbalance may occur as an excess of an element or a deficiency of an element. Most of the elements can become toxic if the level in the body rises above a minimum or standard value.

The importance of nutritional states in maintaining the physical well-being of the human system is very well understandable but the role of diet, including metabolism of dietary constituents is much less well understood. Let us now examine the importance and relevance of the results obtained by us in DMD and the possible mechanisms.

Trace elements act as catalytic agents for enzyme systems of the cells. These elements play a role in enzyme reactions range from weak, ionic strength effects to highly specific associations known as Metalloenzymes. Metal is firmly associated with the protein and there is a fixed number of atoms per

molecule of protein which cannot be removed from this association by dialysis. Removal of the metal by more drastic means leads to loss in the activity of enzyme. This loss cannot be restored readily either by re-addition of the metal.

The minimum requirements of living creatures for the essential trace elements are expressed in proportions or concentrations of the total dry food taken daily. The maximum intake of elements within the normal limits of the human body is called tolerance. The tolerance may be related as the fertility, growth, health or other relevant criteria of different dietary mineral concentrations.

There are safe dietary levels of potentially toxic trace elements. These depend on the extent to which other elements are present.

It may be probably related to the inhibition of Na-K ATPase activity. We must take care of our body not to take these two elements in sufficient amount. We must take proper intake of the copper and zinc enrich diet of our food.

It has been reported in the literature for the importance of trace metals which may have a role to play in the production of seizures and their control in human beings. Zinc, magnesium and copper also play an important biochemical role in the human metabolism.

It has been reviewed and reported in the literature that the living things need 72 biological elements for normal metabolic function, reproduction, and maintenance of the immune system. Calcium is an element which is generally deficient. It is required in every cell in our body and vitally important. If the food is grown on soils which contain all the 72 elements, we may say it is healthy food. Insects and diseases do not attack plants grown in healthy soil. Insects are nature's garbage disposal agents. We choose to kill insects and allow ourselves to eat garbage. Disease is also nature's way of eliminating those things that are not healthy. They may plants, animals and humans.

Food we eat is deficient in over sixty vitally important elements. The food which is deficient to all such types of elements is the basic cause of large numbers of physiological and mental diseases such as auto immune disease, late onset diabetes, degenerative and chronic diseases, allergies and birth defects and neurological disorders.

It has been established in the literature that the routine cocktail of medications with their complicated interactions and side effects should be rejected. We must provide a chance for minerals, vitamins and essential fatty acids and trace elements for healthy body.

Trace elements are essential in the assimilation and utilization of vitamins. Elements help in the digestion. The elements work as a catalyst for hormones and enzymes. They may work as an aid in replacing electrolytes lost through perspiration. Elements protect against toxic reactions.

Reinstatement of trace elements in our soils eliminates all plant diseases, pests and insect attacks. This eliminates the need for use of toxic agricultural chemicals. We may have a healthy food rather than a food which is deficient to all the trace elements. **We must try to keep maintain the levels of zinc and selenium on the higher values up to the normal values. The levels of elements such as copper, calcium, iron, magnesium, potassium, sodium may be put on the lower side of normal values.**

We know that living organisms, including humans, are part of environment they reflect what is present in their surroundings. Traces of a large variety of both natural and man-made compounds can be found in the tissues and fluids of humans as a result of exposure to these compounds in air, soil, water, food and consumer products.

Evidences from analysis of foods and water, as well as from direct measurements of fluids and tissues, reveals that the levels of some harmful elements have decreased now a days.

We are able to detect a number of compounds in the human body that results from the use of consumer products, such as pharmaceuticals and dietary supplements, and from lifestyle choices, such as smoking and alcoholism.

The continuous detection of trace elements in human tissues and fluids has led to legitmate concern about the possible health effects of the presence of elements in human body. To evaluate this fact, it is important to understand how these elements are detected, what trends are in the levels, and what is known about the health impacts of the levels that have been detected.

8 Conclusion

The chemical form of trace element and interactions between different types of trace elements included in the food are very important in deciding between hazard and health. The imbalance of the levels of elements may be adjusted with the proper medication monitoring. Trace elements may act as catalytic agents for enzyme system of the cells. The minimum requirements of living objects for essential trace elements may be expressed in proportions or concentration of the total dry food taken every day. A tolerance of the human system may be adjusted according to intake of these elements. Tolerance is related to the immunity of our human system. If the tolerance is on the lower side of normalcy the immunity may be decreased. We must increase the immunity with the adjustment of proper food and supplementation of suitable trace elements.

Routine use of medicines in bulk with side effects must avoid. We can take minerals, vitamins and essential fatty acids with proper trace elements for healthy human system. A continuous monitoring of trace elements in human tissues and fluids has led to legitimate concern about the probable effects of the presence of trace elements in human system. Our findings suggest that the values of higher levels of trace elements should be adjusted such that these levels must slight below or equal to the normal limits of the particular element. The levels of zinc and selenium should be maintained within the normal limits for DMD cases in comparison to healthy controls. The elements such as copper, calcium, iron, magnesium, potassium, sodium may be reduced up to the normal limits in comparison to healthy persons .

ACKNOWLEDGEMENTS

Authors are thankful to Dr. P. K. Saxena Principal, D.A.V. College, Muzaffarnagar, U.P. for providing necessary conditions to carry research.

REFERENCES

[1]. Petrof, B., Shrager, J., Stedman, H., Kelley, A. and Sweeney, H. (1993) : Dystrophin protects the sarcolemma from stresses developed during muscle contraction. Medical. Sciences, **90**, Retrived from http:// www. pnas. org/content/90/8/3710.full.pdf.

[2]. Emery, A. E. (2002) : The muscular dystrophies. Lancet, **359 (9307)**, 687.

[3]. Bach, R. J. (1999) : Introduction In : Guide to the evaluation and management of neuro muscular disease. Hanley & Belfus. Inc. Philadelphia P. A. , pp. 1-4.

[4]. Meryon, E. (1852) : On grannular and fatty degeneration of the voluntary muscles, Med. Chir. Trans. **35**, 72- 84

[5]. Duchenne, G. B. A. (1868) : Researches Sur la paralysic musculaire pseudo hypertrophic or paralysie myo-sclero sique, Arch. Gen. Med., **11**, 5- 25.

[6]. Maser, H. (1984) : Duchenne muscular dystrophy : Pathogenetic aspects and genetic prevention. Hum. Genet., **66,** 17-40.

[7]. Emery, A. E. (1991): Population frequencies of inherited neuromuscular disease – a world survey. Neuromuscular. Disord. **1(1)**, 19-29.

[8]. Abood, E. A., Jones, M. M. (1991) : Macrophages in developing mammalian skeletal muscle : evidence for muscle fibre death as a normal developmental event. Acta. Anat (Basel) **140 (3)**, 201-212.

[9]. Simonds, A. K., Muntani, F., Heather, S., Fielding, S. (1998) : Impact of nasal ventilation on survival in hypercapnic Duchenne muscular dystrophy, Therax, **53** (11), 949-952.

[10]. Somer, H., Donner, M., Murros, J., Konttinen, A. (1973) : A serum isoenzyme study in muscular dystrophy. Particular reference to creatine kinase, aspartate aminotransferase, and lactic acid dehydrogenase isozymes. Arct. Meyral, **29 (5)**, 343-345.

[11]. Mokri, B., Engel, A. G. (1975) : Duchenne dystrophy : electron microscopic findings pointing to a basic or early abnormality in the plasma membrane of muscle fibre. Neurology, **25 (12)**, 111-1120.

[12]. Engel, J., Furthmayr, H. Odermatt, E., Vender Mark, H., Aumailley, M., Fleischmajer, R., and Timpl, R. (1985) : Structure and macromolecular organization of type VI Collagen, Ann. N. Y. Acad. Sci., **460**, 25-37.

[13]. Gillis, J. M. (1999) : Understanding dystrophinopathies : an inventory of the structural and functional consequences of the absence of dystrophin in muscles of the mdx mouse. J. Muscle. Res. Cell. Motil, **20 (7)**, 605-625.

[14]. Sandri, M., Minetti, C., Pedemonte, M., Carraro, U. (1998) : Apoptotic myonuclei in human Duchenne muscular dystrophy. Lab. Invest., **78 (8)**, 1005-1016.

[15]. Tidball, J. G., Albrecht, D. E., Lokensgal, B. E., Spencer, M. J. (1995): Apptasis precedes necrosis of dystrophin deficient muscle, J. Cell. Sci., **108 (6)**, 2197-2204.

[16]. Matsuda, R., Nishikawa, A., Tanaka, H. (1995) : Visualization of dystrophic muscle fibers in mdx mouse by vital staining with Evans blue : evidence of apoptosis in dystrophin-deficient mouscle. J. Biochem (Tokye), **118 (5)**, 959-964.

[17]. Spencer, M. J., Walsh, C. M., Darsh kind, K. A., Rodriguez, E. M. and Tidball, J. G. (1997) : Myonuclear apoptosis in dystrophic mdx muscles occurs by perforin-mediated cytotoxicity. J. Clin. Invest., **99 (11)**, 2745-2751.

[18]. Bradley, W. G., Hudgson, P., Larson, P. F., Papapetropoulas, T. A. and Jenkison, M. (1972) : Structural changes in the early stages of Duchenne muscular dystrophy. J. Neurol. Neuro Surg. Psychiatry., **35 (4)**, 451-455.

[19]. Bowman, W. (1840) : On the minute structure and movements of voluntary muscle. Philos. Trans. R Soc. London. Biol., **130**, 457- 501.

[20]. Murphy, D. L., Mendell, J. R. and Engel, W. K. (1973) : Serotonin and platelet function in Duchenne's muscular dystrophy. Arch. Neurol. **28**, 239-242.

[21]. Paulsan, O. F., Engel, A. G. and Gomez, M. R. (1974) : Muscle blood flow in Duchenne type muscular dystrophy, limb-gridle dystrophy, polymyositis and in normal controls, J. Neurol. Neuroserg. Psychioatry, **37**, 685-690.

[22]. Jerusalem, F., Engel, A. G. and Gomez, M. R. (1974) : Duchenne dystrophy. I. Morphometric study of the muscle micro vascular. Brain, **97**, 115-122.

[23]. Mc Comas, A. J., Sica, R. E. P. and Currie, S. (1971) : An electrophysiological study of Duchenne dystrophy. J. Neurol. Neurosurg. Psychiatry, **34**, 461-468.

[24]. Panayiotopoulos, C. P., Scarpalezos, S. and Papapetropoulos, T. (1974) : Electrophysiological estimation of motor units in Duchenne muscular dystrophy. J. Neurol. Sci., **23**, 89-98.

[25]. Ballantyne, J. P. and Hansen, S. (1974) : New method for estimation of the number of motor units in a muscle. 2. Duchenne, limb-girdle and facioscapulohumerol, and myotonic muscular dystrophies. J. Neurol. Neurosurg. Psychiatry, **37**, 1195-1201.

[26]. Matheson, D. M. and Howland, J. L. (1974) : Erythrocyte deformation in human muscular dystrophy. Science, **184**, 165-166.

[27]. Miale, T. D., Frias, J. L. and Lawson, D. L. (1975) : Erythrocytes in human muscular dystrophy, Science **187**, 453.

[28]. Miller, S. E., Roses, A. D. and Appel, S. H. (1975) : Erythrocytes in human muscular dystrophy, Science, **188**, 1131.

[29]. Brown, H. D., Chattpadyay, S. K. and Patel, A. B. (1967) : Erythrocyte abnormality in human myopathy, Science, **157**, 1577-1578.

[30]. Peter, J. B. Worsfold, M. and Pearson, C. M. (1969) : Erythrocyte ghost adenosine triphosphate (AT Pase) in Duchenne dystrophy. J. Lab. Clin. Med., **74**, 103-108.

[31]. Roses, A. D., Herbstreith, M. H. and Appel, S. H. (1975) : Membrane protein kinease alteration in Duchenne muscular dystrophy. Nature, **254**, 350-351.

[32]. Mawatari, S., Takagi, A. and Rowland, L. P. (1974) : Adenyl cyclase in normal and pathologic human muscle, Arch Neurol. **30**, 96-102.

[33]. Pearce, G. W., Pearce, J. M. S. and Walton, J. N. (1966) : The Duchenne type muscular dystrophy : Histopathological studies of the carrier state, Brain, **89**, 109-120.

[34]. Roy, S. and Dubowitz, V. (1970) : Carrier detection in Duchenne muscular dystrophy, J. Neurol. Sci., **11**, 65-79.

[35]. Ionasescu, V., Zellweger, H. and Conway,T. W. (1971) : Ribosomal protein synthesis in Ducheme muscular dystrophy, Arch. Bio Chem. Biophys., **144**, 51-58.

[36]. Ionasescu, V., Zellweger, H. Shirk, P. and Conway, T. W. (1973) : Identification of carriers of Duchenne muscular dystrophy by muscle protein synthesis. Neurology, **23**, 497-501.

[37]. Roses, A. D., Roses, M. J., Miller, S. E., Hull, K. L. and Appel, S. M. (1976) : Carrier detection in Duchenne muscular dystrophy. New. Engl. J. Med., **294**, 193-197.

[38]. Hobbins, J. C. and Mahoney, M. J. (1974) : In utero diagnosis of hemoglobinopathies. Technique for obtaining fetal blood. New. Engl. J. Med., **290**, 1065-1067.

[39]. Bodensteiner, J. B. and Engel, A. G. (1978) : Intracellular calcium accumulation in Duchenne dystrophy and other myopathies. A study of 56, 7,000 muscle fibers in 114 biopsies. Neurology, **28**, 439-446.

[40]. Bertorini, T. E., Bhattacharya, S. K., Polmieri, G. M. A., Chesney, C. M., Bifer, D. and Baker, B. (1982) : Muscle calcium and magnesium content in Duchenne muscular dystrophy. Neurology, **32**, 1088-1092.

[41]. Schotland, D. L., Bonilla, E. and Wakayama, Y. (1980) : Application of the freeze fraeture technique to the study of human neuromuscular diseases, Muscle. Nerve., **3**, 21-27.

[42]. Schotland, D. L., Bonilla, E. and Van Meter, M. (1977) : Duchenne dystrophy alteration in plasma membrane structure, Science, **196**, 1005-1007.

[43]. Peluchretti, D., Mora, M., Protti, A. and Cornelio, F. (1985) : Freeze fracture analysis of the muscle fiber plasma membrane in Duchenne dystrophy, Neurology, **35**, 928-930.

[44]. Heimann-Patterson, T. D., Bonilla, E., and Schotland, D. L. (1982) : Cancanavalin A binding of the Cell surfac of Duchenne muscle in vitro. Ann. Neurol., **12**, 305-307.

[45]. Brooke, M. H. (1986) : Muscular dystrophies, In : A clinician's view of neuromuscular disease. Edited by Nancy, McSherry, C. and Victoria, M. V., Williams & Wilkins, Baltimore, London Los Angles Sytdney. PP. 117-154.

[46]. Ionasescu, V., Ionaseesu, R., Feld, R., Write, D., Cancilla, P., Kaeding, L. and Stern, L. Z. (1991 : Alterations in creatine kinase in fresh muscle and cell cultures in Duchenne dystrophy. Ann. Neurol., **9**, 394-399.

[47]. Thompson, E. J., Yasin, R., Vanbeer S. G., Nurse, K. and Al-Ani, S. (1977) : Myogenic defect in human muscular dystrophy, Nature, **268**, 241-243.

[48]. Rothman, S. M. and Bischoff, R. (1983) : Electrophysiology of Duchenne dystrophy myotubes in tissue culture. Ann. Neurol., **13**, 176-179.

[49]. Mawatari, S., Miranda, A., and Rowland, L. P. (1976) : Adenyl Cyelase abnormality in Duchenne muscular dystrophy : muscle cells in culture, Neurology, **26**, 1021-1026.

[50]. Cerri, C. A., Willner, J. H., and Miranda, A. F. (1982) : Adenylate cyclase in Duchenne fibroblasts. J. Neurol. Sci., **53**, 181-185.

[51]. Rowland, L. P. (1980) : Biochemistry of muscle membranes in Duchenne dystrophy, Muscle. Nerve., **3**, 3-20.

[52]. Falk, R. S., Campion, D., Guthrie, B., Sparkes, R. S. and Fox, C. F. (1979) : Phospharylation of the red cell membrane proteins in Duchenne muscular dystrophy. New. Engl. J. Med., **300**, 258-259.

[53]. Fischer, S., Tortolero, M., Piau, J. P., Pelaunay, J. and Schapira, G. (1978) : Protein kinase and adanylate kinase of erythrocyte membrane from patients with Duchenne dystrophy. Clin. Chem. Acta., **88**, 437-440.

[54]. Roses, A. D., Mabry, M. E., Herbstreith, M. H., Shile, E. V. and Balakrishnan, O. V. (1982) : Increased phospharylation of spectrin peptides in Duchenne muscular dystrophy. In : Disorders of the Motor Unit Edited by Schotland, D. L., John Wiley & Sons, New York, PP. 413-420.

[55]. Mabry, M. E. and Roses, A. D. (1981) : Increased ^{32}P-phashorylase of triptic peptides of erythrocytes spectrin in Duchenne muscular dystrophy Muscle Nerve, **4**, 489-493.

[56]. Roses, A. D., Shile, P. E., Herbstreith, M. H. and Balakrishnan, C. V. (1981) : Identification of abnormality ^{32}P-phashorylated cyanogen bromide cleavage product of erythrocyte membrane spectrin in Duchenne muscular dystrophy, Neurology, **31**, 1026-1030.

[57]. Arthur, H., De Niese, M., Jeffrey, P. L. and Austin, L. (1983) : Plasma lipoprotein in Duchenne muscular dystrophy, Biochem. Int. **6**, 307-313.

[58]. Personalhealthfacts. com (1985) : The importance of trace minerals, NFM'S, Nutrition Science, News , pp. 1-4.

[59]. Romeyn, M. (1998) : Vitamins, Minerals and Trace elements. In :Nutrition and HIV. Edited by Jossey-Bass Inc. Sonsome Street San Francisco.

[60]. Herring, W. B., Leavell, B. S., Paixao, L. M. and Yoe, J. H., (1960) : Trace metals in human plasma and red blood cells, American Journal of Clinical nutrition, **Vol. 8,** pp. 846-854.

[61]. Khurshid, S. J. and Qureshi, I. H. (1984) : The role of inorganic elements in human body, The Nucleus, **Vol. 21,** pp. 3-23.

[62]. Suhaila, R., Nasir, K., Shujaat, A., Nasim, U. and Mohammad, Z .I. (2004) : Essential trace metals in human whole blood in relation to environment, Pakistan J. Med. Res., **Vol. 43, No. 2,** pp. 1-5.

[63]. Kumar, S. (1989) : Medico-Physical studies on epilepsy and other neurological disorders, Ph.D. Thesis, University of Delhi, India.

[64]. Mary, R. L. A., Kelvin, A. C., Sheila, D. and William, H. R. (2000) : Nutrient risk assessment implication for food fortification policy, In : Trace elements in man and animals, 10. Edited by Rousel, A. M., Anderson, R. A., Favrier, A., Kluwer Academic Publications, N. Y., Boston, Dodrecht, Lands, Moscow. pp 215 - 220

[65]. Alexander, G. S. (1995) : Minerals and Human health : The rationale for optimal and balanced trace element levels, Tacoma, Life. Sciences. Press. pp 1-5.

[66]. Pike, R. L. and Brown, M. L. (1984) : An Integrated Approach .In : Nutrition., John Wiley & Sons, pp. 197.

[67]. Zumkley, H. (1987) : Trace elements in medicine, Fresenius Z., Anal Chem, **Vol. 327, No. 1,** pp. 6.

[68]. Davies, I. J. J. (1972) : Clinical significance of the essential biological metals, In: Animal health and hygiene (general), William Heineman, London, pp. 48– 26. I.S.B.N. 0433071702 .

[69]. Burns, R. R. and Fell, G. S. (1976) : Estimation and interpretation of plasma zinc fractions, Secott. Med. J., **Vol. 21,** pp. 153-154.

[70]. Prasad, A. S., and Oberleas, D. (1970) : Binding of zinc to amino acids and serum proteins in vitro, J. Lab. Clin .Med., **Vol. 76, No. 3,** pp. 416-425.

[71]. Kelin, D. and Mann, J. (1940) : Carbonic anhydrase : Purification and nature of the enzyme, Biochem J, **Vol. 34, No. 8&9,** pp. 1163-1176.

[72]. Riordan, J. F. and Vallee, B. L. (1976) : Structure and function of zinc metalloenzymes,In Trace Elements in human health and disease. Edited by Prasad, A. S. **Vol. 1**. Academic Press, New York, pp. 227-251.

[73]. Chavapil, M., Zukowski, C. F., Hattler, B. G., Stankova, L., Montgomery, D., Carlson, E. C. and Ludwig, J. C. (1976) : Zinc and activity of cell membrane. In : Trace-elements in human health and disease . Edited by Prasad, A. S. **Vol. 1**, Academic Press, New York, pp. 269-281.

[74]. Prasad, A. S., Schulert, A. R., Sandstead, H. H., Miale. A. Jr., and Farid, Z., (1963): Zinc, iron and nitrogen content of sweat in normal and deficient subjects, J. Lab. Clin .Med., **Vol. 62,** pp. 84-89.

[75]. Walravens, P. A., Doornick, W. J. V. and Hambidge, K. M. (1978) : Metals and Mental Function, J. Ped., **Vol. 93, No. 3,** pp **.**535.

[76]. Henkin, R. I., Patten, B. M., Re, PK., Bronzett, D. A., (1975) : A syndrome of acute zinc loss, Arch Neurol, **Vol. 32, No. 11,** pp. 745-751.

[77]. Dresti, I. E. (1984) : Zinc in the central nervous system : The emerging interactions. In : The Neurobiology of Zinc Part A. Edited by Frederickson, C. J., Howell, G. A. and Kasarskis, E. J., Alan R. L., New York, pp. 1-26.

[78]. Fairbanks, V. F., Fahey, J. L. and Beutler, E. (1971) : Clinical disorders of Iron metabolism, 2nd ed., Grune and Stratton, New York, pp. 1-486.

[79]. Mc Cance and Widdowson, E. M. (1937) : Absorption and excretion of iron, Lancet, **Vol. 2,** pp. 680-684.

[80]. Gramick, S. (1946) : Ferritin IX. Increase of the protein apoferritin in the gastrointestinal mucosa as a direct response to iron feeding. The function of ferritin in the regulation of iron absorption, J. Biol. Chem. **Vol. 164,** pp. 737-746.

[81]. Moore, C. V., Doan, C. A. and Arrowsmith, W. R. (1937) : Studies in iron transportation and metabolism, mechanism of iron transportations : Its significance in iron utilization in anemic states of varied etiology. J. Clin. Invest., **Vol. 16, No. 4,** pp. 627-648.

[82]. Mahler, H. R. and Elowe, D. G. (1953) : DPNH cytochrome reductase, a ferroflavo protein, J. Amer. Chem. Soc., **Vol. 75,** pp. 5769-5770.

[83]. Richert, D. A. and Westerfeld, W. W.(1954) : The relationship of iron to xanthime oxidase, J. Biol. Chem., **Vol. 209,** pp. 179-189.

[84]. Fisher, H. and Zeile, K. (1929) : Synthesis of hematoprophyrin, protoporphyrin and hemin, Ann. European Journal of Organic Chemistry, **Vol. 468 , No. 1,** pp. 98-116.

[85]. Ingram, D. J. E., Gibson, J. F. and Perutz, M. F. (1956) : Orientation of the four heme groups in hemoglobin, Nature, **Vol. 178,** pp. 906-908.

[86]. Holmberg, G. C. and Laurell, C. B. (1947) : Investigations in serum copper I. Nature of serum copper and its relation to the iron-binding protein in human serum. Acta Chem. Scand. **Vol. I,** pp. 944-950.

[87]. Schade, A. L., Reinhart, R. W., and Levy, H., (1949) : Carbon dioxide and oxygen in complex formation with iron and siderophilin, the iron-binding compound of human plasma, Arch Biochem., **Vol. 20, No. 1,** pp. 170-172.

[88]. Lipschitz, D. A., Cook, J. D. and finch, C. A., (1974) : A clinical evaluation of serum ferritin as an index of iron stores. New. Eng. J. Med., **Vol. 290,** pp. 1213-1216.

[89]. Simes, M. A., Addiego, J. E., Jr., and Dallman, P. R., (1974) : Ferritin in serum : Diagnosis of iron deficiendcy and iron overload in infants and children, Blood, **Vol. 43**, **No. 4**, pp. 581-590.

[90]. Aikawa, J. K. (1971) : The relationship of magnesium to diseases in domestic animals and in human, Charles C. Thomas. Springfield, Illinois, pp. 1-145.

[91]. Aikawa, J. K. (1976) : Biochemistry and physiology of magnesium. In: Trace Elements in Humans : Health and diseases, **Vol. II,** Edited by Prasad, A. S., .Academic Press, New York, pp. 47-78.

[92]. Widdowson, E. M., McCance, R. A. and Spray, C. N. (1951) : The clinical composition of the human body, Clin. Sci., **Vol. 10,** pp. 113-125.

[93]. Waterlow J.C. (1992) : Endocrine changes in severe PEM .In: Protein-Energy Malnutrition, Edited by Waterlow, J. C., London, Edward Arnold , pp. 112-125.

[94]. Classen, H. G., (1984) : Magnesium and potassium deprivation and supplementation in animals and man : aspects in view of intestinal absorption. Magnesium, **Vol. 3, No. 4-6**, pp. 257-264.

[95]. Al-Ghamdi, S. M., Cameron, E. C., and Sutten, R. A., (1994) : Magnesium deficiency : Pathophysiologic and Clinical Overview, Am. J. Kidney. Dis., **Vol. 24, No. 5,** pp. 737-752.

[96]. Wester, P. (1987) : Magnesium, Am. J. Clin. Nutr., **Vol. 45,** Supplement, pp. 1305-1312.

[97]. Krasner, B. (1979) : Cardiac effects of magnesium with special reference to anaesthesia : a rewiew, Can Anaesth Soc J., **Vol. 26 No. 3,** pp. 181-185.

[98]. Furukawa, Y., and Chiba, S., (1981) : Effects of magnesium on the isolated, blood-perfused atrial and ventricular preparations of the dog heart, Jpn. Heart. J.,**Vol** . **22, No. 2,** pp. 239-246.

[99]. Stark, G., Stark, U., Pilger, E., Honigl, K., Bertuch, H. and Tritthart, H. A., (1989): The influence of elevated Mg2+ concentrations on cardiac electrophysiological parameters, Cardiovasc. Drugs. Ther., **Vol**. **3, No. 2,** pp. 183-189.

[100]. Haigney, M.C.P., Berger, R., Schulman, S., Gerstenblith, G. ,Tunin. C Silver, B., Silverman, H. S., Tomaselli, G and Calkins, H (1997) : Tissue magnesium levels and the arrhythmic substrate in humans, J Cardiovasc Electrophysiol**.,Vol**. **8, No. 9,** pp. 980-986.

[101]. Ireland, P., and Fordtran, J. S., (1973) : Effect of dietary calcium and age on jejunal calcium absorption in humans studied by intestinal perfusion, J. Clin. Investig., **Vol**. **52, No. 11,** pp. 2672-2681.

[102]. Heaney, R. P., Saville, P. D., and Recker, R. R., (1975) : Calcium absorption as a function of calcium intake, J .Lab. Clin Med.,**Vol. 85, No. 6,** 881-890.

[103]. Wilkinson, R. (1976) : Absorption of calcium, phosphorus and magnesium calcium phosphate and magnesium metabolism. Edited by Nordin, B. E. C., Edinberg, Churchill Livingstone, pp. 36-112.

[104]. Marshall, D. H. (1976) : Calcium and phosphate kinetics calcium, phosphate and magnesium metabolism. Edited by Nordin, B. E. C. Edinberg, Churchill Livingstone, pp. 257-297.

[105]. Morris, H. A., Need, A. G., Horowitz, M., O'Loughlin, P. D., and Nordin, B. E., (1991): Calcium absorption in normal and osteoporotic postmenopausal women, Calcif. Tissue. Int., **Vol. 49, No. 4**, pp. 240-243.

[106]. Ebeling, P. R., Yergey, A. L. and Vleira, N.E. (1994) : Influence of age on effects of endogeneous 1, 25-dihydroxyvitamin D on calcium absorption in normal women, Calcif .Tissue. Int., **Vol. 55 , No.** 5 , pp. 330-334.

[107]. Need, A. G., Morris, H. A., Horowitz, M., Scopacasa, E. and Nordin, B. E., (1998): Nordin. Intestinal calcium absorption in men with spinal osteoporosis, Clin. Endocrinol., **Vol. 48 , No. 2**, pp. 163-168.

[108]. Nordin, B. E. C. (1976) : Nutritional considerations in : Calcium, phosphate and magnesium metabolism. Edited by Nordin, B. E. C., Edinberg, Churchill Livingstone, pp. 1-35.

[109]. Kent, G. N., Price, R. I., and Gutteridge, D. H., Allen, J. R., Barnes, M.P., Hickling, Retallack, R. W., Wilson, S.G., Delvin, R.D., Price, R.I., Simith, M., Bhagat, C.I., Davies, C, St. Johns, A., (1990) : Human lactation : forearm trabecular bone loss, increased bone turnover, and renal conservation of calcium and inorganic phosphate with recovery of bone mass following weaning, J. Bone. Miner. Res.,**Vol**. **5, No. 4,** pp. 361-369.

[110]. Lopez, J. M., Gonzalez, G., Reyes, V., Campino, C. and Diaz, S. (1996): Bone turnover and density in healthy women during breastfeeding and after weaning, Osteoporos. Int., **Vol. 6, No. 2,** pp. 153-159.

[111]. Chan, G. M., McMurray, M., Westover, K., Engelbert-Fenton, K., and Thomas, M. R., (1987): Effects of increased dietary calcium intake upon the calcium and bone mineral status of lacting adolescent and adult women, Am. J. Clin. Nutr., **Vol . 46**, **No. 2,** pp. 319-323.

[112]. Katz, M., and Steihm, E.R. (1977): Host defense in malnutrition. Pediatr. **Vol. 59, No. 4,** pp. 490-495.

[113]. Suskind, R.M. (1977): Malnutritian and the immune response In: Kroc foundation Series, **Vol. 7,** New York, USA, Raven Press, PP 468.

[114]. Bongiorni-Malave, I.B. and Pocino, M. (1980) : Abnormal regulatory control of the antibody response to hetrologous erythrocytes in protein-calorie-malnourished mice, Clin. Immunol. Immunopathol., **Vol. 16 No. 1 ,** pp. 19-29.

[115]. Malave, I., Nemeth, A. and Pocino, M., (1980) : changes in lymphocyte populations in proteins-caloriedefieient mice, Cellular, **Vol. 49, No. 2,** pp. 235-249.

[116]. Gershwin, M. E., Keen, C. L., Fletcher, M. P. and Hurley, L. S. (1988): Trace element deficiencies and immune responsiveness. In : Trace elements in man and animals, Edited by Hurley, L. S, Keen, C. L. Lonnerdal, Bo, and Rucker, R. B, Plenuum press, New York and London, pp. 85-89.

[117]. Rigas, D. A., Rigas, E. C. and Head, C., (1979) : Biophasic toxicity of diethyldithiocarbamate, a metal chelator, to T leymphocytes and polymorphonucuclear granulocytes : Reversal by zinc and copper Biochem. Biophys. Res. Commun. **Vol. 88, No. 2,** pp. 373-379.

[118]. Walten, W. S. and Richard, N. P. Jr. (2003) : Elements metabolism and body composition, Mol. Nucl. Med. in press, pp. 253-300.

[119]. Malcolm, J. J., David, A. J. and Richard, H. T. E. (1985) : Measurements of calcium and other elements in muscle biopsy samples from patients with Duchenne muscular dystrophy, **Vol. 147, No. 3**, pp. 215-221.

[120]. Allen, D. G., Gervasio, O. L., Yeung, E. W. and Wheitehead, M. P. (2010) : Calcium and the damage pathways in muscular dystrophy. Can. J. Pysoiol. Pharmacol., **Vol. 88, No. 2**, pp. 83-91.

[121]. Imbert, N., Cognard, C., Duport, G., Guillou, C. and Raymand, G. (1995) : Abnormal calcium homeostasis in Duchenne muscular dystrophy myotubes contracting in vitro, Cell. Calcium, **Vol**. **18, No. 3,** pp. 177-86.

[122]. Rena, Y. and Yael, H. (1978) : Elements in muscle measured and in vitro with X-ray spectrometry. Muscle and Nerve., **Vol. 1, No. 6,** pp. 486-494.

[123]. Caroline, A. M., Raphael, G., Rena, Y. and Victor, D. (1980) : Elements analysis of skeletal muscle in Duchenne muscular dystrophy using X-ray fluorescence spectrometry, Muscle & Nerve, **Vol. 3, No. 6,** pp. 502-508.

[124]. Hisao, K., Mieko, K. and Yashinori, I. (1991) : Manganese, Copper, Zinc and Iron concentrations and subcellulor distribution in two types of skeletal muscle., Exp. Biol. Med., **Vol. 196, No. 1**, pp. 83-88.

[125]. Turner, P. R., Fong, P. Y., Denetclaw, W. F. and Steinhardt, R. A. (1991) : Increased calcium influx in dystrophic muscle. JCB, Vol. **115, No. 6**, pp. 1701-1712.

[126]. Arthur, J. R. and Duthie, G. G. (1994) : Free radicals and trace elements in muscle disorders and sporis, In : Trace elements and free radicals in oxidative disease, edited by Favier, A. E., Neve, J. and Faure, P. AOCS Press, U. K., pp. 241-248.

[127]. Baharch, M., Jay, R. M. and Mark, A. T. (2005) : Nutritional inadequacy in adults with muscular dystrophy, Muscle & Nerve, **Vol. 31, No. 6**, pp. 713-718.

[128]. Kando, H., Miura, M., Nakagaki, I., Sasaki, S., and Itokawa, Y. (1992) : Trace element movement and oxidative stress in skeletal muscle atrophied by immobilization, Am. Physiol. Soc. **Vol. 262, No. 5 pt 1**, pp. E583-90..

[129]. Gage, V. H., Drori, J. B., Franklin, D. and Schwartz, (1970) : Hypokalemic myopathy and elevation of serum enzymes, Arch. Neurol., **Vol. 22, No. 4**, pp. 335-341.

[130]. Howard, M. K., William, D. S., and Robert, N. R. (1983) : Malignant hyperthermia in a child with Duchenne muscular dystrophy, Pediatrics, **Vol. 71, No. 1**, pp. 118-119.

[131]. William, B., Benedict, C. and Muriance, L. (1963) : Body Potassium content in patients with muscular dystrophy, Anals. N. Y. Acad. Sci., **Vol. 110**, pp. 282-290.

[132]. Kassmann, R. J., Dorothy, C., Peterson, B. S., and Howard, L. A. (1965) : Studies in neuromuscular disease, Neurology, **Vol. 15, No.9**, pp. 855.

[133]. Hull, K. L. and Roses, A. D. (1976) : Stoichiometry of sodium and potassium transport in erythrocytes from patients with mytonic muscular dystrophy. J. Physiol., **Vol. 254**, pp. 169-181.

[134]. Edmonds, C. J., Smith, T., Griffiths, R. D., Mackenzie, J. and Ed. Wards, R. H. (1985) : Total body potassium and water, and exchangeable sodium in muscular dystrophy. Clinical. Science, London. **Vol. 68, No. 4**, pp. 379-85.

[135]. William, H. B., Marianne, L. and Benedict, C. (1967) : The significance of decreased body potassium concentrations in patients with muscular dystrophy and non dystrophic relatives, New. Engl. J. Med., **Vol. 276**, pp. 1349-1352.

[136]. Rowland, L. P., Layzar, R. S. and Kagen, L. J. (1968) : Lack of some muscle proteins in serum of patients with Duchenne dystrophy. Arch. Neurol, **Vol. 18, No. 3**, pp. 272-276.

[137]. Hopf, F. W., Turner, P. R. and Steinhardt, R. A. (2007) : Calcium misregulation and the pathogenesis of muscular dystrophy, Sub Cel. Biochem., **Vol**. **45**, pp. 429-464.

[138]. Neve, J. (2005) : Selenium : An essential micronutrient with extended biological potency at supra-nutritional intakes , Trace elements in medicine **Vol.6,No. 2**, pp. 15-20.

[139]. Westermarck, T. and Atroshi, F. (2005) : Dietary approaches to patients with Duchenne muscular dystrophy (DMD), patients with spielmeyer-sergen disease, and patients with epilepsy, Trace elements in medicine, Vol. **6, No. 2**, pp.27-32.

[140]. Alain, L., Mathieu, R., Alain, K., Pascale, G. and Valérie, A (2009): Selenoprotein function and muscle disease, Biochemica. Et Biophysica Acta, **Vol. 1790, No. 11**, pp. 1569-1574.

[141]. Zunkley, H. (1988) : Clinical aspects of selenium metabolism, Biol. Trace. Elem. Res. **Vol. 15, No. 1**, pp. 139-146.

[142]. Harris, L. S., Robert, L. F., and James, N. E. (1962) : Magnesium and calcium in human muscular dystrophy, Am. J. Dis. Child, **Vol**. **103, No. 6**, pp. 771-776.

[143]. Samuel, W. B., Erik, J. O. Dorothy, F. and Edwin, R. H. (1965) : Plasma and erythrocyte magnesium in muscular dystrophy, Am. J. Dis. Child, **Vol**. **110, No. 2**, pp. 172-175.

[144]. Tulio, E. B., Syamal, K. B., Genaro, M. A. P., Caroly, M. C., David, P. and Barbara, B. (1982) : Muscle calcium and magnesium content in Duchenne muscular dystrophy. Neurology, **Vol. 32, No. 10**, pp. 1088-1092.

[145]. Csenkér, E., Diöszeghy, P., Fekete, I., and Mechler, F. (1982) : Ion concentrations in serum and cerebrospinal fluid of patients with neuromuscular diseases, Arch. Psychiatry, Mervenkr, **Vol. 231, No. 3**, pp. 251-8.

[146]. Carlier, L., Legrand, M., Riviére, H. and Navarro, J. (1993) : Nutritional assessment in Duchenne muscular dystrophy, Dev. Med. Child. Neurol., **Vol. 35, No. 12**, pp. 1074-1082147.

[147]. Walsh, A.,(1956):The application of atomic absorption spectra to chemical analysis, Spectrochim. **Acta Vol. 7,** pp. 108.

[148]. Skoog, D. A., Holler, F. J. and Nieman, T. A. (1998) : Prinicples of instrumental analysis, 5th Edition. Harcourt Brace & Company, Philadelphia. pp. 849.

[149]. John, H., Maxwell, J.D., Stewart, D.A., Parsons, V., Williams, R., (1971) : Altered calcium metabolism in epileptic children on anti-convulsants, British Medical Journal, **Vol**. **4,** pp. 202-204.

[150]. Prasad, R., Singh, A., Das, B. K., Upadhyay, R. S., Singh, T. B., Mishra, O. P. (2009) : Cerebrospinal fluid and serum zinc copper, magnesium and calcium levels in children with idiopathic seizure, Journal of Clinical and Diagnostic Research, **Vol. 3, No. 6,** pp. 1841-1846.

[151]. Lech, T. (2001) : Calcium and magnesium content in hair as a predictor of disease in children, Trace Elements and Electrolytes, **Vol. 18 , No. 3,** pp. 112-121.

[152]. Avci, H., Kizilkan, N., and Yaman, M., (2008) : Comparison of trace elements concentrations in scalp hair of epileptic and normal subjects, Trace Elements and Electrolytes, **Vol. 25 , No. 3 ,** pp. 147-155.

[153]. Barlow, P.J., Francois, P.E., Goldberg, I.J. Richardson, I., Izmeth, M.G., Kumpeson, K., and Sykes, P., (1986) : Trace metal abnormalities in long stay hyperactive mentally handicapped children and agitates senile dements, J Royal Soc Medicine. **Vol. 79, No. 10,** pp. 581-583.

[154]. Khanna, R. S., Kumar, R., Asthana, R. K., Negi, R., Pande, D., Kumar, A. and Khanna, H. D. (2009) : Role of trace element and antioxidants in free radical mediated injury in neonates, MASAUM Journal of Basic and Applied Science, **Vol. 1, No. 3,** pp. 543-547.

[155]. Adnan, M., Ahmed, G., Khaled, O., Indress, A. M., Ahmed, A., Hiatham, T., Wall, H. (2010) : Simultaneous Determination of Cd, Pd, Cu Zn and Se. In Human blood of Jordanian smokers, by ICP-OES, Biological Trace Element Research, **Vol. 133, No. 1,** pp. 1-11.

[156]. Guidotti, T. L., McNamra, J., Moses, M. S., (2008) : The interpretation of trace element analysis in body fluids, Indian Journal of Med. Res., **Vol. 128,** pp. 524-532.

[157]. Deniz, T., Ali, H. T., Saraymen, R (2008) : The effects of antiepileptic drugs on serum and hair trace element levels, Ankara. Universitesi Tip. Fakultesi. Mecmuasi, **Vol. 61, No.2,** pp. 73-76.

[158]. Soylak, M., Saracoglu, S., Divrikli, U., and Elci, L., (2001) : Copper and zinc concentrations of serum samples of healthy people living in Tokat, Turkey, Trace Element and Electrolytes, **Vol**. **18, No.1,** pp. 47-40.

[159]. Delves H. T., Clayton, B. E., and Bicknel, J., (1973) : Concentration of trace metals in the blood of children, Br. J. Prev .Soc. Med**., Vol. 27,** pp. 100-107.

[160]. Kumar, S., Bajaj, M., Jain, D.C. and Yadav, H. S. (1988) : A search for the trace elemental deficiencies in grand mal epilepsy using atomic absorption spectrophotometric technique and catalytic agent in the cellular enzyme reaction, Proc. World .Congress on Clinical. Nutrition, **Vol. 1,** pp. 115A-121A.

[161]. Smith, W. G., and Bone, I., (1982) : Copper, zinc and magnesium plasma levels in epilepsy, J Neurol Neur Surg Psychiatry, **Vol. 45, No. 11 ,** pp. 1072- 1073.

[162]. Kaji, M., Ito, N., Okuno, T., Momoi, T., Sasaki, H., Yamanake, C., Yorifuji, T., and Mikawa, H. (1992) : Serum copper and zinc levels in epileptic children with valporate treatment, Epilepsia, **Vol**. **33, No. 3,** pp. 555-557.

[163]. Kumar, S., Kumar, V., and Jain, D. C. and Mittal. R. (2013): Trace element analysis in epileptic children. Open.J . Appl .Sci , **Vol. 3, No.3,** pp. 449-476.

SOCIETY FOR SCIENCE AND EDUCATION UNITED KINGDOM

JBEMi JOURNAL OF BIOMEDICAL ENGINEERING AND MEDICAL IMAGING

ISSN: 2055-1266
VOLUME 1, ISSUE 5

Application of a Computer-aid Diagnosis of Pneumoconiosis for CR X-ray Images

[1]Koji Abe, [2]Masahide Minami, [1]Ryosuke Miyazaki and [3]Haiyan Tian
[1]Interdisciplinary Graduate School of Science and Engineering, Kinki University, Japan;
[2]Kanazawa Gakuin University, Japan;
[3]Graduate School of Engineering, Kobe University, Japan;
koji@info.kindai.ac.jp; saboten0078@yahoo.co.jp; maminami@dream.com;
tian.haiyan2006@gmail.com

ABSTRACT

This paper presents a method for applying a computer-aided diagnosis (CAD) for pneumoconiosis to chest X-ray images digitalized by the computed radiography (CR) system. When we reported the CAD before, we showed performance of the CAD for chest X-ray images digitalized by a CCD scanner. However, since density distribution of the CR X-ray images is quite different from the images digitalized by CCD scanner, it is necessary to equip some preprocessing into the CAD for applying to the CR images. In this paper, as the first trial for the application, drawing rib edges and additional lines on the CR images by a tablet PC, we examined whether the CAD can be interactively applied to the CR images. Using 51 chest CR X-ray images, we compared the proposed CAD system with the existing system for the images digitalized by CCD scanner.

Keywords: Computer-aided diagnosis; Pneumoconiosis; Chest X-ray image; Medical image processing.

1 Introduction

Pneumoconiosis is interstitial lung disease caused by inhalation of fine particles (e.g., coal pneumoconiosis). In recent years, in addition to coal workers, dental technicians also suffer from the disease. However, since it is difficult for even expert diagnosticians on pneumoconiosis to diagnose pneumoconiosis, disagreement between diagnosticians is often happened. Besides, the experts teach techniques on the diagnosis to immature diagnosticians based on just their experience. For the reasons, computer-aided diagnosis (CAD) systems for pneumoconiosis have been required as a second opinion for diagnosticians. CAD systems for pneumoconiosis have been reported since 1970s [1-4]. Their measurements of abnormalities for pneumoconiosis broadly are two ways: the one measures the abnormalities based on texture analysis [1, 2], another one extracts small round opacities and measures their size and number as well as the real diagnosis by diagnosticians [3, 4]. All the systems were proposed to images obtained by a custom-made scanner (e.g., a drum scanner or a film scanner). Therefore, if the systems were applied in general clinics, the clinics would have to deploy the special scanner, or order scanning chest radiographs to a printing company in spite of high costs.

DOI: 10.14738/jbemi.15.606
Publication Date: 28th October 2014
URL: http://dx.doi.org/10.14738/jbemi.15.606

In order to enhance cost-performance of CAD for pneumoconiosis, a CAD system for pneumoconiosis using images digitalized by a common CCD scanner was reported [5, 6]. This system is composed with a CCD scanner and a tablet PC, and discriminates pneumoconiosis with abnormalities in rib areas. Since the images obtained from X-ray pictures by a CCD scanner are extremely unclear and it is hard to extract rib areas automatically, in this system, the user draws rib edges on the images manually using the tablet PC. The reason why only X-ray pictures are used in diagnosis of pneumoconiosis is because there is a criterion that diagnosticians have to diagnose pneumoconiosis comparing X-ray pictures with the standard X-ray pictures of pneumoconiosis provided by the International Labour Organization (ILO). Similarly, in Japan, the Ministry of Health, Labour and Welfare provided another set of the standard X-ray pictures. And, both of the ILO and the ministry opened new standard images in 2011 [7]. Both of the new standard sets are digital images digitalized by the computed radiography (CR) system. Since a picture digitalized by CR is saved as a digital file, CR enables diagnosticians to read X-ray pictures on a monitor. CR has been already regular radiography in Japan.

With the revision of the standard pictures from X-ray pictures to CR X-ray images, this paper examines whether the prior CAD system for pneumoconiosis using the X-ray images digitalized by a CCD scanner can apply to chest CR X-ray images. Basically, X-ray images digitalized by CCD scanner are unclear. On the other hand, since the shadows in the CR images are appeared clearly, density distribution of the CR image is quite different from the X-ray image digitalized by a CCD scanner. Hence, if we consider to apply the CAD to the CR images, we need to customize the CAD equipping some pre-processing. Therefore, in order to apply the CAD to the CR images, this paper proposes a manual pre-processing method of drawing rib edges and additional lines on the CR images before the diagnosis by the CAD. If the system can apply to either of chest CR X-ray images and images digitalized by CCD scanner, the system is useful in the diagnosis for either of them at a low cost.

2 Pneumoconiosis Classification

The level of pneumoconiosis was indicated by profusion of small round opacities, where categories 0-3 were established. Figure 1 shows samples of the standard images provided by the Japanese ministry. Normal cases belong to category 0, where the opacities are not observed visually. And, abnormal ones belong to category 1, 2, or 3, where the most serious level is category 3 and the opacities are observed most in category 3. Although diagnosticians diagnose pneumoconiosis comparing chest X-ray pictures with the standard pneumoconiosis images prepared in every category, their own experience much depends on the diagnosis. For example, gray levels at the opacities are very similar to intersections of vascular shadows.

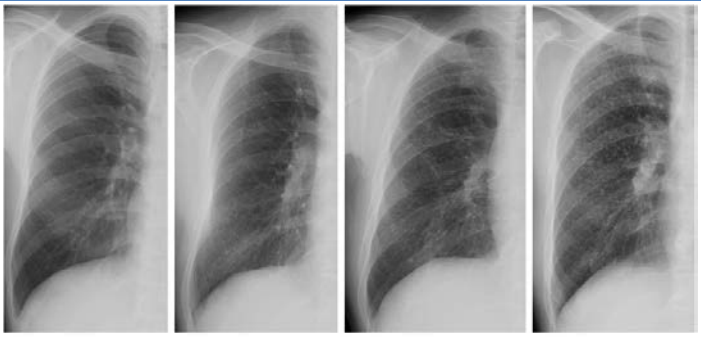

Figure 1: Standard images of pneumoconiosis (Provided by the Ministry of Health, Labour, and Welfare in Japan).

In Japan, the criteria of the classification are defined under the Japanese Pneumoconiosis Law in accordance with criteria of pneumoconiosis in the ILO.

3 CAD for Pneumoconiosis X-ray Images Digitalized by CCD Scanner

3.1 Overview

In the CAD system for pneumoconiosis X-ray images digitalized by CCD scanner [6], abnormalities of pneumoconiosis are measured by extracting characteristics of the density distribution in rib areas. The rib areas are manually designated using a tablet PC. First, the right lung area in chest X-ray pictures is digitalized by a CCD scanner. Next, the chest image is displayed on the tablet PC and the user draws curves along the edges of rib shadows on the image using the tablet PC. And then, the rib areas are designated by the drawn curves. Finally, abnormalities of pneumoconiosis are extracted from the rib areas. The extracted abnormalities are used as valuables for discrimination of the X-ray images into normal or abnormal cases in pneumoconiosis.

3.2 Preprocessing

The right lung area in chest X-ray pictures (35 cm × 35 cm) is digitalized by a CCD scanner. The chest X-ray image is configured with 300 dpi and 256 gray levels. Next, the image is resized into 1000 pixels in height without changing the aspect ratio. And then, the range of the gray value in the image is standardized by the linear histogram stretching.

3.3 Drawing of Rib Edges on the X-ray Image with Tablet PC and Extraction of Rib Areas

The image is displayed on the tablet PC and the user draws 8 curves with white color along the edges of 4 ribs on the image using the tablet PC. The manual for drawing the curves is designed as below.

[Manual for drawing the rib edges]

1. Open the right lung image in a paint tool.
2. Select the round brush and set the thickness of the circle as 4 pixels.
3. Select “white” to the line color.
4. Look at the curve shown in Figure 2(b) as the guide of start points for drawing rib edges.

5. Imaging the curve on the image by yourself, decide the start point for the drawing and start drawing the curve along an edge of a rib.
6. Stop drawing the curve at a location where the edge cannot be seen.
7. Until you finish drawing all couples of the edges for 4 ribs, repeat 5 and 6.

As shown in 4 and 5, Figure 2(b) is shown to the user as the guide for aiming at the location of the start point for the drawing. Figure 2(c) shows an example of the curves drawn to Figure 2(a). Then, as shown in Figure 2(d), the rib areas R_1–R_4 are extracted by the drawn edges (Refer to [6]).

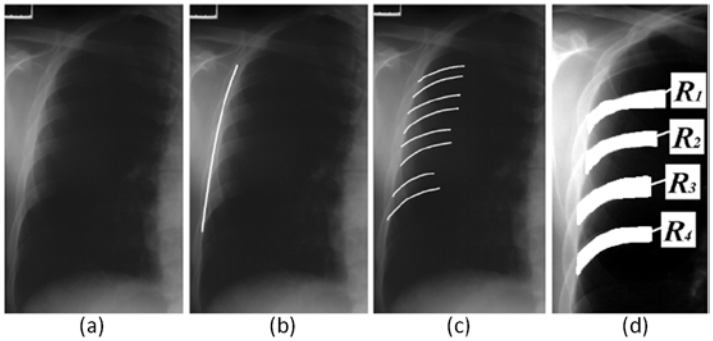

Figure 2: Drawing of rib edges according to the manual and rib areas R_1-R_4 extracted from the edges.

As shown in Figure 1 and Figure 2, we can see that the images digitalized by CCD scanner are extremely unclear than CR images.

3.4 Extraction of Abnormalities and Discrimination of Pneumoconiosis

Figure 3 shows a rib area R_m extracted above, where the first line is regarded as k-th scanning line (k = 1) and the value k is added by 1 whenever the scanning line is shifted to the right by 1 pixel. Besides, the uppermost pixel on k-th scanning line is regarded as j = 1 and the value j is added by 1 whenever the pixel goes down by 1 pixel. The linear histogram stretching is applied to every scanning line. In the scanning on the k-th scanning line, all the pixels on the line are divided into the upper set and the lower set. The boundary of them is obtained by the discriminant analysis for the pixels. In regarding $t_m[k]$-th pixel counted from the uppermost edge as the boundary $t_m[k]$, the upper set is composed of pixels of j = 1 ~ $t_m[k] - 1$ and the lower set is $j = t_m[k] + 1$ ~ $heiR_m[k]$.

As the scanning is conducted from the upper edge to the lower edge along the scanning line regarding $v[j]$ as the gray value of the j-th scanning spot, by using the parameters shown in Figure 3, the abnormality $Abn(R_m)$ of k-th scanning line in R_m is defined as

$$Abn(R_m[k]) = \left[\frac{1}{heiR_m[k]-1} \left(\sum_{j=1}^{heiR_m[k]} |v[j] - avg[k, j]|^2 \right) \right]^{\frac{1}{2}} \quad (1)$$

where

$$avg[k,j]=\begin{cases} if \quad 1\le j\le t_m[k], \left(\sum_{i=1}^{t_m[k]-1} v[j]\right)/\left(t_m[k]-1\right) \\ if \quad j=t_m[k], \; v[j] \\ if \quad t_m[k]<j\le heiR_m[k], \left(\sum_{i=t_m[k]+1}^{heiR_m[k]} v[j]\right)/\left(heiR_m[k]-t_m[k]\right) \end{cases} \tag{2}$$

Next, shifting the scanning line in R_m shifts one by one to the scanning line at the most right side horizontally, the abnormality in R_m, $Abn(R_m)$ is defined as

$$Abn(R_m)=\frac{1}{widR_m}\left(\sum_{k=1}^{widR_m} Abn\left(R_m[k]\right)\right) \tag{3}$$

where $widR_m$ is the number of the horizontal shifts. Then, an abnormality in the whole rib areas *AbnR* is defined as

$$AbnR=\frac{1}{L_R}\left(\sum_{m=1}^{4}\sum_{k=1}^{widR_m} Abn\left(R_m[k]\right)\right) \tag{4}$$

where

$$L_R=\sum_{m=1}^{4} widR_m \tag{5}$$

Besides, the maximum value *AbnRMAX* in $Abn(R_m)$ (m = 1 ~ 4) is represented as another abnormality.

$$AbnRMAX=\max\left\{Abn\left(R_1\right),Abn\left(R_2\right),Abn\left(R_3\right),Abn\left(R_4\right)\right\} \tag{6}$$

Thus, the abnormality *AbnR* represents an overall abnormality of pneumoconiosis in rib areas and *AbnRMAX* represents local abnormalities of pneumoconiosis in all the rib areas.

After the extraction of the abnormalities, regarding the abnormalities as variables for discriminant machines, the diagnosis of pneumoconiosis is conducted by discriminating between normal cases and abnormal cases.

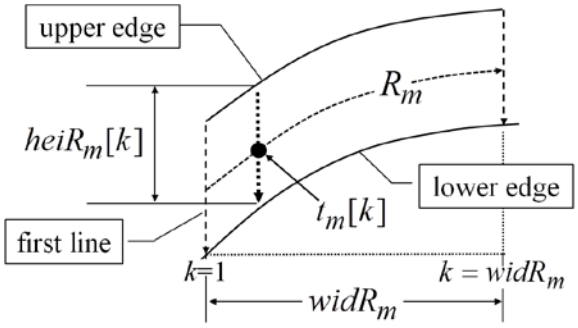

Figure 3: A rib R_m and parameters used in the equations (3)–(5).

4 Customization of the Drawing Manual for Chest CR X-ray images

Figure 4(b) shows a result that a user drew the rib edges to Figure 4(a) according to the manual shown in Sect. 3. Thus, differing from the case of the unclear images digitalized by CCD scanner, the user can confidently draw the edges on the whole ribs. However, due to the drawing, the extracted rib areas would contain the clavicular shadow or the lung marking (a mass of linear shadows appeared in the lung area of chest X-ray images) and they could become noises in extracting the abnormalities from the rib areas. Therefore, to draw the edges on the CR images without containing them, the manual is customized for the CR images as below.

[*Manual for drawing the rib edges* (*for CR X-ray images*)]

1. Open the right lung image in a paint tool.
2. Select the round brush and set the thickness of the circle as 7 pixels.
3. Draw a curve with a color except white along the lower edge of the clavicular shadow (as Ⓐ in Figure 4(c)).
4. Draw a curve with a color except white at left side of the lung marking and separate the lung area into the lung marking and outside of the lung area (as Ⓑ in Figure 4(c)).
5. Draw 8 curves along 4 couples of rib edges with white from the boundary between the lung area and its outside (i.e., left side contour of the right lung) until reaching either of the curves drawn in 3 and 4 as shown in Figure 4(c).

Figure 4(d) shows the rib areas extracted from Figure 4(c).

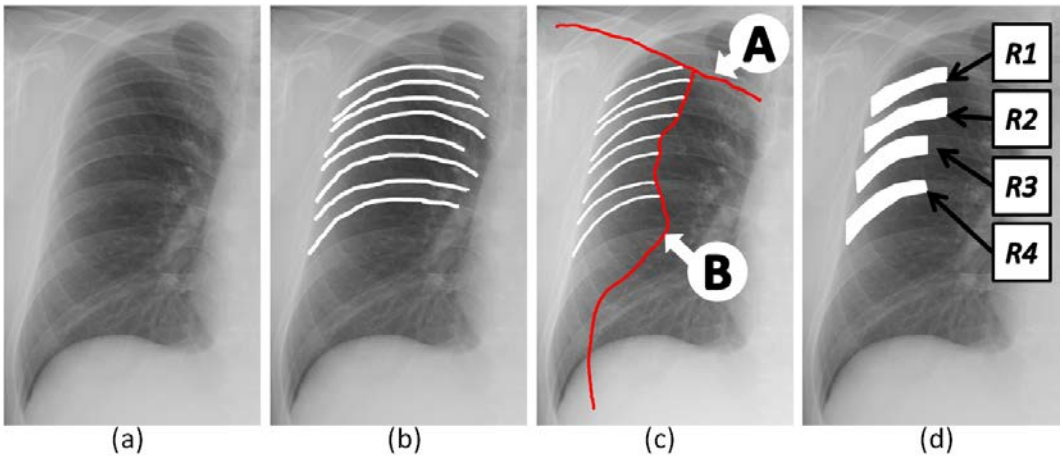

Figure 4: Drawing of the rib edges ((a): original image (b): drawing by the old manual, (c): drawing by the customized manual), and (d) is the rib areas R_1-R_4 extracted from image (c).

5 Experimental Results

The abnormalities were extracted from 51 chest CR X-ray images (resolution: 300 dpi, gray level: 8 bits, format: bitmap image). The number of images which belong in category 0 (normal case) is 36, the number in category 1 is 6, the number in category 2 is 6 and the number in category 3 is 3. All the abnormal cases are the standard image of pneumoconiosis provided by the Japanese ministry. To obtain

the rib areas, three non-experts (represented as userA, userB, and userC) in pneumoconiosis diagnosis drew the rib edges on all the images with a tablet PC (ThinkPad 200Tablet 4184-F5J). The total time used for drawing all the images was about 60 minutes in every user. Table 1 shows the mean and standard deviation (SD) of *AbnR* and *AbnRMAX* extracted from each of the normal and abnormal cases. From Table 1, we can see both of two abnormalities in abnormal cases are higher than normal cases, and the abnormalities are appropriately extracted for the discrimination of pneumoconiosis in both of the proposed methods.

Table 1: The mean value and the standard deviation of the abnormalities in the proposed method.

Abnormalities	User	normal		Abnormal	
		mean	SD	Mean	SD
AbnR	userA	2.3	0.2	3.1	0.5
	userB	2.2	0.2	3.0	0.4
	userC	2.1	0.2	3.0	0.5
AbnRMAX	userA	2.5	0.3	3.5	0.6
	userB	2.5	0.3	3.5	0.5
	userC	2.4	0.3	3.3	0.5

Next, we examine performance of the proposed method from the discrimination of the images into normal or abnormal (i.e. pneumoconiosis) cases by regarding the abnormalities as variables for the discriminations. As the way of the discrimination, Random Trees (RT), a Neural Network (NN), a linear Support Vector Machine (SVM) were applied. Training set and test set were chosen by the leave-one-out cross validation [8] in all the discriminations. In fact, every discrimination was conducted as the following procedure:

1. Choose one image from all the images as test data, and use the other images as training set.
2. Discriminate the test data between normal and abnormal cases.
3. Repeat the procedure from 1 to 2 to every combination changing the test data.

Table 2 shows the recall (*Rec.*) and the precision (*Pre.*) in the discriminations. *Rec.* and *Pre.* are defined as

$$Rec. = \frac{X_{h \cap c}}{X_h} \times 100 \tag{7}$$

$$Pre. = \frac{X_{h \cap c}}{X_c} \times 100 \tag{8}$$

where X represents the number of images, X_h is the number of the correct answers, and X_c is the number of images discriminated by the proposed method. Table 2 shows the ratios have been more than 80% except one part (*Rec.* of abnormal case in NN by userA).

Table 2: Experimental results of the discrimination of pneumoconiosis by the proposed method.

User	Case	RT		NN		SVM	
		Rec.	*Pre.*	*Rec.*	*Pre.*	*Rec.*	*Pre.*
userA	Normal	97.2%	92.1%	97.2%	89.7%	91.7%	94.3%
	Abnormal	80.0%	92.3%	73.3%	91.6%	86.7%	81.3%
userB	Normal	91.6%	94.2%	94.4%	97.1%	88.8%	100%
	Abnormal	86.6%	81.2%	93.3%	87.5%	100%	78.9%
userC	Normal	91.7%	97.0%	94.4%	97.2%	94.4%	97.2%
	Abnormal	93.2%	82.4%	93.2%	87.5%	93.2%	87.5%

6 Discussions

Figure 7(a)(b)(c) show the distribution maps of all the data by the abnormalities, where ○ is normal case and × is abnormal case. From the figures, we can see the two cases are roughly separated without depending on users, and this suggests that the CAD could be sufficiently applied to the CR images by the customization.

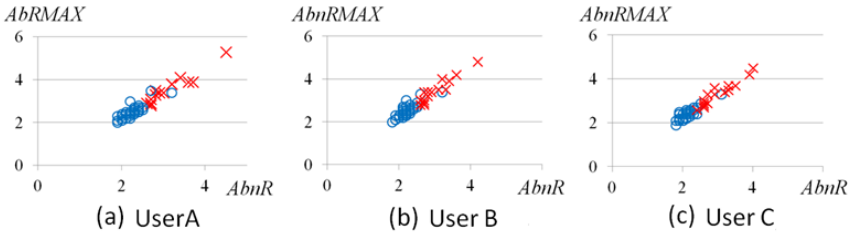

Figure 7: Distribution maps of all the image data by the abnormalities.

Figure 8 shows results of an image drawn by each user. From the results, we can see that there are difference of the drawing between the users. In addition, although there were no significant difference in the discrimination ratios shown in Table 2 between the users, it is suggested that there is possibility the abnormalities could be depended on the user if the drawing is depended on users. Therefore, it is necessary to reduce the difference between users by improving the manual more strictly.

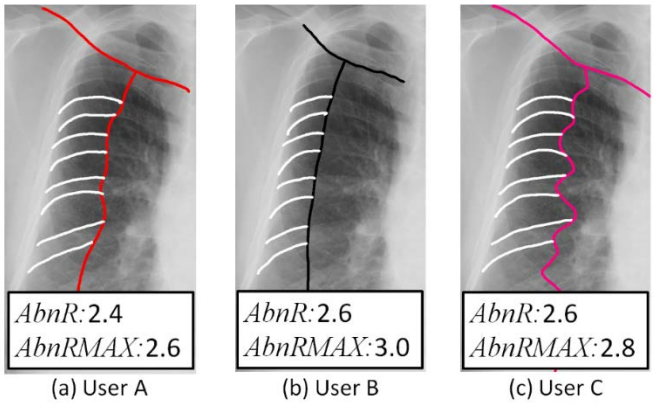

Figure 8: Results of the drawing for an image by the 3 users.

Finally, we compare experimental results of the discrimination between the proposed method and the existing CAD, i.e., the proposed method is the CAD which apples to the CR X-ray images by the customization of the rib drawing and the existing CAD works to the X-ray images digitalized by CCD scanner. Table 3 shows experimental results of the discrimination for the existing CAD using the same 51 X-ray images digitalized by CCD scanner. Comparing Table 2 with Table 4, we can confirm there is no significant difference between the two CAD systems. In Japan, there is the license test of mammography, where the candidates have to correctly read the X-ray pictures of more than 80 % to pass the test. If we follow this line, the results of Table 2 show that the CAD can be applied to the CR images sufficiently.

Table 3: Experimental results of the discrimination by the existing method (using images digitalized by CCD scanner).

User	Case	RT		NN		SVM	
		Rec.	*Pre.*	*Rec.*	*Pre.*	*Rec.*	*Pre.*
userA	Normal	95.7%	95.7%	95.7%	95.7%	95.7%	95.7%
	Abnormal	83.3%	83.3%	83.3%	83.3%	83.3%	83.3%
userB	Normal	95.7%	95.7%	97.9%	97.9%	97.9%	97.9%
	Abnormal	83.3%	83.3%	91.7%	91.7%	91.7%	91.7%
userC	Normal	97.9%	97.9%	100.0%	97.9%	97.9%	100.0%
	Abnormal	91.7%	91.7%	91.7%	100.0%	100.0%	92.3%

7 Conclusion

For the sake of application of the CAD system for pneumoconiosis for images digitalized by CCD scanner to chest CR X-ray images, this paper proposed a preprocessing of customizing the manual for drawing rib edges in the CAD. Experimental results for examining the proposed method using 51 chest CR X-ray images showed that the customization was effective enough for the diagnosis and there was no significant difference between the CAD which applied to the CR images and the existing CAD which works to the X-ray images digitalized by CCD scanner.

As future works, it is necessary to improve the manual more strictly to reduce difference of the drawing between users.

REFERENCES

[1]. R.P. Kruger, W.B. Thompson, and A.F. Turner, *Computer diagnosis of pneumoconiosis.* Trans. on Systems, Man. and Cybernetics, 1974. SMC-4(1): pp. 40-49.

[2]. H. Kobatake and K. Ohishi, *Automatic diagnosis of pneumoconiosis by texture analysis of chest x-ray images*. Proc. IEEE ICASSP, 1987. pp. 633-636.

[3]. A.M. Savol, C.C. Li, and R.J. Hoy, *Computer aided recognition of small rounded pneumoconiosis opacities in chest X-rays.* IEEE Transactions on PAMI, 1980. 2(5): pp. 479-482.

[4]. T. Kouda and H. Kondo, *Computer-aided diagnosis for pneumoconiosis using neural network.* Biomed. Soft Comput. Hum. Sci., 2001. 7(1): pp. 13-18.

[5]. M. Nakamura, K. Abe, and M. Minami, *Quantitative Evaluation of Pneumoconiosis in Chest Radiographs Obtained with a CCD Scanner.* Proc. of the 2nd International Conference on the Applications of Digital Information and Web Technologies (ICADIWT 2009), 2009. pp. 673-678.

[6]. K. Abe, T. Tahori, M. Minami, M. Nakamura, and H. Tian, *Computer-aided diagnosis of pneumoconiosis X-ray images scanned with a common CCD scanner.* Automation Control and Intelligent Systems, 2013. 1(2): pp. 24-33.

[7]. International Labour Organization (ILO), *Guidelines for the use of ILO international classification of radiographs of pneumoconiosis (Revised edition 2011).* Geneva: International Labour Office.

[8]. F. Mosteller, *A k-sample slippage test for an extreme population*. The Annals of Mathematical Statistics, 1948. 19(1): pp. 58-65.